Since January 2020 Elsevier has created a COVID-19 resource centre with free information in English and Mandarin on the novel coronavirus COVID-19. The COVID-19 resource centre is hosted on Elsevier Connect, the company's public news and information website.

Talanta 230 (2021) 122026

Contents lists available at ScienceDirect

Talanta

journal homepage: www.elsevier.com/locate/talanta

Review

Nanomaterial application in bio/sensors for the detection of infectious diseases

Elham Sheikhzadeh [a,*], Valerio Beni [b], Mohammed Zourob [c,d,**]

[a] Department of Chemistry, Faculty of Science, Ferdowsi University of Mashhad, Mashhad, Iran
[b] Digital Systems, Department Smart Hardware, Unit Bio–& Organic Electronics, RISE Acreo, Research Institutes of Sweden, Norrkoping, 60221, Sweden
[c] Department of Chemistry, Alfaisal University, Al Zahrawi Street, Al Maather, Al Takhassusi Road, Riyadh, 11533, Saudi Arabia
[d] King Faisal Specialist Hospital and Research Center, Zahrawi Street, Al Maather, Riyadh, 12713, Saudi Arabia

ARTICLE INFO

Keywords:
Nanomaterial
Infectious disease
Electrochemical method
Optical method
Lateral flow strip
Pathogen detection

ABSTRACT

Infectious diseases are a potential risk for public health and the global economy. Fast and accurate detection of the pathogens that cause these infections is important to avoid the transmission of the diseases. Conventional methods for the detection of these microorganisms are time-consuming, costly, and not applicable for on-site monitoring. Biosensors can provide a fast, reliable, and point of care diagnostic. Nanomaterials, due to their outstanding electrical, chemical, and optical features, have become key players in the area of biosensors. This review will cover different nanomaterials that employed in electrochemical, optical, and instrumental biosensors for infectious disease diagnosis and how these contributed to enhancing the sensitivity and rapidity of the various sensing platforms. Examples of nanomaterial synthesis methods as well as a comprehensive description of their properties are explained. Moreover, when available, comparative data, in the presence and absence of the nanomaterials, have been reported to further highlight how the usage of nanomaterials enhances the performances of the sensor.

1. Introduction

Infectious or transmissible diseases are those diseases that can be transmitted by bacteria, viruses, fungus, and parasites [1]. According to the World Health Organization reports consumption of unsafe foods, that are polluted with harmful bacteria, viruses, parasites, or chemical substances leads to 200 types of sickness including cancers, sepias, homoerotic diarrhea, etc. [2]. Moreover, diarrhea-associated infections related to the intake of contaminated food or water are the third cause of mortality in developing countries, and around a million people's death is reported for this every year [2–4].

Facing threats like Ebola, dengue, Zika, severe acute respiratory syndromes (SARS-Cov-2), Middle East respiratory syndrome (MERS), and severe known as well as unknown pathogens endanger human health and, in a large view, economic welfares [5]. Bacteria such as *Escherichia coli O157: H7*, *Salmonella enterica serovar Typhimurium*, *Klebsiella pneumonia*, *Listeria monocytogenes*, *Enterococcus faecalis*, *Campylobacter*, *Acinetobacter baumannii* and Viruses like *influenza virus H5N1*, H_3N_2, *HIV*, *HPV*, and *enterovirus 71* cause enormous hospitalizations and death all over the world. Therefore, the development of new, fast, and reliable approaches to detect these sources of infection are crucial to prevent the epidemic of these diseases [6,7].

Nanomaterials with specific electrical, optical, magnetic, chemical and mechanical properties have been found effective application in many areas including biosensors or chemical sensors, diagnostics methods, drug delivery, energy harvesting, and tissue engineering [8]. This unquestionably owes to the intrinsic high surface area to volume ratio of these materials that can present more recognition sites and quicker signal transduction procedure [9]. Nanomaterials according to the European commission's recommendation 2011, "is a natural, incidental or manufactured material containing particles, in an unbound state or as an aggregate or as an agglomerate and where, for 50% or more of the particles in the number size distribution, one or more external dimensions is in the size range 1 nm–100 nm" [10]. They can be categorized into four groups based on the material using in their fabrication 1) carbon-based nanomaterials that are carbons with different morphology such as hollow tubes, ellipsoids or spheres e.g. Graphene, Graphene oxide, Carbon nanotubes (CNTs), Fullerenes (C60), Carbon

* Corresponding author.
** Corresponding author. Department of Chemistry, Alfaisal University, Al Zahrawi Street, Al Maather, Al Takhassusi Road, Riyadh, 11533, Saudi Arabia.
E-mail addresses: Elham.Sheikhzadeh@mail.um.ac.ir (E. Sheikhzadeh), mzourob@alfaisal.edu (M. Zourob).

https://doi.org/10.1016/j.talanta.2020.122026
Received 4 November 2020; Received in revised form 14 December 2020; Accepted 15 December 2020
Available online 17 December 2020
0039-9140/

black and carbon nano onion. 2) Inorganic-based nanomaterials, these groups involve metal (Au, Ag, Pt, Ni, Cu), metal oxide nanoparticles (ZnO, TiO_2, MnO_2, Fe_2O_3, Al_2O_3), SiO_2, semiconductors such as silicon and ceramics, and inorganic semiconductor nanocrystals which also called quantum dots (CdS, ZnO, CdS). 3) Organic-based nanomaterials, these groups are nanomaterial from organic material such as (dendrimers, micelles, liposomes, and polymer NPs). 4) Composite-based nanomaterials, that are multi-phase nanoparticle and nanostructured materials with one phase on the nanoscale size which can combine either with other nanoparticles or bulk-type materials (e.g., hybrid nanofibers) or more complicated structures, such as metal-organic frameworks (MOF). The composites may be any combinations of carbon-based, metal-based, or organic-based nanostructured materials with any form of metal, ceramic, or polymer bulk materials [11,12]. In the present review, we will focus on electrochemical and optical sensors for infectious diseases which used nanomaterials like metallic nanoparticle (Ag, Au), magnetic nanoparticle, bimetallic nanoparticle, silica nanoparticle, graphene family, carbon nanotube, carbon dot, quantum dots, and upconversion nanoparticles.

2. Nanomaterial

2.1. Magnetic nanoparticle (MNP)

Magnetic nanoparticles are well known for special magnetic properties like superparamagnetism and high magnetic susceptibility [13]. These nanoparticles have found extensive applications due to their unique advantages including low production cost, large surface area, high mass transference, direct capture, easy separation, improving the washing steps, and minimizing the matrix effect. Besides their application in sample enrichment, they have been shown to enhance sensor sensitivity, increase the signal-to-noise ratio, and decrease the time of analysis [14,15]. The role of the MNPs is dependent on their sizes that can be influenced by the preparation method [16]. MNPs with a size of less than 30 nm possess superparamagnetic properties making these good candidates for enrichment applications because of an immediate response to the applied magnetic field [17]. Different types of Magnetic nanoparticles like iron oxides (Fe_2O_3 and Fe_3O_4); ferrites of manganese, cobalt, nickel, and magnesium; multifunctional composite MNPs, such as Fe_3O_4-Ag, Fe $_3O_4$-Au, Fe_3O_4-SiO_2 are reported. Among them, Fe_3O_4 is the preferred magnetic nanoparticle in biosensor development because of its superparamagnetic property, biocompatibility with antibodies and enzymes, and ease of preparation [14]. Among the demonstrated manufacturing methods, like thermal decomposition, microemulsion, electrochemical, solvothermal, sol-gel, sonochemical, and co-precipitation for synthesis Fe_3O_4 nanoparticle; co-precipitation is the most used technique in the synthesis Fe_3O_4 [17]. More details about different synthesis method of iron oxide nanoparticles and surface modification [17–19] properties of iron oxide nanoparticles [17], magnetic $CoFe_2O_4$ [20] magnetic nanoparticle [21] are available in these references.

2.2. Gold nanomaterials

Gold nanomaterials with a wide variety of shapes, such as rods, spheres, cubes, wires, and cages, are among the most popular nanomaterials for sensor applications [22]. Their intrinsic properties, such as good biocompatibility, large surface area, ease of synthesis and modification, and high chemical and thermal stability make Au nanomaterial ideal choice as substrates and transducers for sensors. The optical properties of these materials depend on their size and shape which can be controlled/tuned during the synthesis process. Besides, the surface of gold nanomaterial can be modified by electrostatic, hydrophobic, and covalent bonding; for example, the strong bond between gold atoms and nitrogen or sulfur, enable efficient attachment of molecules via the well-established thiol or amine chemistry [9].

2.2.1. Gold nanoparticle (AuNPs)

Gold nanoparticles (AuNPs) are polycrystalline Au nanostructure with a quasi-spherical shape and typically 5–100 nm diameter size. In electrochemical sensors, AuNPs, have found application due to their ability to improve the charge transfer processes [23] and the electrode's conductivity [24]. AuNPs are extensively applied as a colorimetric indicator, because of their surface plasmon resonance property [25,26]. Along with their optical and electrochemical properties, AuNPs are very attractive in biosensing since their high surface area offer unprecedented opportunities for high loading of biomolecules such as antibodies, enzymes, and aptamers; moreover, gold nanoparticles have been shown to maintain high bioactivity of immobilized biomolecules [23]. Chemical reduction or ligand passivation methods and their variants are popular approaches for manufacturing AuNPs. Peng et al. discussed various methods for the synthesis of gold nanomaterial family [9].

2.2.2. Gold nanorods (AuNRs)

Anisotropic Nanorods are cylindrical rod-shaped particles with uniform diameters ranging from a few nanometers to hundreds of nanometers, with aspect ratios (length to width) larger than 1 but typically smaller than 10 [27]. The main features of AuNRs are depending properties like intensities and spectral positions of SPR-bands, aggregative stability, electroconductivity, and redox potential by physical size [28]. One of the peculiarities of the AuNRs is those to present two distinct surface plasmon resonances; one along with the longitudinal ax and one on the transversal ax. The longitudinal plasmon resonance generates radiation in a wide range from visible to near-infrared regions depending on the AuNRs aspect ratio and their size which is a distinguishable feature of nanorods when compared to nanoparticles [28,29]. Among the different approaches proposed to producing AuNRs, seed-mediated growth is the most commonly used because of a simple procedure, adjustable aspect ratio, great uniformity, and adaptability for post-modification [9,30]. There are promising reviews about the synthesis and properties of gold nanorods [30] gold nanorods and their nanocomposites synthesis and recent applications in Analytical chemistry [28].

2.2.3. Gold nanocluster (AuNCs)

AuNCs are molecular like arrangements consisting of several hundred Au atoms with an average size of 2 nm. They are located between Au atoms and AuNPs and can be fabricated by atoms to clusters and nanoparticles to clusters approaches. Atoms to cluster approach based on template-based synthesis and ligand-protected methods. While, nanoparticles to clusters methods are etching surface atoms of gold nanoparticles by appropriate ligand, or solvents [31]. AuNCs are characterized by photoluminescence [32]and high catalytic properties [33]; on the other end, AuNCs do not present the surface plasmon resonance properties characteristic of the AuNPs and AuNRs [9]. Zhang et al. discussed synthesis methods and biomedical and biosensing applications of Au nanoclusters in a recent review [34].

2.3. Silver nanoparticles (AgNPs)

Silver nanoparticles (AgNPs) present unique plasmonic properties that can be influenced by different parameters, such as size, shape, uniformity, composition, dispersion, etc. [35]. Moreover, these nanomaterials have prominent benefits including low cost, simple preparation, high extinction coefficients, and sharp extinction band [36]. AgNPs can be produced, similarly to their counterparts AuNPs, by chemical reduction using reducing agents like $NaBH_4$, tri-sodium citrate, thiosulfate, and polyethylene glycol. Polyvinyl pyrrolidone (PVP), polyvinyl alcohol (PVA), and CTAB are often used to stabilize particles and avoid sedimentation and agglomeration of nanoparticles [37].

2.4. Bimetallic nanoparticles

Bimetallic nanoparticles are consist of two different metal NPs and can have various morphologies and structures. They can be classified based on structures into mixed and segregated structures. Mixed forms subdivide into alloy and intermetallic. In alloyed nanoparticles nanocrystals of two metals are randomly mixed; however, in intermetallic structures, the two metals are mixed in an ordered way. The segregated structures are categorized as subcluster, core-shell, multishell core-shell structures, and multiple core structures. A subcluster is a separate distribution of two metals with a shared interference. Core-shell structures are composed of a metal core surrounded by a shell of the second metal. Multishell core-shell structures are an alternative arrangement of metals forming a shape like onion rings. Multiple core materials are multiple small cores coated by a single shell. Various types of bimetallic nanoparticles are platinum, nickel, iron, palladium, and gold-based bimetallic nanoparticles [38]. Due to the collaborative effect of two different metals, bimetallic nanoparticles display novel features such as tunable surface plasmon band and optical properties and improved stability and dispersibility that make them attractive materials in electrochemical and optical sensors [39,40]. They can prepare with chemical, physical, and biological methods [41]. Some interesting reviews for synthesis, properties, and application of bimetallic nanoparticle [39,42], noble metal bimetallic nanoparticle [43] are provided in the former references.

2.5. Quantum dots (QDs)

Quantum dots (QDs) is a family of nanomaterials with outstanding optical properties like narrow emission, wide absorption spectra, size-controlled emission from visible to the infrared range (400–4000 nm), good photostability, and high quantum yields. Generally, these are composed of atoms from IIB-VI, III–V, or IV-VI groups of the periodic table that have 1–10 nm size dimensions which is smaller than the exciton Bohr radius [44–46]; their nanocrystal (dots) nature defines the quantum controlled mechanics of their optical properties. Capping agents on the surface of QD including alcohols, primary amines, carboxylic acid thiols, and long-chain organophosphorates play a pivotal role in the application of these materials. Ligands facilitate modification of the surface with biomolecules and responsible for colloidal stability, solubility, particle size distribution as well as growth or agglomeration [47,48].

2.6. Graphene group

Graphene is one of the carbon allotropes with a plane two-dimensional nanostructure. This possesses excellent optical and electronic properties, converting it into a fast-growing material for designing optical and electrochemical sensors [49,50]. There are different graphene-based nanomaterials, pristine graphene, graphene oxide (GO), and reduced graphene oxide (rGO). GO was regarded as a result of chemical exfoliation and oxidizing of layered crystalline graphite [51]. rGO is the product of GO reduction via physical, chemical, or electrochemical methods. These differ from each other in terms of, composition, purity, lateral dimensions, oxygen content, surface chemistry, and electric properties [52,53]. GO is strongly hydrophilic with oxygenated functional groups that facilitate chemical functionalization of it. The presence of versatile functional groups such as OH, COOH, and CHO allows interaction with biomolecules to improve the selectivity of the biosensors [54] but reduce the electrical conductivity due to its insulating nature for electrochemical application [55]. rGO demonstrated an improvement in electrical conductivity and remaining oxygen groups, converted it to a useful material in developing biosensors. Graphene and graphene derivatives can be coupled with different materials, such as metal oxides, metal nanoparticle, and organic polymers obtaining in this way diverse nanocomposites with tailored properties [56,57]. Interesting reviews about graphene-based electrochemical biosensors that discussed different types and synthesis methods [55] and reduced graphene for electroanalytical sensing platforms [58] are available in the former papers.

2.7. Carbon nanotube (CNTs)

Carbon nanotubes (CNTs), including single-wall and multiwall carbon nanotubes (SWCNTs and MWCNTs, respectively) [59] have attracted great attention in sensors due to their high surface area, high electrical conductivity, high thermal conductivity, and great mechanical strength. CNTs also possess specific inherent optical properties as, for example, potent resonance Raman scattering and Near-Infrared photoluminescence [60]. CNT can produce by three main synthesis methods including chemical vapor deposition, electric arc method, and laser deposition method [61].

2.8. Carbon dot or carbon particles (CD)

Carbon dots (CDs), as a new type of fluorescent carbon-based nanomaterial, have promising properties to design the fluorescent sensor to conventional fluorescent probes like superior optical properties, strong absorption, bright photoluminescence, excellent light stability, resistance to light bleaching, low toxicity, environmental-friendly, good biocompatibility, and facile synthesis [62,63]. CDs are zero-dimensional carbon-dominated nanomaterial, with a size of less than 20 nm which consisted of sp^2/sp^3carbon skeleton and abundant functional groups/polymer chains [62]. Functional groups are OH, COOH, and NH_2 [64,65]. Although there is considerable debate about the classification of CDs, they can be categorized into carbon quantum dots (CQDs) graphene quantum dots (GQDs), carbon nanodots (CNDs), and polymer dots (PDs) [62]. Two main synthesis routes, the top-down include arc discharge, laser ablation, electrochemical synthesis, nanometer etching, hydrothermal/solvothermal/special oxidation cleavage, and the bottom-up method involves combustion, pyrolysis, hydrothermal, solvothermal, and microwave assistant pyrolysis have been reported for the preparation of carbon dots [62,63,66].

2.9. Upconversion nanoparticles (UCNPs)

Upconversion nanoparticles (UCNPs) with near-infrared (NIR) excitation characteristics have received considerable attention in bioimaging (e.g. nanoprobe) [67]. The most used of UCNP-based nanoparticles are in fluorescence resonance energy transfer, FRET sensor. The UCNP's fluorescence were quenched or recovered after the additions of analytes via modulating the absorption of energy acceptors or the distance between donors and acceptors [68].UCNP are a special class of nanomaterial doped with lanthanide ions; these consist of three components, a sensitizer (Yb^{3+}) for absorbing energy from a laser source, an emitter that works as a luminescence hearts of UNCPs (Tm^{3+}, Er^{+3}, Ho^{+3}), and a host matrix. The host matrix has a substantial influence on optical features, fluorescence efficiency, and chemical properties. Fluorides due to their high chemical stability, low photon energy, are well-suited hosts for UCNPs. Synthetic procedures like co-precipitation, thermal decomposition, hydro/solvothermal synthesis, and sonochemical methods have been reported in the manufacturing of UCNPs [67]. These nanoparticles are characterized by low toxicity, sharp emission band, long fluorescence lifetime, less light scattering, high photostability, tunable multicolor emission, high light penetration depth, and larger anti-stocks shifts, when compared with more conventional fluorochromes, making them particularly useful for biosensor applications [68,69].

2.10. Silica nanoparticles

Numerous silica nanoparticles (SiNPs) and hybrid silica

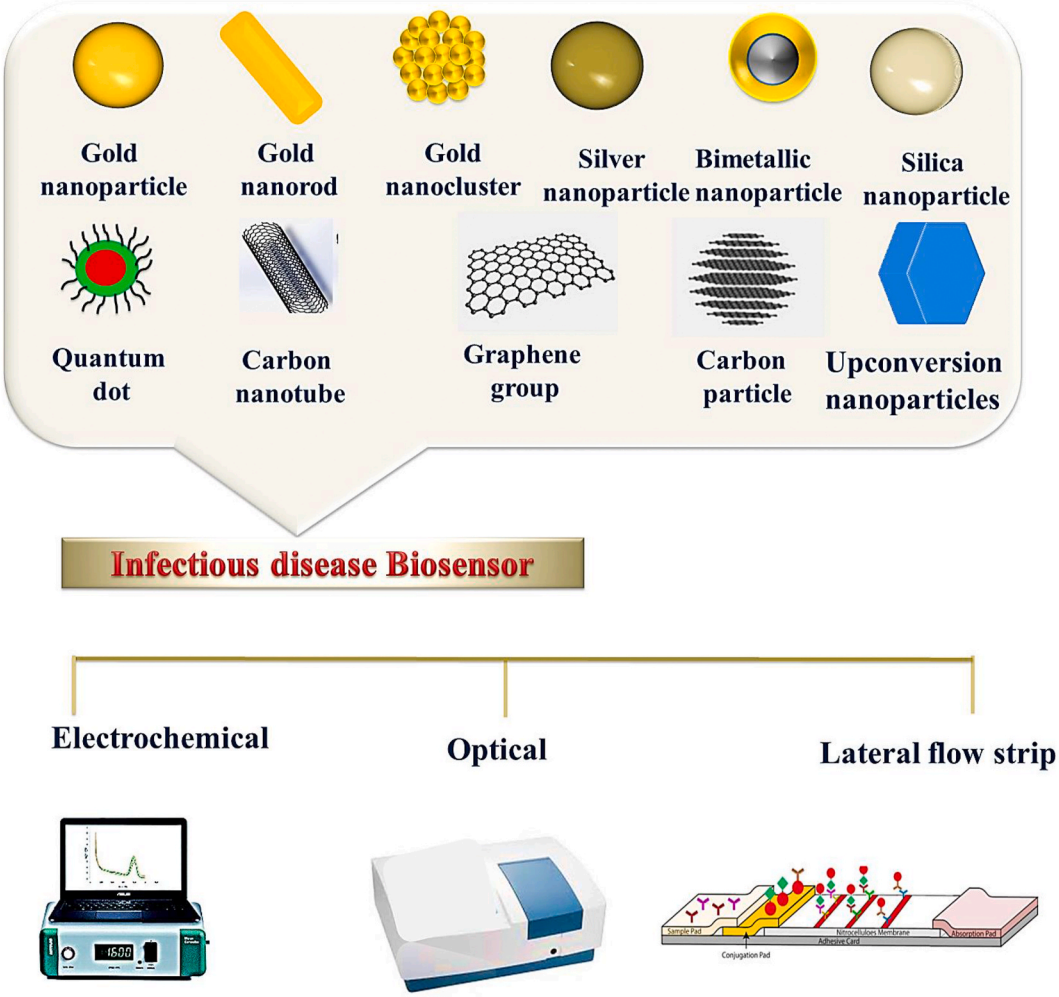

Fig. 1. Schematic of different nanomaterials and biosensors used in detection infectious disease.

nanoparticles with solid or porous structures can be prepared via diverse methods such as hydrothermal, sol-gel, and reverse emulsion [70]. Silica nanoparticles can be further modified with organic dye which leads to rich color particles [71]. SiNPs are characterized by high stability, biocompatibility, chemical inertness, large surface area, transparency, and easy functionalization using silane chemistry [72,73]. Besides, silica can be used as a protective and stabilizing layer of magnetic nanoparticles or noble metal particles. Silica covering of gold particles is usually carried out with the Stöber method allowed thickness control with adjusting reaction time and reagent concentration [73]. A schematic of nanoparticles which are described in this section and the applied biosensors is illustrated in Fig. 1.

3. Biosensors for infectious disease based on nanomaterials

3.1. Electrochemical biosensors

Electrochemical detection methods are widely used because of their easy procedure, high sensitivity, and ready to scale down for portable applications [74,75]. Also, screen printed technology facilitates the large scale fabrication of portable, low-cost analytical systems that can operate with small sample volume [76]. Nanomaterials have found extensive application in electrochemical sensors ranging from analyte separation/concentration (e.g. magnetic particle [77–90]) to the catalyst of redox reactions [23,90–102], enhancer of electrodes' surface conductivity [24,103], to grafting elements for efficient loading of biomolecules [79,93,104], as well as excellent sensitivity that achieve with QDs [105–108].

Magnetic beads are commonly used in rapid assays to capture the targets from crude samples before detection [15]. The use of these not only allows to pre-concentrate the analyte (e.g. biomarkers) but also to reduce interferences that lead to an increase in the sensitivity and specificity of the sensors. Importantly superparamagnetic properties of magnetic nanoparticles allow their re-dispersion, with limited/no agglomeration, in the absence of the magnetic field. The surface of MNPs can be easily engineered, using specific coating providing in this way an appropriate functional group for the immobilization of biomolecules; furthermore, it has been shown that immobilization of biomolecules reduces their biodegradation when in contact with complex environmental or biological systems [78,90].

Electrochemical immunosensors have been effectively used for the detection of pathogens [78,90,91] due to simple handling methods, high sensitivity, and good applicability in real samples. Moreover, the sandwich assay enables the construction of a more specific and sensitive immunosensor in comparison to direct detection [23].

Fei et al. reported on the preparation of Fe_3O_4/SiO_2/AuNPs and their application in electrochemical immunosensing. Fe_3O_4-NPs were prepared using the co-precipitation method; these, following capping with SiO_2 and pre-functionalization with 3-Mercapto-propyltriethoxysilane (MPTES), were coated by AuNPs that served as anchoring element for *S. pullorum* and *S. gallinarum* antibodies. *S. pullorum* and *S. gallinarum* in the sample were captured by the Fe_3O_4/SiO_2/AuNPs and separated from the samples by applying an external magnetic field. Au-Nps/Fe_3O_4NPs with carrying bacteria, re-dispersed in buffer solution contained

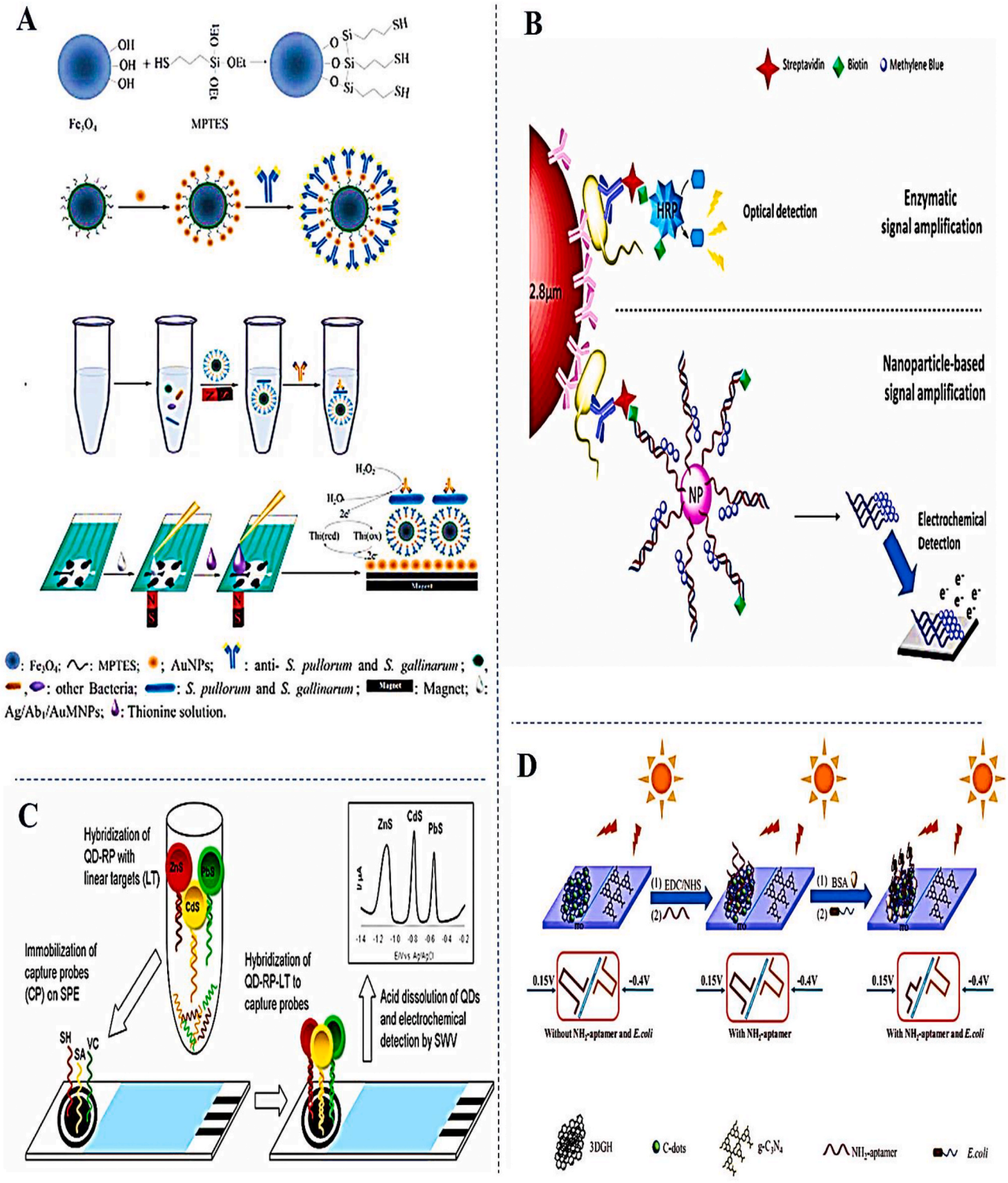

Fig. 2. A) Schematic diagram of the synthesis process of the Fe_3O_4/SiO_2 nanoparticle, immobilization antibody, capturing *S. pullorum and S. gallinarum* from sample, sandwich complex dropped on AuNPs/4-SPCE electrode with permission ref [90], B) Presentation of the assay with enzymatic amplification colorimetric detection and nanoparticle-based amplification and electrochemical detection with permission ref [15] C) Biosensor with npcRNA for simultaneous detection of three pathogens with permission of ref [105] D) Ratiometric photoelectrochemical aptasensor with permission [119].

horseradish peroxidase (HRP) labeled anti-*S. pullorum* and *S. gallinarum* to form a sandwich complex. The sandwich complex was dropped on 4-channel screen-printed carbon electrode already modified with electrodeposited AuNPs and supplied with a magnet, followed by the addition of thionine and hydrogen peroxide. To detect *S. pullorum* and *S. gallinarum* the reduction peak current change of the CV before and after reaction of HRP with hydrogen peroxide was recorded. The antibody immobilized efficiently on the Fe_3O_4/SiO_2/AuNPs surface and 93.95% of the electrode signal was maintained after 30 days of storage indicated the ability of Fe_3O_4/SiO_2/AuNPs to retain the bioactivity of the adsorbed antibody [90]. The schematic of this procedure is depicted in Fig. 2A. Wang et al. [80]developed a portable electrochemical system,

based on a personal glucose meter (PGM), for detecting *E. Coli O157: H7* and *S. aureus*. In the reported work glucoamylase-quaternized magnetic nanoparticles (QMNP) were used to capture and detect bacteria, via a competitive mechanism. Following the capture of bacteria, via electrostatic interaction, on the positively charged QMNPs nanoparticles, Glucoamylase was released to the solution; this was then used to catalyze the hydrolysis of amylose, added in the solution into glucose which was then detected by PGM. QMNPs also prevented the growth of the bacteria which led to killing and monitoring pathogens at the same time [80]. Luo et al. used PGM to develop a rapid, portable, and sensitive immunosensor for *S. pullorum* and *S.gallinarum*. In this work capture of pathogens, performed using MNP-antibody, was followed by the introduction of an enzymatic label (antibody- SiNps-glucose oxidase (GOx). The so generated sandwich system, following magnetic capture and cleaning, was dispersed in a glucose solution. Glucose concentration monitoring before and after hydrolysis of glucose by GOx revealed that the reduction in glucose concentration was proportional to the logarithm concentration of bacteria. The immune nanoparticles used in this work were shown to retain their activity after storage at 4 °C for at least 90 days [109].

Oxidoreductase Enzymes, like Horseradish peroxidase (HRP), are generally used in immunoassays to improve signal and reduce noise. Nanoparticles with peroxidase-like activity (e.g. Au@Pt bimetallic nanoparticle) are an attractive alternative to enzymes in immune assays resulting in more stable and cost-effective sensors [79,92]. For example, Zhu and coworkers fabricated two sandwich-type immunosensor with Fe_3O_4@SiO_2-Ab1/*E.coliO157: H7*/rGO-NR-Au@Pt-Ab2s for *Escherichia Coli O157: H7* detection [78,79]. One of the immunosensor utilized HRP [78] while the second one used Au@Pt nanoparticles instead of the enzyme [79]. The non-enzymatic system could reach a LOD of 4.5×10^2 CFU mL^{-1} and a linear range of 4×10^3 to 4×10^8 CFU mL^{-1}; while the enzyme-based system was linear in 4×10^2 to 4×10^8 CFU mL^{-1} concentration range with a LOD of 91 CFU mL^{-1}. Besides, 91.0% of the initial response was retained after 5-weeks' storage of the Non-enzymatic electrode. Mo et al. also demonstrated the ability of non-enzymatic labels, reduced graphene oxide –natural red -Au@Pt, to retain their activity (85.46% of the initial signal) even after ten weeks of storage [92].

Gold nanomaterials have been widely used in electrochemical sensors due to biological compatibility, electrical conductivity, the high surface-to-volume ratio [22]. Moreover, gold nanomaterials can effectively couple with other nano/materials to produce various Au-based nanocomposites biosensor like poly(diallyldimethylammonium chloride)-functionalized graphene oxide and AuNps [98] chitosan/MWCNT/Polypyrrole/AuNPs [24] rGO/AuNR/poly thionine [110] to develop new electrochemical sensors with improving sensitivity, selectivity, and stability.

Xiang et al. developed a sandwich electrochemical immunosensor for the detection of *Salmonella* based on AuNPs dispersed in oxidized chitosan film on a glassy carbon electrode surface. In the reported work the presence of AuNPs in the film provided a more conducive platform for the immobilization of antibody, improved the catalytic activity of film for H_2O_2 reduction and the immobilized HRP-antibody structure preserve high catalytic activity on the biocompatible substrate. The developed sensor presented good selectivity and reproducibility with higher sensitivity when compared to the sensor based on pure chitosan film [111]. Lin et al. compared two impedimetric biosensors, based on self-assembled thiolated protein G, which was used for oriented immobilization of goat anti - *E. coliO157: H7 IgG* using a bare gold electrode and gold nanoparticles modified electrode. Thiolated protein G was applied on the gold electrode surface while for the AuNP modified electrode, the gold electrode surface was first modified with a layer of 1, 6-Hexanedithiol, then colloidal AuNPs and thiolated protein G were applied on the surface. The AuNPs modified electrode was shown to have 2.2 times larger active area and a LOD 48 CFUmL^{-1} for detection *E. Coli O157: H7* which is 3 times lower than those recorded for the bare gold electrode [94]. Lin et al. reported on a regenerable and sensitive impedimetric immunosensor for the detection of type 5 adenovirus; the sensor was based on a multi-layered architecture assembled onto the surface of an Au electrode. The Au electrode was coated with AuNPs, grafted onto the sensor surface via 1, 6 hexane dithiol layers. 11-mercaptoundecanoic acid was then self-assembled on the sensor surface to attach monoclonal anti-adenovirus-5 antibodies. Regenerating the surface was carried out by applying a constant negative potential that could clean the gold electrode surface completely and enable the reuse of the electrode [95]. Ariffin and co-workers reported on ultrasensitive *E. coli* DNA biosensor based on a screen-printed carbon paste electrode modified with colloidal AuNPs and aminated hollow silica spheres (HSiSs) respectively. HSiSs was non-conductive and AuNps promote the electron transfer from the intercalated DNA hybridization redox label to the SPE surface. HSiSs was treated with glutaraldehyde before attachment of aminated DNA. The sensor was able to detect target DNA in the 1.0×10^{-12} μM -1.0×10^{-2} μM concentration range, with a low LOD of 8. 17 $\times 10^{-14}$ μM via the DPV method; these performances were ascribed to the high loading of DNA probes taking place on the inner and outer surface of hollow silica, and to the conductivity increasing effect of AuNPs [96]. Bonnet and co-workers reported on a nanoparticle sandwich immunoassay based on the boron-doped diamond electrode for *E. coli* detection in platelet lysate. The system was based on solid-phase oligodeoxyribonucleotide (ODN) synthesis on nano-sized silica particles which was immobilized on micrometric silica beads. The nano-micro structures retained on the DNA synthesis column and ODN could synthesize on the silica nanoparticles with OH group via phosphoramidite chemistry. Then ODN-functionalized nanoparticles hybridized with methylene blue DNA probes. The methylene blue -ODN-functionalized nanoparticles were released from micrometric silica beads and used in the detection procedure. Capturing bacteria from the platelet lysate with antibody functionalized magnetic beads, followed by the formation of a sandwich complex by the second antibody with the streptavidin group. Then above mentioned methylene blue-ODN-functionalized silica nanoparticles, carried out the biotin group, coupled with sandwich structure via biotin/streptavidin chemistry. In the last step, the magnetic beads were suspended in RNase free water and the methylene blues labeled oligonucleotides were released. The boron-doped diamond electrode surface was grafted with a 4-aminobenzyl amine to produce a cationic surface. Then released methylene blue-labeled oligonucleotides were deposited on the surface while negative potential applied for electrostatic attachment. The square wave method was applied to detect the different concentrations of *E.coli.* The proposed system could achieve detection of 10–100 CFU mL^{-1} *E.coli* in platelet concentrates; this was 3 orders of magnitude more sensitive than the assay without nanoparticles. Moreover, the electrochemical system could provide 10 times superior LOD than that ELISA method with the same magnetic sandwich complex ELISA method which used HRP as a biocatalyst for TMB reduction [15]. The schematic of this assay is presented in Fig. 2B. DNA sensor for the invA gene of *Salmonella* was developed based on the combination of AgNCs (as a label) and cysteine-rich DNA reporting probes. Hybridization of target DNA and reporting DNA probes with the capture probe immobilized on AuNPs modified GCE electrodes resulted, following growth of the AgNCs (at the cystine groups of the reporting probes), in a clear DPV signal (oxidation of Ag). The sensor was demonstrated to have a linear response to DNA target concentration in a wide range between 1 fM and 0.1 nM with a LOD 0.162 fM [97]. Fei et al. reported on an immunoassay for the detection of *S. pullorum* and based on the combination of magnetic concentration and NP signal generation; more specifically AuNPs were used as redox labels in replacement of more conventional enzymatic labels. Fe_3O_4/SiO_2/antibody1 captured *S.pullorum* from sample solution. After magnetic separation, the formed complex was incubated with/Ab_2/AuNPs/rGO to produce a sandwich structure. The sandwich structure was dropped on the 4-SPCE electrode surface while applying magnet below the electrode. To generate an electrochemical signal

AuNPs were per-oxidation, by applying a constant potential followed by a DPV scan to reduce the in-situ generated $AuCl^{-}{}^{4}$ to Au^{0}. The recorded DPV signal correlated with the log CFU concentration of the bacteria and the system showed a LOD of 89CFU mL^{-1} [77]. Nanocomposite of poly (diallyldimethylammonium chloride) graphene oxide (GO-PDDA) and AuNPs was reported in the manufacturing of an immunosensor for the detection of *E.coli DH5 α* in the dairy product. The nanocomposite was shown to provides a superior microenvironment for the immobilization of the antibody and 51.7% and 82.9% signal enhancement was achieved in comparison to sensor containing only GO or AuNPs. The sensor was shown to present a LOD 35 CFU mL^{-1} [98]. Valipour and Roushani investigated the application of AgNPs and thiol graphene quantum dot (AgNPs/GQD-SH) in the development of an immunosensor for the detection of hepatitis C virus core antigen. In the proposed sensor, the glassy carbon surface was first modified with the GQD-SH solution, and then AgNps were attached via thiol groups of the GQD-SH/GCE surface. The antibody was immobilized on AgNps by chemisorption between AgNps and an amino group of anti-HCV core antigen. The electrochemical response was generated by the DPV monitoring of a redox probe (riboflavin). DPV currents decreased with the increase of the concentration of the antigen; The system was show to allow to detect 3×10^{-12} g L^{-1} of the hepatitis C virus core antigen with a broad linear range of 5×10^{-11}-6×10^{-5} g L^{-1} [112].

Pandey et al. proposed the use of a gold electrode decorated by reduced graphene oxide wrapped copper oxide and cysteine, in the development of *E. coli O157: H7* immunosensor. Cysteine was used for the attachment of nanocomposite to the gold surface through the SH group and also as a green route for synthesis rGO. Antibody covalently bond via N-(3-dimethylaminopropyl)-N′-ethyl carbodiimide hydrochloride (EDC)/N-hydroxysuccinimide (NHS) coupling reagent through the carboxylic acid functional group of rGO. The presence of the Cu in the composite was shown to improve the LOD and sensitivity (slope of the calibration curve) of the sensor due to inducing stronger interactions between GO and Cysteine [113].

Bhardwaj et al. fabricated a paper-based electrochemical immunosensor that used carbon paste as a working electrode for the detection of *S. aureus*. EDC/NHS chemistry was utilized to activate carboxylic acid groups on the SWCNT surface and immobilization of the antibody, then SWCNT-antibody solution-dropped on the carbon paste surface. The DPV response of the sensor was shown to increase with the increase of the concentration of the bacteria; accordingly, to the authors, these results could be associated with three mechanisms: a) deficiency in antibody monolayer coverage as a result of bacteria binding, b) extracellular electron transfer of bacteria with redox mediator in solution and Ab-SWCNT, c) the presence of sodium ion on the bacteria cell wall [114]. Carboxylate graphene nanoflakes, prepared from MWCNT with wet chemical methods, were electrophoretically deposited on ITO coated glass substrate, and the so prepared surface used for the manufacturing a DNA sensor for the detection of a nucleic acid of *Escherichia coli O157: H7*. The developed genosensor presented higher sensitivity, ca. 2 order of magnitude when compared with resembling rGO counterpart sensor [115]. A dual aptamer sandwich complex consisting of a primary biotinylated aptamer (immobilized onto streptavidin magnetic bead) and a secondary aptamer conjugated with AgNPs was reported for the detection of *S.aureus*. The formed MB-Apt1/*S.aureus*/Apt2-AgNPs sandwich was collected and transferred in HNO_3 solution (0.1 M) were AgNPs were dissolved to Ag^{+}. The reduction of the formed Ag^{+} was used as the analytical response of the sensor. Ag reduction signal was shown to be linear concerning *S.aureus* log concentration ($10–10^{6}$ CFU mL^{-1}); the sensor was reported to present a LOD of 1 CFU mL^{-1} [116].

A Nanoporous gold structure was manufactured on a glassy carbon electrode by the combination of electrodeposition of Au-Cu alloy and selective dealloying of Cu from the previous deposited film. The so prepared nanostructured surface was used, following attachment of thiolated *S. Typhimurium* aptamer on the surface, for the development of an impedimetric bacteria biosensor. The proposed sensor was shown to present significant improvement, when compared to the planer Au electrode, in aptamer loading and surface stability. The aforementioned aptasensor was shown to present a low detection limit and excellent selectivity toward other bacteria and was demonstrated in the detection of *S. Typhimurium* in egg and rotten egg samples [99]. QDs embedded metal-organic framework (ZIF-8) particle were designed as signal-amplifying tags for the ultrasensitive and specific detection of ^{1}*E. Coli O157: H7*. (CdS/ZIF-8) particles were modified with polyethyleneimine to introduce amino groups on their surfaces, before reaction with glutaraldehyde for immobilization *E. coli O157: H7* antibody (CdS@ZIF-8/PEI/Ab). Glassy carbon electrode which was modified with p-aminobenzoic acid utilized to immobilize antibodies via EDC/NHS chemistry. The prepared electrode was incubated with bacteria and CdS@ZIF-8/PEI/Ab to form a sandwich complex on the electrode surface. Electrochemical detection of pathogens was made possible by the releasing of the Cd (II) ions from the CdS/ZIF-8 in HCl solution followed by their quantification via DPV. A LOD of 3 CFU mL^{-1} and a wide linear range $10–10^{8}$ CFU mL^{-1} were reported; the sensor was also shown to be ca. 16 times more sensitive than the sensor using the CdS QD due to the large number of QD encapsulated in the MOF structure [117].

Vijian et al. reported on the multiplex detection of *Vibrio cholera*, *Salmonella sp*., and *Shigella sp;* in the reported work QDs (PbS, CdS, or ZnS) modified specific reporting probes were used to provide specificity to the sensor (QD-RP). Two hybridization strategies, the step-by-step and premix sandwich hybridization methods were applied for single and multiple pathogen detections. Premix sandwich hybridization methods had better results. For this strategy denaturing the PCR product of Non-protein coding RNAs (npcRNA) with different concentrations of three pathogens, were incubated with QD-RP conjugates. Then, Non-protein coding RNAs (npcRNA) QD-RP, one for each targeted DNA, were applied on SPE modified with a capture probe, followed by, QDs dissolution (using HNO3) and voltammetric detection, via SWV, of released Zn^{2+}. $Cd^{2+}$and Pb^{2+}ions. Voltammetric detection of the heavy metal ions was made possible by the in-situ formation of a bismuth-film electrode. The prepared sensor presented the excellent LOD values of 22 aM (*Salmonella sp*.), 34aM (*Salmonella sp*.) and 42aM (*Shigella sp*) for single pathogen detection, and 51aM (*Salmonella sp*.), 53aM (*Salmonella sp*.), and 38aM (*Shigella sp*) for multiplex pathogen respectively [105]. The schematic of this procedure is illustrated in Fig. 2C.

Electrochemiluminescence aptasensor for the detection of *E.coli* using AgBr nanoparticles/3D nitrogen-doped GO hydrogel (AgBr/3DNGH) nanocomposite as the catalyst to enhance the electrochemiluminescence (ECL) of luminol was reported by Hao et al. Luminol was mixed with the AgBr/3DNGH before apply on the glassy carbon surface. The glassy carbon surface is then modified with a chitosan layer and aminated aptamer respectively. After capturing *E.coli* to the surface, ECL intensity was shown to decrease linearly in the 0.5–500 CFU mL^{-1} dynamic ranges; the sensor showed a LOD of 0.17 CFU mL^{-1}. The introduction of nitrogen in the GO structure was shown to improve the catalytic ability of the AgBr/3DGH composite; furthermore, the combination of AgBr and 3DNGH presented significantly improved catalytic performances when compared to the single material system [118].

A glassy carbon electrode was modified with electrodeposited Graphene oxide and decorated with $CdTeQDs_{551}$-capture DNA_{HBV} and $CdTeQDs_{607}$-capture DNA_{HCV} was used for the detection of HBV and HCV virus, followed by hybridization with the target probe. In the proposed biosensor AuNP-modified reporting probes, specific for the viruses were used as signal generation element. Virus detection was based on the ability of the AuNPs present in the specific reporting probes to quench the electrochemiluminescence of the CdTe QDs in an unreacted capture probe. The unreacted capture probe decreased with increasing concentration of target probe so the ECL signal was raised with increasing concentration of target probe in the range 0.0005–0.5 nmol L^{-1} and 0.001–1.0 nmol L^{-1} with LOD of 0.082 and 0.34 pmol L^{-1} for Hepatitis B and Hepatitis C virus respectively [106]. Hua and co-workers developed a sensitive potentiometric resolved ratiometric

Table 1
Electrochemical biosensors List of Abbreviation, Amperometry (AM), Antibody (Ab), (Aptamer (Ap), Au Nanoparticle citrate synthesis(AuNPsC), Biomolecule(Bio), Cyclic voltammetry (CV), Differential pulse voltammetry (DPV), Differential pulse anodic stripping voltammetry (DPASV), Electrochemiluminesense (ECL), Electrochemical Impedance Spectroscopy (EIS), Electropolymerized Au nanoparticle(AuNPsE), Horseradish peroxidase (HRP), Linear sweep voltammetry (LSV), Potentiometry (PT), Personal glucose meter(PGM), poly(diallyldimethylammonium chloride (PDDA), Square wave voltammetry (SWV), Square wave voltammetry anodic stripping voltammetry (SWVAW) [189–247].

Nanomaterial	Nanomaterial remark	Bio	Pathogen	Method	Linear range	LOD	Remark	Real sample	Ref
$AuNPs_E$	AuNPs 25nm, Ab attachment & enhancement of current of redox peak. Electrodeposited AuNPs coated electrode surface more uniformly & strongly	Ab	*S.pullorum & S.Gallinarum*	CV	10^4-10^9 CFU mL^{-1}	3.0×10^3 CFU mL^{-1}	Selective, Stable, Activity of Ab enhanced by Ionic Liquids as electrode modifier.	Egg Chicken Meat	[23]
$AuNPs_E$, $AuNPs_C$, Fe_3O_4/SiO_2/AuNPs	AuNPs 25nm Enhancement electrochemical signal & attachment to Fe_3O_4/SiO_2– SH Np with SH group Fe_3O_4MN co-precipitation method Fe_3O_4/SiO_2/AuNPs 250 nm	Ab	*S.pullorum & S.Gallinarum*	CV	10^2 -10^6 CFU mL^{-1}	3.2×10^2 CFU mL^{-1}	Selective, 4-SPCE reduced the detection time & improves the reproducibility, Increase sensitivity by MNP	Chicken	[90]
GO-PDDA@AuNP	GO-PDDA@AuNP nanocomposites biocompatible& enhance electrochemical signal, $AuNPs_C$ 18nm, , Ab-Au-Thionine 108% increase in comparison with Ab-Thionine	Ab	*E. Coli (DH5α)*	CV	50 -5.0×10^6 CFU mL^{-1}	3.5×10^1 CFU mL^{-1}	Selective, Stable, Non- enzymatic, 90.8% of the response remained after 15 days	Fresh milk Yogurt Expired yogurt	[98]
Chitosan MWCNT Polypyrrole AuNPs	AuNPs increase the conductivity of the film	Ab	*E. Coli O157: H7*	CV	3×10^1 -3×10^7 CFU mL^{-1}	3×10^1 CFU mL^{-1}	Specific, Disposable, 89.3% of signal remained after 2 weeks	-	[24]
rGO-NR-Au@Pt Fe_3O_4@SiO_2	Highest Reduction peak current when Pt/Au molar ratio is 1:1	Ab	*E.coli O157: H7*	CV	4.0×10^2 - 4.0×10^5CFUmL^{-1}	91CFUmL^{-1}	Specific, Non- enzymatic 91.0% response remained after 5 weeks.	Pork Milk	[78]
rGO-NR-Au@Pt Fe_3O_4@SiO2	Au@Pt 30 nm, Fe_3O_4@ Solvothermal method 200 nm, Silica shell 30 nm Stöber method, Magnetic separation achieved in 10 seconds, rGO increase redox current	Ab	*E.coli O157:H7*	CV	4×10^3-4×10^8 CFU mL^{-1}	4.5×10^2 CFU mL^{-1}	Specific, Au@Pt good peroxidase-like catalytic activity, Non- enzymatic 91.0% response remained after 5 weeks.	Pork Milk	[79]
rGO-NR-Au@Pt PANI $AuNPs_C$	AuNPs work as a linker between PANI & Ab The AuNPs increase signal	Ab	*E.coli O157: H7*	CV	8.9 $\times10^3$- 8.9 $\times10^9$ CFU mL^{-1}	2.84×10^3 CFU mL^{-1}	Specific, Non-enzymatic, Regenerable up to 5 times, 85.46 0% responses remained after 10 week.	Milk & pork	[92]
Functionalized -MWCNT-Chit@Th	Thionine dye (Th) immobilized on functionalized-multi-walled carbon nanotube chitosan composite	Ab	*Uropathogenic E. coli*	CV	10^2-10^9 CFU mL^{-1}	50 CFU mL	Selective, Easy preparation	Urine	[189]
Silica Np	Silica nanoparticle make quantitative measurement applicable	Ab	*E.coli*	CV	10^5-10^8 CFU mL^{-1}	10^3 CFU mL^{-1}	Fast, Easy	-	[190]
rGO–AuNPs –Ionic liquid	Electrochemical synthesis of rGO & AuNPs simultaneously. The composite showed better current response. AuNPs 100nm	Ab	*E. Sakazakii*	CV	10^3-10^9 CFU mL^{-1}	1.19×10^2 CFU mL^{-1}	Selective, RSD 6.2% n=7 3.9% signal change after 4 weeks.	Infant milk	[91]
$AuNPs_C$–coated with reduced GO oxide, Fe_3O_4/SiO_2	AuNPs & rGO simultaneously synthesised by citrate, $AuNPs_C$ 25nm capture Ab, rGO improve the peak current of the electrode, Fe_3O_4 magnetic co-precipitation	Ab	*S. Pullorum*	DPV	10^2- 0^6 CFU mL^{-1}	8.9×10 CFU mL^{-1}	Selective, Non – enzymatic, AuNPs label signal	Chicken liver	[77]
GO/Au composite	AuNPsC 30 nm prepared in-situ in Go solution the intrinsic characteristics of GO preserved, Carboxyl groups in GO stabilizes the newly formed Au nanoparticles	Ab	*C. sakazakii*	DPV	2.0×10^2–2.0×10^7 CFU mL^{-1}	2.0×10^1 CFU mL^{-1}	Specific, Synthesis of new antibody, Stable, 90% signal remained after 3weeks	Powdered infant formula	[191]
Composite rGO/Thionine/ AuNPs	$AuNPs_E$ Composite formed with mixing rGO, Thionine & AuNPs. Thionine with positive charge linking between rGO & AuNPs	Ab	*C. sakazakii*	DPV	8.8×10^4- 8.8×10^8 CFU mL^{-1}	1×10^4 CFU mL^{-1}	Selective, 86.8% of the initial response remained after 30 days.	Infant milk powder Milk	[192]
Chitosan-AuNP composite film	$AuNPs_C$ AuNPs/Chi has very good conductivity & demonstrates excellent electron-transfer ability. The optimum ratio of AuNPs/Chi is 1.	Ab	*Salmonella*	DPV	10 - 10^5 CFU mL^{-1}	5 CFU mL^{-1}	Selective, Simple fabrication	Tap water, Milk	[111]
AuNPs	$AuNPs_C$	Ab	*Salmonella*	DPV	100 - 700 Cell mL^{-1}	100 cells mL^{-1}	Fast, Low cost, disposable, Non-enzymatic	Skimmed milk	[193]
SWCNT	Peak current increased following the deposition of SWCNTs	Ab	*S. aureus*	DPV	10^1-10^7 CFU mL^{-1}	15, Milk 13 CFU mL^{-1}	Low cost, RSD 10.5% after 5 weeks	Milk	[194]
PANI Coated MNP AuNPs	γ -Fe_2O_3 solvothermal method nanoparticle core is 20 nm PANI-coated MNPs50 to 100 nm. AuNPs prepared in Alkaline solution with a dextrin capping agent.	Ab	*E.coli O157:H7*	DPV	10^1- 10^6 CFU mL^{-1}	10^1 CFU mL^{-1}	Detection based on AuNPs signal	-	[81]
AuNR@SiO_2	AuNRs with seed-mediated method AuNR@ SiO_2, AuNRs 10 nm in mean diameter & about 40 nm in length	Ab	*E.coli*	DPV	1.0×10^2–5.0×10^4CFU mL^{-1}	60 CFU mL^{-1}	Selective, Better LOD with AuNRs, 2% current response after 2 weeks.	Fresh milk Yogurt Expired yogurt	[195]
rGO/polyetheyleneimine	Electrodeposition rGO/PEI, rGO/PEI film formation cause a significant increase in redox current	Ab	*E. coli UTI89*	DPV	10^1 -10^4 CFU mL^{-1}	10^1 CFU mL^{-1}	Sensitive, 2.8 % loss peak current after 2 weeks storage	Urine Human serum	[196]
PPy-rGO/AuNPs	Deposited PPy on GO Surface prevent aggregation	Ab	*E. coli K12.*	DPV	10^1- 10^7	1.0×10^1	Selective, 8.8% signal decrease after	Water	[197]

PPy@Fc/AuNPs	of the GO& 6 times increase in surface area, $AuNPs_C$ 10 nm, GO & rGO decrease charge transfer resistance	b		V	CFU mL^{-1}	CFU mL^{-1}	40 days	Milk	
Sulfonated rGO-PEDOT-AuNPs	AuNPs composites effectively facilitated the electron transfer, AuNPs 13 nm	A b	*E. Coli O157: H7*	DP V	7.8×10^{1}–7.8×10^{6} CFU mL^{-1}	3.4×10^{1} CFU mL^{-1}	Specific, 92% of its initial response after 2 weeks	Spring water Milk	[198]
Poly(amidoamine) dendrimer-(PAMAM)encapsulated AuNPs/ CNT	AuNPs 3nm, $HAuCl_4$: PAMAM ratio 55:1 the best ratio, Ab-CNT-HRP showed better DPV signal rather Ab- HRP, CNT –COOH 30nm	A b	*E.coli*	DP V	10^{2}- 10^{6} CFU mL^{-1}	5.0×10^{1} CFU mL^{-1}	Selective, 90.2% signal after 5 assay Milk Infant milk Powder Yogurt Expired yogurt		[199]
AuNPs enclosed PANI	AuNPs 10nm prepared with mixing aqueous aniline & $HAuCl_4$ solution (353 K)	A b	*E. Coli O157: H7*	DP V	10^{0}- 10^{6} CFU mL^{-1}	300 cell mL^{-1}	Specific	Beef	[200]
CdS quantum dots-encapsulated metal-organic frameworks as	DPV signals are amplified greatly by using CdS/ZIF_8, CdS/ZIF_8, with regular rhombic do-decahedron shape & an average diameter of 670 nm.	A b	*E. coli O157: H7*	DP V	10 to 10^{8} CFU mL^{-1}	3CFU mL^{-1}	Selective, ,16 times increase in CdS@ZIF-8 sensitivity rather than conventional sensor using CdS QDs,	Milk	[117]
$AuNPs_{S}$,C60@AuNPs,CdS & PbS nanoparticle	$AuNPs_{E}$ CdS 4nm PbS 10nm	A b	E.coli O157: *H7* & *V.cholerae O1*	DP V	5×10^{1}- 1×10^{6} CFU mL^{-1}	32CFU mL^{-1}	Selective, Simultaneous detection	Stool water	[201]
Mesoporous graphitic-C_3N_4	mpg-C_3N_4 has lower resistance than the bulk g-$C_3N_4$12-nm used SiO_2 particle as a hard templet	A b	*Avian leukosis viruses J*	DP V	$10^{2.08}$-$10^{4.0}$TCID50 mL^{-1}	120 TCID50 mL^{-1}	Specific, 90.75% signal remained after 14 days	Normal avian serum	[202]
AuNPs-rGO-Chitosan, AgNPs-rGO	Au^{3+} & Ag^{+} reduced to AuNPs by chitosan at 80º C.	A b	*Avian influenza virus H7*	LS V	1.6×10^{-9}-1.6×10^{-5} g L^{-1}	1.6×10^{-9} g L^{-}	Selective, 91.2% signal retained after 30days	-	[203]
MNB	Superparamagnetic amino magnetic beads 200nm	A b	*Avian influenza A (H7N9) virus*	LS V	1×10^{-8}–2×10^{-5} g L^{-1}	6.8×10^{-9} g L^{-1}	Bi-MBs increase the detection signal 4 times.	Skim milk	[204]
GO-COOH MWCNT SiO_2Np Chitosan	SiO_2Np Sol-gel method, MWCNT significantly improve the electron transfer	A b	*HIV p24 Virus*	DP V	$5.\times 10^{-10}$–8.5×10^{-6} g L^{-1}	1.5×10^{-8} g L^{-1}	93.45% - 87.56% initial signal after 15 & 30 day	Human plasma	[205]
Go	Go–methylene blue & chitosan	A b	*HA proteins of H5N1 & H1N1*	DP V	2.5×10^{-11}- 5×10^{-10} mole L^{-1}	8.3×10^{-12} mole L^{-1}	Dual sensor, Rapid response time, Simple fabrication	-	[206]
AgNPs GQD-SH	$AgNPs_C$ 13 nm, Graphene quantum dot-SH prepared from MWCNT & cystamine	A b	*Hepatitis C virus core antigen*	DP V	5×10^{-11}-6×10^{-5} g L^{-1}	3×10^{-12} g L^{-1}	90% signal remained after 20 days	Human serum	[112]
Fe_3O_4.COOH, AuNPs	MNP 180 nm $AuNPs_C$ 20nm	A b	*L.monocytogenes*	EIS	3.2×10^{2}–3.2×10^{4} CFU mL^{-1}	3.2×10^{2} CFU mL^{-1}	Selective, 95% separation efficiency due to MNP, Microelectrode reusable 50 time	Lettuce sample	[207]
Iron/gold core/shell &CdSe nanocrystals	Magnetic iron thermal decomposition method 10 ±3 nm & 15±3 nm due to the gold coating	A b	*Salmonella Typhimurium*	PT	10^{2}-10^{7} Cell mL^{-1}	20 cells mL^{-1}	Rapid, Easy to perform	Bovine milk	[208]
Fe_3O_4@poly(dopamine)	Fe_3O_4 co-precipitation, Quasi-spherical with magnetic core 12nm, & 4nm polymeric layer,	A b	*L.pneumophila*	AM	10^{4}-10^{8} CFU mL^{-1}	1×10^{4} CFU mL^{-1}	Selective, 30-day stability	Water	[209]
Magnetic bead AuNPs	Magnetic bead 150 nm coated with GOx & dopamine (PMNCs), PMNCs capture 89% or bacteria cells in the range of 10^{2}- 10^{5} AuNPs glucose reduction method	A b	*E.coli O157: H7*	AM	10^{2}-10^{6} CFU mL^{-1}	5.2×10^{1} $CFUmL^{1}$	Specific, Green synthesis AuNPs Ground beef 10^{3}-10^{6} $CFUg^{-1}$LOD of 190 CFU g^{-1}	Ground beef	[82]
AuNPs	$AuNPs_C$, superparamagnetic polystyrene beads	A b	*E. coli O157: H7&S. aureus*	AM	10^{2}-10^{5} CFU mL^{-1}	148 CFU mL^{-1}	Selective, Electrocatalytic properties AuNPs towards hydrogen	minced Beef Water	[210]
AuNPs, AuNPs/HRP	$AuNPs_C$ 15 nm regular shape & uniform, AuNPs increase the fixed amount of HRP & the monoclonal Ab, & promote the electron transfer between the enzyme & the electrode surface	A b	*Salmonella*	AM	10^{1}–5×10^{4} CFU mL^{-1}	5 CFU mL^{-1}	86.45% response signal after13 day, Preparation & purification of new Salmonella plasmid virulence antibody	Milk	[104]
Magnetic nanoparticle	Magnetic nanoparticle illustrated an obvious higher matrix effect & higher agglomeration effect but better LOD After 8h enrichment	A b	*Salmonella*	AM		598 for micro particle & 291 for nanoparticle CFU mL-1 LOD 0.04CFUmL^{1}(pre enriched or 8h),		Milk	[83]
SilicaNp, MNP	Antibody- MNPs co-participation method, MNPs10nm, narrow size distribution, Magnetic separation obtained in 1 min, Silica nanoparticle 50 nm inverse microemulsion	A b	*S. Pullorum S.Gallinarum*	PG M	1.27×10^{2} -1.27×10^{5} CFU mL^{-1}	7.2×10^{1} CFU mL^{-1}	Simple, Portable, Easy to use, Specific, without requiring expensive instruments, Immune nanoparticle stable for 90 days.	-	[109]
Au@Pt/SiO2 NPs Fe_3O_4NP/SiO_2	poly-(4-styrene sulfonic acid- co -maleic acid) (PSSMA) as a linker between Au@Pt & SiO_2 MNP 300 nm spherical nanocrystal solvothermal method clusters, Silica thickness 50 nm	A b	*E. coli O157: H7*	PG M	3.5×10^{2} - 3.5×10^{8} CFU mL^{-1}	1.83×10^{2} CFU mL^{-1}	Selective, Very good stability Portable, Low cost, Easy to use Ab-Fe_3O_4 @SiO_2 NPs & Ab/invertase-Au@Pt/SiO2 NPs stable for 90 days.	Milk	[84]
ST-magnetic nanobeads	Streptavidin magnetic nanobeads size 150nm	A b	*E. coli O157: H7*	PG M	10^{2}- 10^{7} CFU mL^{-1}	79 CFU mL	Selective, Portable, recoveries from 80% to 94.8% Portable	Milk	[85]

Fe_3O_4	Hydrothermal, MNPs 200 nm are regular spherical particles, Good separation in a few second	Ab	*E. coli O157: H7*	PGM/ICA	2.08×10^5-2.08×10^8 CFU mL^{-1}	1.04×10^4 CFU mL^{-1}	Selective, Portable ,	Milk	[86]
Magnetic nanoparticle, Silica Np	Fe_3O_4 Co-precipitation 10nm coated with silica layer 2nm,60 s separation, SilicaNp reverse microemulsion method uniform particle 50 nm	Ab	*C.sakazakii*	PGM	9×10^2-9×10^7 CFU mL^{-1}	4×10^1 CFU mL^{-1}	Selective, Portable, 100-70% signal retained after 1- 90 days	Powdered infant milk	[87]
AuNPs	AuNPs 10nm, AuNPs enhance the transfer of electrons, The electroactive surface area of the Au NP-modified electrode2.2 times of the planar gold electrode	Ab	*Heat killed E. coli O157: H7*	EIS	10^2–10^7 CFU mL^{-1}	48for AuNPs & 140 CFU mL^{-1} planer electrode	Selective, AuNPs 3 time lower LOD	-	[94]
GO-wrapped copper oxide-cysteine	Cu-doped rGO Cysteine facilitated strong adsorption leading to faster electron transfer kinetics in comparison to that of the electrode without GO	Ab	*E. coli O157: H7 E. coli DH5a*	EIS	10^1–10^8 CFU mL^{-1}	3.8 CFU mL^{-1}	Selective, 90.2% signal remained after 40 days,8 times regeneration, Cu in composite structure increase the sensitivity & LOD	Tap Water, Juices, Skimmed milk	[113]
Streptavidin Fe_3O_4	Streptavidin Fe_3O_4 150 nm	Ab	*E. coli O157: H7*	EIS	10^4–10^7 CFU mL^{-1}	1400 cells	1400 cells in less than 1 hour.	Ground beef	[211]
G/GO	Composite of Graphene/Graphene oxide GO resulted in an enhanced conductance value.	Ab	*S.Typhimurium*	EIS	10^1-10^7 CFU mL^{-1}	10^1 CFU mL^{-1}	Specific, Using a specific antibody against specific surface antigen OmpD for the first time	Lichi & orange juices	[212]
AuNPs	AuNPs 10nm Au NPs promoted electron transfer between the electrode surface & the redox probe	Ab	*Type5 Adenovirus*	EIS	10–10^8 virus particle mL^{-}	30 virus particle mL^{-1}	Selective, Sensitive, 30 times regeneration RSD 5.1%		[95]
SilicaNps –MB-DNA	Rhodamine encapsulated in the core of SilicaNps 50 nm	Ab	*E. coli*	SWV	10^1–10^4 CFU mL^{-1}	1×10^1 CFU mL^{-1}	The Nps amplify sensitivity 1000 times compared with the assay run without NPs	Platelet concentrates	[15]
HA-NH2-CNT	Stable film	Ab	*Hepatitis B virus core protein*	SWV	1-6×10^{-6} g L^{-1}	3×10^{-8} g L^{-1}	Easy synthesis		[213]
AuNPs MNP	PANI coated MNP 50-100 nm, AuNPs-conjugated PbS nanoparticles & capture antibody	Ab	*E. Coli O157: H7*	SWASV	10^1–10^6 CFU mL^{-1}	10 CFU mL^{-1}	Optimize antibody to maintain colloid stability. 94.96% bacteria capture with MNP		[214]
Au Nanorod	AuNRs 32.8 ± 1.8 nm (length) & 6.7 ± 1.2 nm width, growth seed method, Rct sharply decreased after AuNRs deposition	T4-bacteriophages *E. coli K.12*		EIS	10^3 CFU mL^{-1}	Low cost			[215]
polyethyleneimine (PEI)-functionalized carbon nanotube	Functionalized CNT directly grown on the surface caused uniform surface deposition of oriented phage & immobilization with minimal particle aggregation.	T2-bacteriophage *E.coli B*		EIS	10^3–10^7 CFU mL^{-1}	1.5×10^3 CFU mL^{-1}	Specific, Induced immobilization methods result in 15 X higher loading of phage particles on the electrode surface		[216]

(CNTs)	Antimicrobial peptide clavanin A	*K.pneumoniae, E. faecalis, E. coli, B. subtilis*		EIS		1.0×10^2–1.0×10^6 CFU mL^{-1}	Differentiate between gram-positive & gram-negative bacteria, High sensitivity to gram-negative bacteria		[217]
AuNPs	$AuNPs_C$ 15nm	DNA probe *Vibrio cholerae*		DPV	4 to 10^3 CFU mL^{-1}	2 CFU mL^{-1}	Selective	Stool	[218]
AuNPs/hollow silica spheres	AuNPs- doped with aminated HSiSs exhibited high electron transfer performance, AuNPs for increasing the biosensor conductivity	DNA probe *E. coli DNA*		DPV	1×10^{-18}-1×10^{-8}mol L^{-1}	8.17×10^{-20}mol L^{-1}	Regenerable 4 times	River water	[96]
$AuNPs_E$, AgNCs+ AuNPsC	Peak currents increased after the electrodeposition of AuNPsE, AuNPs carried capture probe. AuNPs cause loading more sDNA, AgNCs work as the signal inducer	DNA probe PCR product of *Salmonella*		DPV	1×10^{-15}-1×10^{-11} mol L^{-1}	1.62^{-16} mol L^{-1}	DPV responses maintained 88.2% & 71.4% of its initial signal response respectively after 5 & 10 days of storage, invA gene sequence of Salmonella in PCR samples		[97]
Au nanoaggregate	AuNAs prepared at physiological pH enhance the electrochemical signal &cause high loading of the ssDNA probe. Crystallite size of AuNAs 7.9 nm & 13.5.	Salmonella specific DNA str& *S. Typhi*		DPV	4×10^{-18}-2.4×10^{-16} mol L^{-1}	Selective, stability 60 Day &reusability of 6 time, signal 8 % loss after 60 days, The electroactive area & greater for AuNAs-ITO than for bare ITO.		Urine & blood	[93]
rGO & NiO nanoparticle	Electro reduction of GO, Redox peak current increased after Go reduction on the surface, Electrodeposition of NiO nanoparticle, NiO 125 nm	Selected part *S.enteritidis* gene *s. enteritidis gene*		DPV	1.0×10^{-13} -1.0×10^{-6} mol L^{-1}	3.12×10^{-14} mol L^{-1}	Selective, 96 .3 % of the initial after 10 day PCR product of gene sequence		[219]
PPy- rGo, $AuNPs_E$, AuNPs-HRP-SA	$AuNPs_E$, $AuNP_C$ size 10 nm, Chemical reduction of GO,PPy- rGo & $AuNPs_E$ increased peak current. Signal decrease without using AuNPs	*S. Typhimurium strains invA gene S. Typhimurium*		DPV	1.0×10^{-16} -1.0×10^{-10} mol L^{-1} 9.6 -9.6×10^4 CFU mL^{-1}	4.7×10^{-17} mol L^{-1} 8.07 CFU mL^{-1}	Sensitive, Good regeneration ability 91.6 % signal after 3 cycle regeneration, 84.6% original signal after 7-day storage, PCR product of salmonella		[220]
MWCNT	More sensitive sensor with MWCNT	*DNA probe 16S rDNA for E. coli*		DPV	7-12×10^{-3} g L^{-1}	1.7×10^{-8} mol L^{-1}	Selective PCR amplified products		[221]
$AuNPsE$, $AuNPs_C$ CNT doped with polyaniline, Fullerene nanoparticle	Flower-like CNTs-PAN nanohybrids possessed large surface area, excellent electronic conductivity, & redox activity, Fullerene nanoparticle prepared by mixing poly(amino-amine)dendrimers & fullerene.	IS6110 DNA the sequence of Mycobacterium tuberculosis M. tuberculosis		DPV	1×10^{-15} - 1×10^{-8} mol L^{-1}	3.3×10^{-16} mol L^{-1}	Selective, Current response of five electrodes retained from 94.5% to 96.9% after 10 days storage	Sputume	[222]
rGO/AuNR /poly thionine	AuNRs with seed growth mediated method rGO/Au NR/PT excellent electric conducting material & accelerated the electron transfer.	DNA probe Human papillomavirus		DPV	1×10^{-15}-1×10^{-8}mol L^{-1}	4.03×10^{-14} mol L^{-1}	Selective, Sensitive, Wide linear range	Human serum	[110]

		(HPV)						
Graphene-COOH nanoflakes, rGO	COOH Graphene nanoflakes prepared from MWCNT 50nm with a wet chemical method Electrophoretic deposition of Graphene nanoflakes 2 order higher LOD than rGO, better electron transfer kinetics rather rGO	DNA probe *nucleic acid Escherichia coli O157: H7*	EIS	10^{-17}-10^{-6} mol L^{-1}	1×10^{-17} mol L^{-1}	15% Loss after the 6th cycle of regeneration, The 18% decrease in the signal response after 30 days		[115]
GO-iron oxide-chitosan hybrid nanobiocomposite	Electrophoretic deposition GO-iron oxide-chitosan monodispersed spherical shape 8 to 12 fast electron transfer kinetics	DNA probe *E.coli*	EIS	10^{-14}-10^{-6} mol L^{-1}	1×10^{-14} mol L^{-1}	Selective, 10.37, 10 % loss of the initial value after 6 cycles of regeneration &after 6-week storage		[223]
AuNPs	$AuNPs_C$ 16 nm	DNA probe, *Leishmania DNA*	Am	0.5-500 parasites mL^{-1} blood	0.8 parasites mL^{-1} blood	AuNPs primer 8 week lifetime	Dog Blood Parasite	[224]
GO-Tetracycline ZrO_2 Np	ZrO_2increased the conductivity of the electrode	DNA sample, *Mycobacterium avium subspecies paratuberculosis DNA*	EIS	6.37×10^{-15}M (2×10^{-14} g/L) $6.37\ 10^{-15}$M (20×10^{-8}g/L)	6.37×10^{-15}M (2×10^{-14} g/L)	Rapid	Faecal sample Cattle	[225]
SiNPs doped MB	Silica Np reverse microemulsion method, SiNPs/ MB 100 nm	Viral DNA, hepatitis C virus DNA	EIS	100–10^6 Copies mL^{-1}	90 Copies mL^{-1}	Selective, Regenerable, 10-day stability	Serum	[226]
QD	Quantum dot reverse micelles, the narrow absorbance peak of high mono dispersion of QDs in aqueous solution	non-protein-coding RNA, sequences npcRNA sequences of Vibrio cholera, Salmonella sp. & Shigella sp	SWASV	$1\text{-}6\times10^{-17}$	2.2×10^{-17} (VC-PbS), 3.4×10^{-17}, (SA-CdS) & 4.2×10^{-17} (SH-ZnS) mol L^{-1}	Simultaneously detection npcRNA sequences of Vibrio cholerae, Salmonella sp., & Shigella sp in the attomolar range.	PCR product	[105]
Porous AuNPs	AuNPs strongly facilitate the electron transfer & provides the higher surface roughness & the active area which higher coverage, Ag nanoplates as a template for seed-growth method 60– 110 nm diameter distribution	multi-functional DNA hemagglutinin (HA) protein Ap + HRP-DNAzyme with hemin HA protein in AIV H5N1	CV	10^{-12}-10^{-7} mol L^{-1}	10^{-12} mol L^{-1}	Selective	Chicken serum	[101]
MoS_2-rGO nanocomposite	rGO avoid restacking MoS_2 nanocomposite .	Ap *Vi polysaccharide antigen mediated detection of enteric fever*	SWV	10^{-10} -10^{-6} g mL^{-1}	10^{-10} g mL^{-1}	Selective, New aptamer	Blood, Urine	[227]

AuNPs	$AuNPs_E$ Capture probe, AuNPs increase LOD & Linear range	Ap	*S.Typhimurium*	DPV	20-2 × 10^8	16 CFU mL^{-1}	Selective	Bottled mineral water	[228]
AgNPs	AgNPs 20 nm prepared by $NaBH_4$	Ap	*S. aureus*	DPASV	10^1-10^6 CFU mL^{-1}	1 CFU mL^{-1}	Excellent sensitivity, Specific	Tap & river water	[116]
$AuNPs_C$, AgNPs Hollow gold/silver nanospheres, Ag@Au core-shell, Au@Ag core-shell, Ag/Au alloy	Ag@Au better result core enhance the physical properties & the shell offers chemical stability & biocompatibility for the immobilization of aptamers, 30 to 100 nm	Ap	*E.coli*	DPV	10^3-10^5 CFU mL^{-1}	90 CFU mL^{-1}	Comparison of different nanoparticle		[229]
AuNPs, UiO-67/GR	$AuNPs_C$,	Ap	*S.Typhimurium*	DPV	2×10^1-2×10^8 CFU mL^{-1}	5 CFU mL^{-1}	Selective, 93.1% current reserved after 15 days n=6	Milk	[230]
Nanocomposite of rGO -azophloxine	Chemical reduction of Go, GO-Ap formed by π-π stacking. Doping of rGO with AP dye improves its free charge carrier density	Ap	*S.Typhimurium*	DPV	10^1-10^8 CFU mL^{-1}	10^1 CFU mL^{-1}	Fast 5 min incubation time, Low cost, 5.1 % increase in current response after 20day	-	[54]
rGO/CNT	rGO-CNT Hydrothermal method, Hybridization of rGO with carbon nanotubes (CNT) avoid the aggregation of graphene sheets because of Working CNT as a spacer	AP	*S.Typhimurium*	DPV	10^1-10^8 CFU mL^{-1}	10^1 CFU mL^{-1}	Selective, 20-day stability,	Chicken	[231]
rGO-TiO_2	Chemical reduction of Go, Noticeable increase in current density observed after coating rGO-TiO_2 compared with rGo.	Ap	*Salmonella enterica*	DPV	10^1-10^8 CFU mL^{-1}	10^1 CFU mL^{-1}	Selective, Fast 5min incubation, Stability to 21 days, & a 10% decrease in signal after30 days.	Chicken	[232]
$AuNPs_E$, $AuNPs_C$	$AuNPs_C$ 18 nm spherical & homogeneously distributed AuNPs on the electrode surface enhanced the peak current 2 times	Ap	*Salmonella*	DPV	2×10^1-2×10^6 CFU mL^{-1}	20 CFU mL^{-1} 200 CFU mL^{-1} in milk	Selective, Easy to use	Milk	[233]
rGo + chitosan	Electro reduction Go-CHI solution, Current increased after RGO-CHI deposition	Ap	*Salmonella*	DPV	10^1–10^6 CFU mL^{-1}	10^1CFU mL^{-1}	Selective, Thiol-aptamer gave a higher current compared to amine aptamer, Specific	Chicken	[234]
SWCNT	SWCNT attachment of aptamer with π-π stacking	Ap	*Escherichia coli O157:H7*	DPV	1.7×10^1-1.1×10^7 CFU mL^{-1}	10^1 CFU mL^{-1}	Selective	Tap water	[235]
Go	Methylene blue anchored Go	Ap	*C. sakazakii*	DPV	2×10^1-2×10^6 CFU mL^{-1}	7 CFU mL^{-1}	Specific, 88. 4%of its original response after 15-day storage,	Powdered infant milk	[236]
$AuNPs_C$	$AuNPs_C$ thiocyanuric acid/gold nanoparticles worked as the amplifier	Ap	*Avian influenza virus H5N1*	EIS	0.25 -16 HAU	0.25 HAU for the pure virus & 1 HAU for the tracheal	Specific, 57-fold increase for the 1 HAU samples with an amplifier	Swab samples of chicken	[237]

						Chicken swap		
Go/silica-cobalt	GO/Si-10Co has a small size while rGO/Si-10Co has mesopores with a large size. rGO/Si-10Co Showed a higher surface area.	Ap	*Salmonella*	EIS	10^{1}-10^{8} CFU mL^{-1}	10^{1} CFU mL^{-1}	5 min incubation time with bacteria	[238]
Nanoporous gold	Nanoporous gold prepared by electrodeposition of Au-Cu alloy at the surface of the electrode & dealloying of Au-Cu film from Cu.	Ap	*Salmonella*	EIS	6.5×10^{2} -6.5×10^{8} CFU mL^{-1}	1CFU mL^{-1}	New, facile, & cost-effective nanoporous gold Synthesis, Regenerable, Distinguish between live & dead bacteria cells.	Egg, Rotten egg [99]
rGO & COOH-MWCNT	Electrodeposition GO-MWCNT & electrochemical reduction to rGO-MWCNT GO oxide with a uniform length	Ap	*Salmonella*	EIS	75 to 7.5×10^{5} CFU mL^{-1}	25 CFU mL^{-1}	Selective, The current of rGO –MWCNT is bigger than MWCNT alone	[239]
MWCNT -COOH	Electrodeposition MWCNT increased peak current 2 times.	Ap	*S.Typhimurium & S.enteritidis*	EIS	10^{1}-10^{5} CFU mL^{-1}	6.7×10^{1}&5.5×10^{1} CFU mL^{-1} *S. Typhimurium & S.enteritidis*	Selective, Sensitive, Low cost of preparation	Chicken [240]
GO -Platinum nano cauliflower hybrid	Chemical reduction of GO, Pt was electrodeposited on GO-nano cellulose, Pt nano cauliflowers with structures ranging from 10 nm nodes to 2 µm.	Ap	*Escherichia coli O157: H7*	EIS	4 to 10^{5} CFU mL^{-1}	4 CFU mL^{-1}	POC biosensing, Electroactive surface area (ESA) increased by an order of magnitude after deposition of Pt nano cauliflower structures	[241]
MWCNT-COOH	Bridged Rebar Graphene synthesized from MWCNT using modified chemical assisted unscrolling method followed by bridging with terephthalaldehyde	Ap	*E. coli O78:K80: H11*	EIS	10^{1}- 10^{6} CFU mL^{-1}	10^{1} CFU mL^{-1}	Specific, New aptamer	Water Juice Milk [242]
AuNPs, Carbon nanoparticles/ cellulose nanofibers	Significant increase in the peak current & decrease in Rct CNFs with AuNPs/CNPs nanocomposite.	Ap	S. aureus	EIS	1.2×10^{1}- 1.2×10^{8} CFU mL^{-1}	1 CFU mL^{-1}	Selective, Discriminate between live and dead bacteria cells	Human blood serum [243]
AgNPs	$AgNPS_E$100 nm modification of GCE by AgNPs enhanced electron -transfer of modified electrode & reduce charge transfer resistance	Ap	P. aeruginosa	EIS	10^{2}- 10^{6} CFU mL^{-1}	33 CFU mL^{-1}	Selective, First impedimetric for *P. aeruginosa*	Human blood serum [102]
GQD	Aptamer molecules attached on the surface of GQD by chemisorption between GQD & amine groups of aptamer by π-πstacking interactions	Ap	hepatitis C virus (HCV) core antigen	EIS	10-70×10^{-9} g L^{-1} & 7-40×10^{-8} g L^{-1}	3.3×10^{-9} g L^{-1}	96 -85% initial signal after 10 &14 days	Human serum [244]
AgBrNPs anchored 3D nitrogen-doped GO hydrogel	AgBr/3D N-doped GO hydrogel, AgBr nanoparticles was around 50–180 nm, Smaller impedance of AgBr/3DNGH due to presence of	Ap	*E.coli*	ECL	0.5 to 500 CFU mL^{-1}	0.17 CFU mL^{-1}	Simple operation process, low-cost, 12 Day storage time	Meat [118]
$AuNPs_E$, rGO	Chemical reduction of GO, $AuNPs_E$ rGO & AuNPs increase electrical conductivity & electron	Ap	*S. aureus*	ECL	1.5×10^{2}- 1.5×10^{8} CFU mL^{-1}	28 CFU mL^{-1}	Selective, Enzyme free High ECL with AuNPs &	Urine [245]
MoS2-PtNPs	transferability						catalytic activity of hemin	
GO COOH/porcine IgG	GO-COOH strong immobilization ability to porcine IgG for its large surface & the high number of carboxyl groups. COOH- GO facilitated electron transfer	S. aureus protein A *s S. aureus*		ECL	1.0×10^{3}–1. 0×10^{9} CFU mL^{-1}	3.1×10^{2} CFU mL^{-1}	Selective, Simple fabrication, Short assay timer. 91.3% of initial signal remained for 15 days.	Milk, Human Saliva [246]
Ru(bpy)3^{2+}-PtNps complex Fe_3O_4@Au Nps, rGO	Fe_3O_4@ Au NPs 50nm was more suitable, Ru-PtNps 12nm, rGo & Ru-PtNps decreased charge transfer resistance	Ab	*Clostridium. perfringens*	ECL	10^{3}-10^{7} CFU mL^{-1}	10^{2} CFU mL^{-1}	Specific, POC analysis	Infected Wound [88]
CdTe QDs, AuNPs, GO	$AuNPS_C$, Electrochemical reduction of GO	DNA probe *Hepatitis B virus& Hepatitis C virus DNA*		ECL	*Hepatitis B virus* 5×10^{-13} - 5×10^{-10} *Hepatitis C virus* 1×10^{-12}-1×10^{-9} mol L^{-1}	*Hepatitis B* 8.2×10^{-14} *Hepatitis C virus* 3.4×10^{-13} mol L^{-1}	Sensitive, Multiplex sensing,92% signal value remained after 15 days	Human Serum [106]
Fe_3O_4/Van/PEG	Amin terminated Fe_3O_4 100 − 200 nm Vancomycin coated	Bacteria DNA *L.monocytogenes*		ECL	10^{2}-10^{6} CFU mL^{-1}	10 CFU mL^{-1}	Selective, Fe_3O_4/Van/PEG Biocompatible & 90% Capture bacteria	[89]
Fe_3O_4@GO	Fe_3O_4 Co-Precipitation method	Ab	*V.parahaemolyticus*	ECL	10-10^{8} CFU mL^{-1}	5 CFU mL^{-1}	Specific, 92.97± 4.5% initial signal n =5 after 1 month, High & stable ECL signal, RSD 7.8% n=5,Recoveries94.4–112.0%,Simple instrumentation(a laboratory built ECL)	Seafood, Seawater [247]
Hydrogel-loaded carbon quantum dots(Cdots/3DGH) &Graphene-like carbon nitride (g-C_3N_4)	g-C_3N_4 prepared from melamine powder, Cdots/3DGH prepared by dissolving glucose 10 mL GO oxide, followed by Autoclave	Ap	*E.coli,* Ratiometric Photoelectrochemical		2.9 -2.9×10^{6} CFU mL^{-1}	0.66 CFU mL^{-1}	Stability, good reproducibility, & repeatability .	Milk [119]
CdSe quantum dots (QDs) sensitized Ho^{3+}/Yb^{3+}-TiO_2	CdSe QDs size 5nm, CdSe QDs increases the photocurrent response of TiO_2& enabled it to be excited under the visible light	Ab	*V.parahaemolyticus* Photoelectrochemical		10^{2}-10^{9} CFU mL^{-1}	25 CFU mL^{-1}	Excellent selectivity, High sensitivity, RSD 5 electrode 1.2%	Shellfish products [107]
AuNPs integrated with ZnAgInS QDs	$AuNPS_C$, ZnAgInS QDs 10 nm, AuNPs integrated with ZnAgInS QDs with EDC/NHS with the help of mercaptoacetic acid, $AuNPS_C$ & ZnAgInS QDs ratio 1:100 is the best ratio	Ab	*Hepatitis B virus surface antigen* Photoelectrochemical		5×10^{-9}- 3×10^{-5} g L^{-1}	5×10^{-10} g L^{-1}	Selective, GNPs/ZnAgInS/GCE showed 33 times higher photo current in comparison ZnAgInS/GCE, 94.5% of initial signal after 2 week	Human serum [108]
AuAg Nanoshells	AuAg NSs with increased resistance to chemical oxidation generates a strong electrochemical signal.	*Escherichia coli & Salmonella*		DPV		10^{2} CFU mL^{-1}	Low cost. Fast (10min), Easy to operation, need any additional	water [120]
	Monodisperse hollow AuAg NSs 60 nm with a thin outer shell of 10 nm,	*Typhimurium*					reagent, substrate, AuAg NSs act as a natural redox enzymes electrochemical signal	

photoelectrochemical aptasensor based on three-dimensional graphene hydrogel-loaded with carbon quantum dot (C-dots/3DGH) and graphene-like carbon nitride sheet (g-C_3N_4); the proposed sensor presented superior photoelectrochemical ability. Appling different bias voltage, the cathodic and anodic current produced, respectively, C-dots/3DGH and g-C_3N_4 could be detected and differentiated; the proposed dual signal system allowed not only to detect selectively an analyte but also to take into account possible influence of the environment on the sensor response. To demonstrate this, the authors reported on an *E.coli* aptasensor in which the aptamer was immobilized on the C-dots/3DGH surface. In the presence of *E.coli* if on one end the cathodic current, associated with the C-dots/3DGH, was reduced due to the

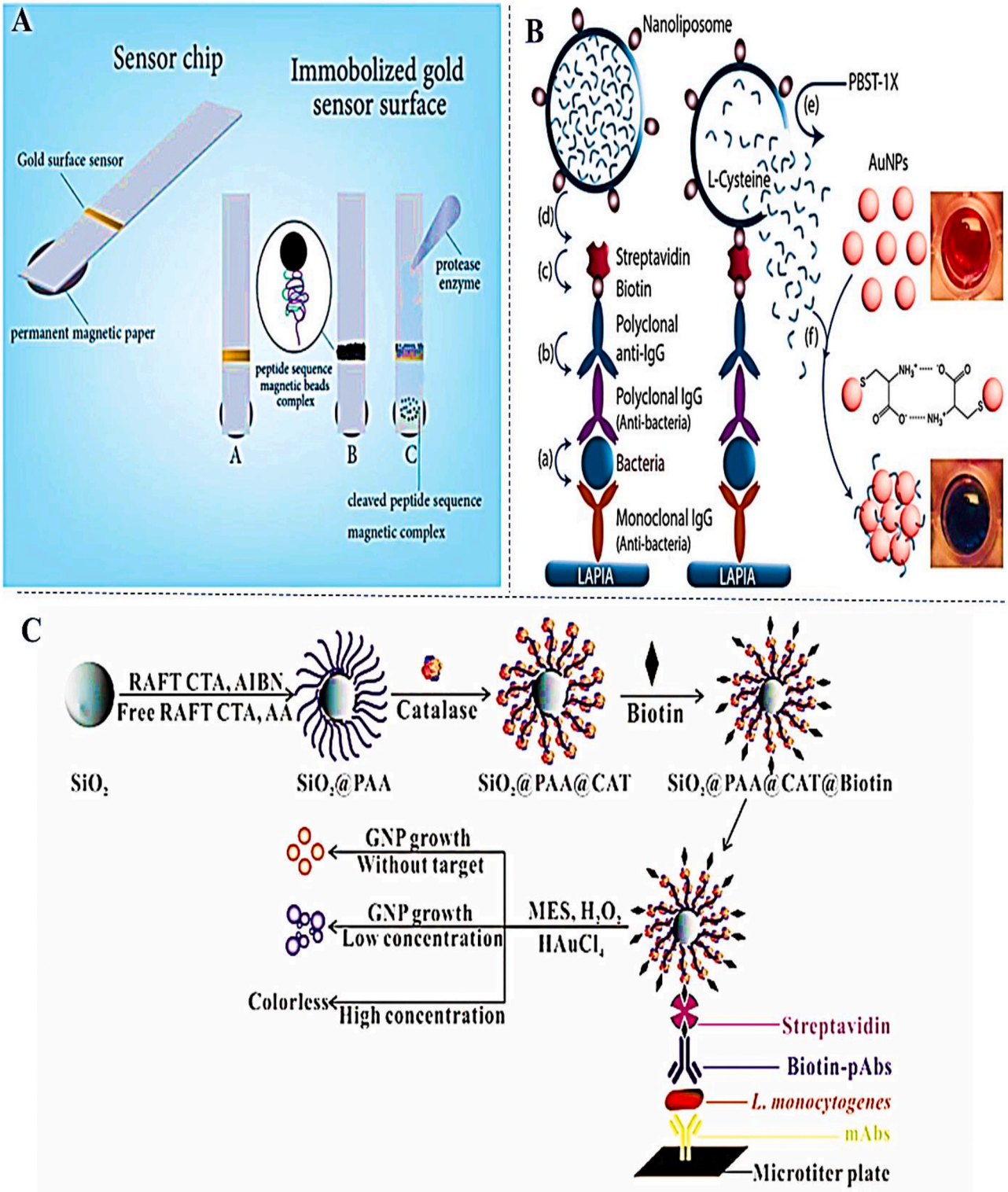

Fig. 3. A) Schematic of pyrolytic biosensor schema with permission ref [125]. B) Liposome enhanced plasmonic immunosensor with permission ref [126], C) Quantitative Immunoassay Based on SiO_2@PAA@CAT-Catalyzed growth of AuNPs with permission ref [127].

blocking effect of aptamer and target on the other end no effect on the anodic current was recorded; subsequently variation in the anodic current was used to estimate environmental change. The quantitative measurement of the target pathogen was carried out by calculating the ratio of cathodic current to anodic current. The aptasensor showed a linear range of (2.9 CFU $mL^{-1}$to 2.9 $\times$ 10^6 CFU $mL^{-1}$with an excellent LOD of 0.66 CFU mL^{-1} [119]. The schematic of this procedure is shown in Fig. 2D

Simple and facile detection of *S.Typhimurium* and *E.coli* was demonstrated by the use of hollow electrocatalyst Au-Ag nanoshells that enabled the in situ generations of the readable electrochemical signal; *S. Typhimurium* and *E.coli* were mixed with PVP-coated Au-Ag nanoshells and incubated for short time. To generate an electrochemical signal the mixture was dropped to SPCE. Au-Ag nanoshells were deposited, by

Table 2
Colorimetric biosensors, List of Abbreviation Colorimetry (CO) [248–276].

Nanomaterial	Nanomaterial Bio remark	Pathogen	Method	Liner range	LOD	Remark	Real sample	Ref
(Magnetic nanobeads) MNP-COOH	*S. aureus* proteases peptide	*Methicillin-Resistant S.aureus*	Visual	7.5-7.5×10^6 CFU mL^{-1}	7CFUmL^{-1}	40 and 100 CFUmL^{-1} in real sample, Selective, 6-month stability	Ground beef, turkey sausage, Lettuce, milk	[122]
MNP-COOH	*E. coli O157: H7* proteases peptide	*E.coli O157: H7*	Visual	121-1.21×10^6 CFU·mL^{-1}	12 CFU·mL^{-1}	30-300 CFU mL^{-1} in complex food matrices, rapid response time, 6 months, stability. Selective, Low cost and, Ease of use	Ground beef, turkey sausage, Lettuce, milk	[123]
MNP-COOH	*P. gingivalis* proteases peptide	*Porphyromonas gingivalis*	Visual	10^1-×10^9 CFU·mL^{-1}	49CFUmL^{-1}	Easy to perform, Fast (30 s response time)	Saliva samples	[124]
MNP-COOH	*Listeria* protease peptide	*Listeria monocytogenes*	Visual	2.17 x10^2 – 2.17 x10^8 CFUmL^{-1}	2.17 x10^2 CFU mL^{-1}	Selective, Easy to perform, Fast (30 s response time)	Whole milk Ready to eat meat	[125]
Blue, orange, and green dye coated polymer nano-beads	Ab Lactoferrin	*S. Typhimurium, S.enteritidis, S. aureus and C. jejuni.*	Visual	10-10^8 CFU·mL^{-1}	10 CFU·mL^{-1}	Selective Portable, User friendly 10 CFU·mL^{-1} S.Typhimurium and C.rjejuni, 100 for S. enteritidis *S. aureus* CFU·mL^{-1} meat surface	Chicken meat	[248]
$AuNPs_C$, Nanoliposome	Cysteine-loaded liposomes pH 7.25, AuNPs shows a very high stability	Ab *E. coli O157: H7, S.Typhimurium L.monocytogenes.*	Visual	10^1-10^3 CFU mL^{-1}	Single-digit pathogen	Enzyme free, *E.coli O157: H7* Milk, *S.Typhimurium* Apple juice, *L.monocytogenes.* Ground beef		[126]
Blue Silica Np, Blue Silica Np-NH_2, Blue Silica Np-COOH, MNPs- COOH	Blue Silica Np spherical shape 45nm, Reverse microemulsion method, tiny color change in basic solution& faintly lighter in acidic solution	Ab *S. pullorum & S. gallinarum*	Visual	8.8×10^1-8.8×10^9 CFU mL^{-1}	8.8 ×10^1 CFU mL^{-1}	Milk powder 8.8×10^2CFUmL^{-1}, Inexpensive, Specific, Immune Np stable for 90 days	Milk powder	[70]
Blue SilicaNp, Blue Silica Np-NH, Magnetic bead	Blue Silica Np spherical shape 50nm, Reverse microemulsion method, color Stable in acidic &basic solution	Ab *S. pullorum & S. gallinarum*	Visual	10^1-10^8 CFU mL^{-1}	10^1 CFU mL^{-1}	Selective, Non- enzymatic, Immune Np stable for 90 days	Chicken serum	[71]
AuNPs	AuNPs coated with streptavidin larger than 13 nm	Ab *E.coli & Salmonella*	Visual	10-10^3 CFU mL^{-1}	10CFUmL^{-1}	Selective, Detect only live cell, total assay time is about 30 min when the sample is gently agitated	Lake water, Whole milk	[249]
AuNPs	AuNPs coated with streptavidin larger than 13 nm	Ab *Salmonella*	Visual	10-10^3 CFUmL^{-1}	10CFUmL^{-1}	Selective	Tomato	[250]
SilicaNp MNP with SiO_2	Silica Np 50 nm reverse emulsion, MNP Co-participation	Ab *S.pullorum and S. Gallinarum.*	Visual/CO	8.4 × 10^3 8.4 × 10^7 CFU mL^{-1}	1.7 × 10^3 CFU mL^{-1}	Specific,96- 55% of the initial signal were preserved after storage of HRP-IgG-SiNps &IgG -MN P for 30- 120 days	Chicken liver	[72]
SiO_2@PAA@CAT, MNP-COOH	SiO_2+Polyacrylic acid size 80 nm Stöber method, Magnetic particle 180nm, High loading of catalase enzyme By SiO_2 nanoparticles modified with PAA brushes	Ab *Listeria monocytogenes*	Visual /pELISA	8 × 10^1- 8 × 10^8 CFU·mL^{-1} Visual and 8 × 10^0- 8 × 10^6 with a microplate reader	8CFU·mL^{-1}	5 order of magnitude more sensitive than	Lettuce	[127]
AuNPs		Ab *Salmonella enterica*	Visual /CO	10^3-10^7 CFU mL^{-1}	500 CFUmL^{-1}	Selective,	Milk	[251]
MNP, AuNPs	Fe_3O_4- COOH 180 nm Dextran-capped AuNPs mono-dispersed particles with 15 nm	Ab *E. Coli O157: H7*	Visual / CO	10^2-10^6 CFU mL^{-1}	41 CFU mL^{-1}	Selective	Milk	[252]
MNC/Pt	Fe_3O_4 Hydrothermal method MNC/ Pt 100nm,PtNps 16nm	Ab *E.coli O157: H7*	Visual/CO	10^1-10^5 CFU mL^{-1}	10^1 CFU mL^{-1}	Selective, MNCs/*E. Coli* were separated from free MNCs by magnetophoretic Chromatography, Easy to perform, fast, Strong catalytic activity of Pt particle cause low LOD	Milk	[136]
$AuNPs_C$	AuNPs probes labeled with HRP as probes to produce signal created by catalyzed TMB reaction	Ab *E.coli O157: H7*	CO	10^2-10^5 CFU mL^{-1}	100 CFU mL^{-1}	Net fishing enrichment method, 200 CFUmL^{-1}Pineapple juice	Pineapple juice	[253]
MNP-COOH	MNP-COOH 100nm coated with vancomycin	ALP-IgG *S. aureus*	CO	12-1.2×10^6 CFU mL^{-1}	3.3 CFUmL^{-1}	Specific	Lake water, Milk, Urine Saliva	[254]
MNPS,AuNPs, Ag nanoclusters	MNPS Hydrothermal method $AuNPs_C$ spherical 18.1nm	Ab/Ap *Listeria monocytogenes*	Visual/ CO	10-10^6 CFU mL^{-1}	10 CFU·mL^{-1}	Specific	Pork	[255]
Au-CNT nanohybrids	Au CNT nanohybrids in situ synthesis with HCOONa The optimum 10 nm	Ab *Influenza virus A (H3N2)*	Visual /CO	10-50000 PFU mL^{-1}	3.4 PFU mL^{-1}	100 times and 500 times more sensitive than ELISA& commercial kit		[135]
AuNPs	$AuNPs_C$ 13nm	Ab *Influenza A virus H3N2*	Visual/CO	0-80 HAU	7.8 HAU	Specific, Easy to operate		[256]
Magnetic Nano beads, AuNPs	Superparamagnetic Nano beads 200nm Electrodeposited AuNPs	Ab *Human enterovirus 71 (EV 71)*	Visual	1× 10^{-11}-6×10^{-7} gmL^{-1} Amperometry	1× 10^{-9} Visual g mL^{-1} 1× 10^{-11}gM	Selective, Investigate two different method, No pre-treatment or solution transfer,	Clinical serum sample	[257]

AuNPs	$AuNPs_C$ 20 nm for a capture probe, cationic cystamine 40nm, CTAB capped AuNPs 30 nm core/shell-like structure, cystamine-AuNPs capable of acting as hydrogen bond and enhance color detection	RNA probe	*Hepatitis C virus RNA*	Visual/CO	1-3 IU μl^{-1}	4.57 IU μl^{-1}	Simple, Rapid, RNA folding impact on the aggregation behavior	Clinical serum sample	[128]
AuNPs film AuNPs + CdTe QDs	Coating AuNPs on glass, 96-well polystyrene plates, Au NPs more densely deposited onto the hydrophobic surface than onto the hydrophilic surface, CdTe QDs2.85nm, +AuNPs 40 nm prepared with cystamine solution	Ab	*Influenza virus A H1N1 & H3N2*	Visual/CO	10 $^{-8}$gL^{-1} -10 × 10^{-2}g L^{-1} 10–50,000 PFUA mL^{-1}	5.05×10^{-11} g mL^{-1} 24.3 PFUA mL^{-1}	The peroxidase-like catalytic activity of Au NP films and colloidal AuNPs, 116 times better than ELISA		[130]
$AuNPs_C$, Magnetic nanobeads QD	Superparamagnetic 500nm, In situ, synthesized QDs with S.aureus,	Ab	*Enterovirus 71*	Visual/CO	5 ×10^{-7} - 3×10^{-5} g L^{-1}	1× 10^{-6}g L^{-1}	Selective, Self-synthesized nanoparticles,	Human throat swab	[258]
AuNPs	$AuNPs_C$	Ap	*C. sakazakii*	Visual	7.1 × 10^3 7.1 × 10^7 CFU mL^{-1}	7.1 × 10^3 CFU mL^{-1}	Selective, Easy to operate	Powdered infant formula	[259]
AuNPs	$AuNPs_C$	Ap	*Campylobacter coli& Campylobacter jejuni*	Visual	10^5 -10^8 CFU mL^{-1}	7.2×10^5 CFU mL^{-1}	Can distinguish live and heat-killed bacteria,	Chicken carcass	[260]
Au@Pd nanoparticles	The thickness of palladium layer 1-2 nm cause a redshift for Au@PdNps	Ap	*Campylobacter jejuni*	Visual/ CO	10 -10^6 CFU mL^{-1}	100 CFU·mL^{-1}	Selective, After 6 months RSD peroxidase-like activity change4.2%,	Milk	[40]
AuNPs	$AuNPs_C$ peroxidase-like activity of AuNP17 nm	Ap	*Pseudomonas aeruginosa*	CO/ electrochemical	60.0 to 6. 0 × 10^7 CFU mL^{-1}	60.0 CFU mL^{-1}	Selective, Applying , two different method	-	[261]
Au Nanorods, Magnetic nanoparticle, MnO_2 Nanoparticle	Au Nanorods silver ion-assisted seed-mediated growth a monodisperse and uniform rod,Magnetic nanoparticle 242.7 nm	Ap/ Ab	*Listeria monocytogenes*	Visual/CO	10× 10^6 CFU mL^{-1}	10CFUmL^{-1}	Selective, Detection in pork sample Without pre-enrichment, MnO_2 peroxidases like nano artificial enzyme	Minced pork	[133]
$ZnFe_2O_4$/rGO	$ZnFe_2O_4$/rGO Good peroxidase-activity, Stable than HRP	Ap	*S.Typhimurium*	Visual/CO	11 - 1.10 × 10^5 CFU mL^{-1}	11 CFU mL^{-1}	Selective	Milk	[134]
Fe_3O_4 MNP	MNP 20nm co-participation	Ap	*S. Typhimurium*	Visual/CO	-	7.5 × 10^5 CFU mL^{-1}	Peroxidase behavior Fe_3O_4 MNP	-	[131]

Fe_3O_4Nano cluster	Fe_3O_4 Solvothermal method Fe_3O_4Nano cluster Fe_3O_4+ poly-L- lysine layer Show higher catalytic activity	Ap	*Listeria monocytogenes*	Visual/CO	5.4×10^3-×10^8 CFU mL^{-1}	5.4×10^3	Selective	Milk	[262]
AuNPs	AuNPsC 16 nm	Ap	*S. Typhimurium*	Visual/CO	10^2-10^9 CL 10-10^9 AM CFU mL^{-1}	10 CL, 100 Am CFU mL^{-1}	Sensitive, Peroxidase behavior of AuNPs	Apple juice	[132]
AuNPs	$AuNPs_C$	Ap	*Sh. flexneri*	Visual/CO	10^2-6 CFUmL^{-1}	80 CFU·mL^{-1}	Selective, Portable	Smoked salmon	[263]
AuNPs	AuNPsC	Ap	*E. coli O111:B4LPS*	Visual/CO	2.5-20× 10^{-3} g L^{-1}	1×10^{-3} g L^{-1}	Specific		[264]
Au@Pt NR	NRs aspect ratio 3.8, Pt nanodots with sizes of 3–4 nm	Ab	*Measles IgM antibodies*	Visual / LAMP	10^{-5}-10^{-3} g L^{-1}	10^{-5} g L^{-1}	1000 times more sensitive than ELISA, More stable in different temperatures and pH than HRP	-	[265]
AuNPs	$AgNPs_C$ 20nm	Phosphatidylcholine-phospholipase C gene (plcB) *Listeria monocytogenes*		Visual / LAMP	2.82-2.82×10^8 CFU mL^{-1}	8×10^{-10}g and 2.82 CFU mL^{-1}	Fast, Specific, 10 times more sensitive than the conventional PCR assay	Chicken Meat	[266]
AuNPs	$AuNPs_C$ 10 to 20 nm	DNA probe *Hepatitis C Virus (HCV) RNA*		Visual/CO	3.70 ×10^{-7}- 3 ×10^{-6} mol L^{-1}	5 ×10^{-7} mol L^{-1}	Investigate free patchy end in differential adsorption of ssDNA and dsDNA over citrate-modified Au NPs and set up rules	-	[267]
AuNPs	$AuNPs_C$ 13nm	Genomic DNA from bacterial cultures *Emetic Bacillus cereus*		CO/asymmetric PCR	9.2 × 10^1 -9.2 × 10^6 CFUmL^{-1}	9.2 × 10^1 Milk 9.2 × 10^2 CFUmL^{-1}	Selective, Viable detection of the pathogen	Milk	[268]
AuNPs	$AuNPs_C$ 12.867 ± 2.399 nm and 13.705 ± 2.557 nm	DNA probe *Mycobacterium avium DNA*		Visual		1.03× 10^{-2} gL^{-1}	Specific	-	[269]
Flower-shaped AuNPs	Flower-shaped AuNPs 68.7 ± 2.8 nm, AuNPs +planet extract	DNA probe *Amplicons of hlyA gene & genomic DNA of Listeria monocytogenes*		Visual	4.84 × 10^{-8} 1.004× 10^{-7} g	4.84 × 10^{-8} g	Green synthesis method, Fast, Simple, Selective	-	[270]
AuNPs	AuNPs 6-10 nm	DNA probe *DNA S. aureus ,*		Visual/CO	5-40 ×10^{-3}g L^{-1}	8.37×10^{-3}g L^{-1}	Selective	-	[271]
CTAB capped gold nanoshells	CTAB capped gold nanoshells 23±0.58	-	*S.aureus, P.aeruginosa, S. enterica, E. coli*	Visual/CO	10^1-10^7 cells mL^{-1}	10CFUmL^{-1}	Rapid, Simple, Without biomolecule, Answer to a broad range of pathogen		[272]

$AuNPs_C$	$AuNPs_C$ 18±3 nm	-	*E.coli*	Visual	10^4- 0^7 CFU mL^{-1}	1.02×10^3CFUmL^{-1}	Rapid, reliable, and cost-effective, Without biomolecule	-	[273]
Au nanorods	Au nanorode seed-mediated growth method 59 ± 8 nm and a width of 11 ± 1 nm	-	*E.coli*	Visual/ CO	-	1×10^5 CFU mL^{-1}	Simple, Rapid inexpensive, portable, disposable devices, User friendly, without biomolecule	-	[274]
AuNPs	$AuNPs_C$ 20 nm	-	*E. coli. S.Typhimurium ,Klebsiella pneumonia*	Visual, FRET	10-10^7 cells mL^{-1}	10 cells mL^{-1}	Rapid, Simple, Without biomolecule, Answer to a broad range of pathogen	Tap water and lake water	[129]
Van-coated Au NPs	9.5 nm, Molar ration 1:1 $HAuCl_4$ to Van the most stable	-	*Gram-positive bacteria*	Visual	0–8 × 10^8 CFU mL^{-1}	1×10^9 CFU mL^{-1}	Ag enhancement, Without biomolecule	Orange juice Tap water	[275]
MPBA-AgNPs	AuNPs citrate & $NaBH_4$	-	*Gram-negative bacteria*	Visual/UV/Smart phone	5×10^4 -1×10^7 CFU m L^{-1}	9×10^3 CFU m L^{-1}	Rapid, Low cost, Selective Without biomolecule		[276]

applying a constant potential followed by a DPV scan to oxide the residual Ag atoms to Ag^+ in PBS solution. The proposed electrode was demonstrated to be able to measure 10^2 CFU mL^{-1} of bacteria without using specific biomolecule [120]. More examples of the electrochemical bio/sensors are presented in Table 1.

3.2. Colorimetric biosensors

Colorimetry is a well-established method with widespread use in sensor development; this transduction method presents few advantages as low cost, simple/no instrumentation, and ease of fabrication. Naked-eye detection is a fascinating branch of colorimetric methods that enables qualitative detection of analytes; on the other end, the use of spectrophotometric reading allows quantitative measurements [121].

Enzyme induced disaggregation of black magnetic nanobeads (MB) network, based on peptidic crosslinking, was explored by the Zourob team, in the development of optical sensing of several pathogens. MB networks were placed on gold substrates, located on a paper surface, and kept in position with a magnet. Upon addition of bacterial extract, that contains proteases to the sensing surface, disaggregation of the MB network, due to the peptide digestion, take place exposing in this way the underneath Au. The percentage of the observable area was shown to be proportional to the bacteria protease concentration. The proposed sensors could achieve LOD of 7, 12, 49, 2.17 × 10^2 CFUmL^{-1} for *Methicillin-Resistant S.aureus, E.coli O157: H7, Porphyromonas gingivalis, Listeria monocytogenes* respectively [122–125]. The schematic of this procedure is presented in Fig. 3A. Nanoliposomes contain cysteine were demonstrated in the development of optical ELISA tests for the detection of *Salmonella*, *Listeria, E. coli O157,* and rabbit IgG antibody. In the proposed strategies the nanoliposomes were used as a label in the sandwich assay. Optical detection was made possible by the ability of the cysteine, released following rupture of the nanoliposome, to aggregate AuNPs with a subsequent blue shift of the AuNPs plasmonic. The purposed sensor showed 6 orders of magnitude enhancements for IgG detection, down to aM levels, in comparison to the conventional ELISA method which used HRP as a biocatalyst for TMB reduction [126]. The schematic of this assay was illustrated in Fig. 3B.

Silica nanoparticle with poly(acrylic acid) brushes worked as a carrier for high loading of catalase enzyme; the enzyme loaded particles were used as a label in ELISA for sensitive visual detection of *L.monocytogenes* (10 CFUmL^{-1}). The proposed assay was based on the differences in AuNPs formation when different concentrations of the reducing agent (hydrogen peroxide) were present in the reaction chamber. In the absence of target analyte the fast reduction of gold ions by hydrogen peroxide, both added in the ELISA well, quasi-spherical non-aggregated gold nanoparticles with red color were formed. By contrast in the presence of analyte the catalase enzymes, loaded on the silica labels, were then able to degrade the hydrogen peroxide giving rise to an aggregated nanoparticle with characteristic blue color. High loading of the enzyme increased LOD 2 and 5 orders of magnitude in comparison with catalase plasmonic ELISA (without silica nanoparticle) and HRP based ELISA methods [127]. The schematic of this assay is depicted in Fig. 3C.

Gold nanomaterials are among the most used material in colorimetric detection. The different detection approached based on Au nanomaterials can be classified into three "groups": (i) approaches based on aggregation/disaggregation, (ii) approaches based on catalytic properties of the Au nanomaterials, and (iii) growth of hybrid nanomaterials [9]. AuNPs modified with a thiolated Hepatitis C Virus (HCV) specific probe was used to detect unamplified HCV RNA. In the proposed assay probe modified AuNPs were incubated with unamplified HCV RNA at 95 °C for a fixed time; two positively charged gold nanoparticles (cysteamine and CTAB) capped used to promote aggregation of the above-mentioned AuNPs. When no complementary target was present in the solution aggregation of the AuNPs, due to electrostatic interaction was recorded (red to blue color change); on the other end in the presence of HCV RNA the solution remained red. Cysteamine capped AuNps provided sharper color. The biosensor showed a LOD of 4.57 IUμL^{-1} [128]. AuNPs were also used to transduce the interaction of antibiotics with the bacterial outer membrane; this was shown to enable the sensitive detection of bacteria down to 10CFU mL^{-1}. More specifically in their proof of concept work, Singh et al. used Colistin, a cationic antibiotic, as a bacteria recognition element and as an AuNPs aggregation inducing element [129].

Visual detection can be enhanced by the catalytic activity of nanomaterials to a chromogenic substrate like 3,3′,5,5′-tetramethylbenzidine (TMB) [130–132]. Peroxidase activity of nanomaterial has been also exploited in colorimetric sensing. For example, a sandwich-type biosensor based on apt-MNP and IgY- BSA-MnO_2 nanoparticles was reported for the detection of *L. monocytogenes.* The MnO_2 in the label was then used to oxidize TMB to TMB^{2+}; oxidizedTMB^{2+} reacted with AuNRs resulting in a gradual degradation of the AuNRs with associated variation in their aspect ratio. The shift of longitudinal localized surface plasmon was shown to correlate linearly with the log concentration of *L. monocytogenes* in the 10–10^6 CFU mL^{-1}concentration range [133]. Wu et al. developed a colorimetric sandwich-type aptasensor in which $ZnFe_2O_4$/reduced GO nanocomposite was used to catalyze the oxidation of the TMB by consuming H_2O_2 that resulted in the formation of a blue color product which is then measured by micro-reader; detection of *Salmonella enterica serovar* down to 11 CFU$mL^{-1}$was demonstrated [134]. In another study, the nanocomposite of AuNPs and CNT was shown to have higher catalytic activity in comparison to AuNPs and CNT alone toward the oxidation of TMB by H_2O_2. The proposed nanocomposites were utilized in an immunosensor for the sensitive detection of influenza A H_3N_2 virus down to 10 PFU mL^{-1} [135].

Magnetic nanoparticles covered with platinum (Pt/MNC) were exploited as a dual functional element in an *E.coli O157: H7* immunoassay; these were used to (i) carry the biorecognition element, half-fragment of monoclonal *E.coli O157: H7* antibody, and as (ii) catalyst for the oxidation of TMB. Nanoparticles were added to milk solution containing *E.coli O157: H7* followed by incubation for short time and separated with a permanent magnet. A precision pipette was used to

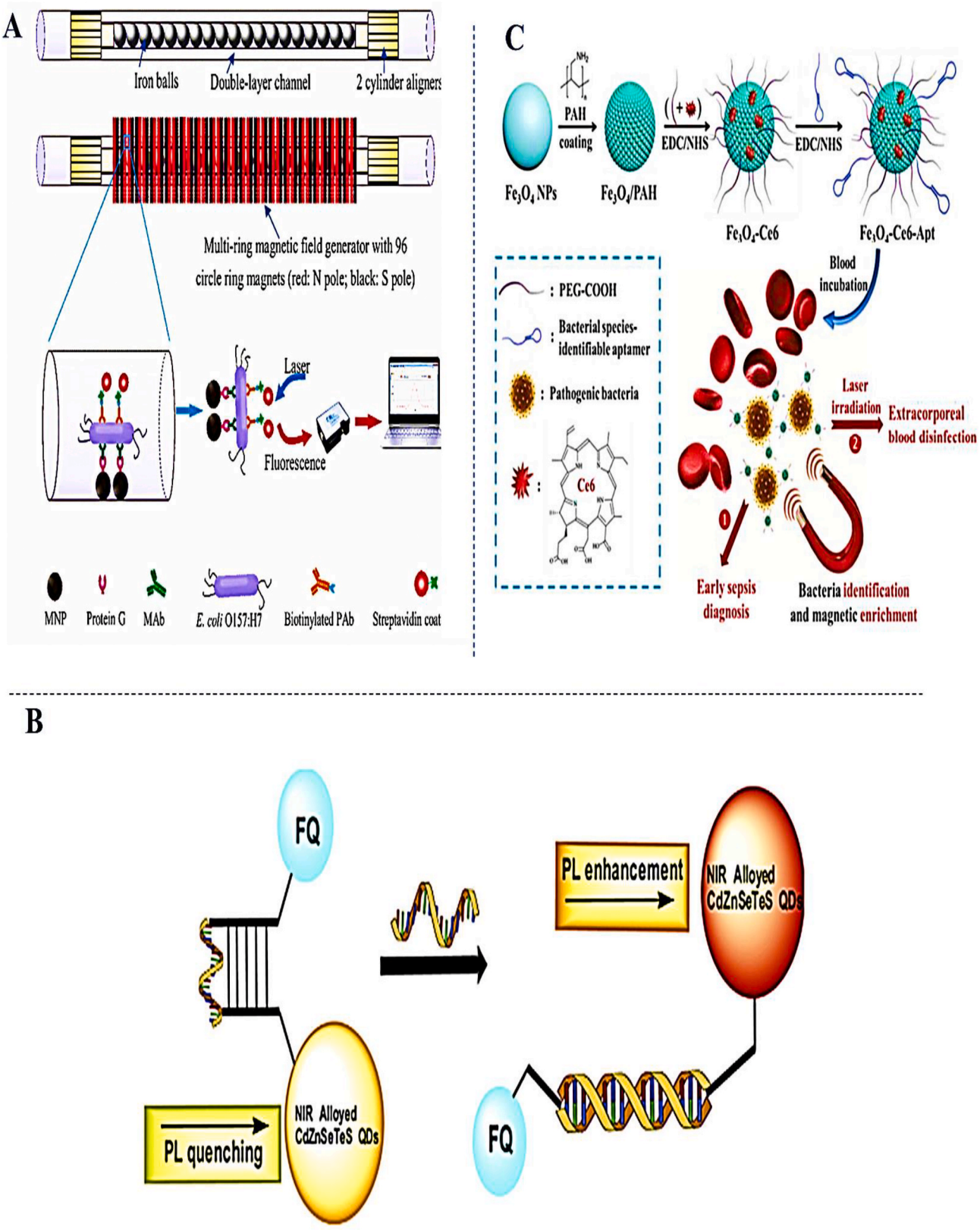

Fig. 4. A)The illustration of double channel coated by immunomagnetic bead and QDs with permission ref [139], B) The Schematic of NIR alloyed QD-MB designed biosensor with the permission of ref [144] C) The pattern of the Fe_3O_4-Ce6-Apt system for early sepsis diagnosis [148].

Table 3
Fluorometric biosensors Abbreviation Fluorescence (FL), Fluorescence energy transfer resonance (FRET) Emission (em), Reverse assay strategy (RAS) [277-312].

Table 3

Nanomaterial	Nanomaterial remark	Bio	Pathogen	Method	Linear range	LOD	Remark	Real Sample	Ref
Magnetic nanobeads-COOH CdTe QD - MPA	Aqueous synthesis of QD, Fluorescence of mercaptopropionic acid-modified CdTe QDs is highly sensitive to H_2O_2, λabs=566 nm, λ em=590 nm, Carboxylated magnetic nanoparticles180 nm	Ab	*E. coli O157: H7*	FL/Quenching	1.18×10^3 1.18×10^6 CFU mL^{-1}	5×10^2 CFU mL^{-1}	Specific, Novel method based on extreme bioactivity of catalase to H_2O_2 & sensitive H_2O_2 QD	Milk	[277]
MNP QD	Carboxylated magnetic nanoparticles180 nm CdSe/ZnS core shell, λ em=614 nm	Ab	*E. coli O157: H7*	FL	8.9×10^0 8.9×10^5 CFU mL^{-1}	1.4×10^1 CFU mL^{-1}	Specific	Milk	[139]
Fe_3O_4@Au CdTe QD	CdTe QD 3nm, Chitosan Coated CdTe 40 nm Fe_3O_4@Au, Fe_3O_4 Co-precipitation Au Shell CTAB	Ab	*E.coli*	FL	10^2-10^8 CFU mL^{-1}	30 CFUmL^{-1}	Selective, Fast, Sensitive	Urine	[278]
QD, Magnetic beads	Carboxyl QDs 2–10 nm in size Magnetic beads (1150 nm	Ab	*E. coli O157: H7 & Enterica*	FL/RAS	*S. enterica* 10^2 -10^7 *E.coli* 50-10^8 CFU mL^{-1}	*E.coli* 30 CFU mL^{-1} S. enterica 60 CFU mL^{-1}	Multiplex,50time sensitivity enhancement than ELISA	Milk	[279]
CdSe /ZnS AuNPs	core-shell CdSe/ZnS QDs AuNPs citrate 20nm	Ab	*Vibrio parahaemolyticus*	FL Turn on	10-10^4 CFU mL^{-1}	1050CFU mL^{-1} in real sample 50CFU mL^{-1}	Selective, core-shell CdSe/ZnS QDs stable for 2 month, Shrimp Ground beef Salted vegetables		[142]
CdSe/ZnS QD	CdSe/ZnS QD 5-8 nm	Ab	*Salmonella*	Visual/FL	-	10cell mL^{-1}	Selective, Simple, POC analysis.	Stool	[280]
MNP-COOH liposomes	MNP-COOH 30 nm Liposomes 244.3nm	Ab	*C. sakazakii*	FL	10^3-10^7 CFU ml^{-1}	3.3×10^3 CFU ml^{-1}	2 cells/10g After 6 h enrichment 10^3CFU mL^{-1} without pre-incubation	Powdered infant milk	[281]
CdTe-COOH AuNPs 14.5	two particles become less than 10 nm and AuNPs citrate 14.5 nm+ 11-MUA	Ab	Vibrio choleraeouter membrane protein W	FL/FRET	$2-10\times 10^{-9}$ mol L^{-1}	2×10^{-9} mol L^{-1}	Simple, Fast	-	[282]
AuMNPs CdSeInS QD	AuMNPs decorated with GO MNP Co-precipitation method	Ab	Influenza virus H_1N_1	FL	1×10^{-12}g L^{-1}-1×10^{-8}g L^{-1}	7.27×10^{-13}g L^{-1} Human serum 6.07×10^{-9}g L^{-1}	Specific	Human serum	[143]
Alloyed quaternary CdSeTeS QDs AuNPs	Alloyed quaternary 3.8 nm CdSeTeS hot-injection organometallic route & capped with L-cysteine AuNPs40 nm synthesized from HAuCl4 in HEPES buffer with cysteine cape	Ab	Influenza virus H_1N_1	FL	10^{-8} - 10^{-7} g L^{-1}	3×10^{-11} g L^{-1} Human Serum 4×10^{-10} g L^{-1} 10 PFU mL^{-1}	Selective	Human Serum	[283]
SiQDs AuNRs	Silica-coated quantum dots (SiQDs) QD 3.5 nm average size, Silica shell of 15 nm, the Aspect ratio of the AuNRs rise 3.8 times by increasing concentration of AgNO3, CTAB-coating over AuNRs worked as a bilayer, preventing aggregation and allowing its growth by face-sensitive surface adsorption	Ab	Mycobacterium tuberculosis Ag85B antigen	FL	1×10^{-6} -$^1\times 10^{-13}$g L^{-1}	1.3×10^{-10} gL^{-1}	Selective	Urine	[284]
CdZnSeTeS QDs	QDs 9nm highly, Homogenous and monodispersed PL enhancement was considerably higher for the NIR alloyed QD-MB than for the conventional CdSe/ ZnS QD-MB probe	molecular beacon strains of influenza virus H1N1 RNA		FL	2 -10 copies/mL	Specific		Human serum	[144]
AuNPs	AuNPsC	Ab/DNA probe *E. coli O157:H7, S.choleraesuis L.monocytogenes*		FL	10^1-10^7 CFU m L^{-1}	*E. coli O157: H7*3.4 × 10^1, *S. Choleraesuis* 6.4 × 10^0, *L.monocytogene* 7.0 × 10^1 CFU m L^{-1} Selective, Simultaneous		Milk	[285]
FITC-doped Silica NPs SilicaNPS-COOH	Silica reverse microemulsion method monodisperse particles 60 nm FITC-doped silica NPs increase photostability of dye-doped silica	Ab	*E. coli O157: H7*	FL microscopy & flow cytometry -	9× 10^5 CFU mL^{-1}	FITC-doped silica NPs brighter fluorescence and higher photostability		Ground Beef	[286]
UCNPs	Hexagonal uniform UCNP 50 nm	Ab	*E.coli*	FL	42 to 4.2 × 10^7 CFU mL^{-1}	42 CFU mL^{-1}	Selective	Pork Milk	[287]
UCNPs MNP	UCNP hexagonal shape 105 nm MNP hydrothermal method 110nm	Ap	*E.coli*	FL	58 to 5.8 × 10^6 CFU mL^{-1}	10 CFU mL^{-1}	Selective	Pork sample	[150]
$NaYF_4$:Yb/r AuNPs	AuNPs monodispersed 13 nm $NaYF_4$:Yb/Er monodispersed with an average diameter of 35 nm	Ap	*Escherichia coli 8739*	FL/FRET	5-10^6 CFU mL^{-1}	3 CFU mL^{-1}	Specific	Tap/Pond water Milk	[145]
CdTe QD Fe_3O_4	CdTe CD 2nm	Ap	*S.Typhimurium*	FL	10^1-10^{10} CFU m L^{-1}	1CFU m L^{-1}	Specific,	Water Milk	[140]

QD, Thulium-doped UCNPS, Magnetic bead	QD1-2 nm size Down-conversion of QDs & Upconversion of UCNP afford a suitable detection platform without spectral overlap	Ap	*S. aureus, & S.Typhimurium*	FL	50-10^6 CFU mL^{-1}	16 and 28 CFU $mL^{-1}$for *S.aureus, & S. Typhimurium*	Selective, Simultaneous detection, of *S.aureus, & S. Typhimurium,*	-	[141]
GO		Ap	*S. enteritidis*	FL	10^2 -10^7 CFU mL^{-1}	25 CFU mL^{-1}	Selective, truncated aptamer lower dissociation constant and 2 times lower LOD than full sequence	Milk	[288]
CDs , GO	CD	Ap	*P. aeruginosa*	FL/FRET	10^1 -10^7 CFU mL^{-1}	9CFU mL^{-1}	Selective, Easy to perform, High-throughput sequencing method to select aptamer .	Mineral water	[149]
Fe_3O_4	Fe_3O_4 Co-participation method coated with silica layer with NH_2 group 283 nm, MCM-41 type silica particles 187 nm wit	Ap/DNA probe *S. aureus*		FL	800-10^4 CFU mL^{-1}	682 CFU mL^{-1}	Selective	Whole blood	[289]
MBs-COOH Van-BSA-MBs	MBs-COOH 180nm	Ab	*S. aureus*	Flow cytometry	3.3×10^1 - 3.3×10^5 CFU mL^{-1}	3.3×10^1 CFU mL^{-1}	Selective, Sensitives Water, Milk, Fruit juice		[290]
Hollow silica nanosphere, Fe_3O_4@SiO_2@ PAA	Hollow silica nanospheres 350 nm prepared by ammonia-catalyzed hydrolysis and condensation of TEOS in an aqueous ethanol solution. Fe_3O_4angular and amorphous particles with sizes ranging from 7 to 20 nm.,Fe_3O_4@SiO_2 quasi-spherical 30 to 50 nm	Ab	*E. coli O157: H7*	FL	4- 4×10^8 CFU mL^{-1}	3 CFU mL^{-1}	Specific, bio-conjugated FHSNs stable for 60 days, 96.7% of initial response remained after 60 days	Milk, Orange juice, River water,	[146]
CdTe QD	CdTe QD 4.5nm	Ap	*E. coli O157:H7*	FL	10^2 - 10^7 CFU m L^{-1}	10^2 CFU mL^{-1}	Selective, Recoveries 76-91%.	Meat, Green sprouts, Chicken Milk	[3]
AuNCs@Van	Vancomycin as reducing & stabilizing agent AuNCs uniform spherical and monodisperse with an AuNCs@Van diameter of 2.0±0.6 nm. Fluorescence stable in different buffers and at varying pH, only falling off significantly at pH below 4. The fluorescence quantum yield 13%	Ap	*S. aureus*	FL	32-10^8 CFU mL^{-1}	70 CFU mL^{-1}	Specific, Good sensitivity, Excellent linear range Recoveries 96.94% - 101.24%	Milk, Human serum	[291]
AuNCs@Van AuNPs	AuNCs@Van , Vancomycin as reducing & stabilizing agent	Ap	*S. aureus*	FL	20-10^8 CFU mL^{-1}	10 CFU mL^{-1}	Selective, Facile	Milk, Orange juice, Serum	[147]

CdSe/ZnS	Water-soluble QD	Ap	*E. coli O157: H7*	FL	10^2 -10^5 CFU mL^{-1}	10^2 CFU mL^{-1}	Specific, Sensitive	Tap water	[292]
QD	Red, yellow, green QDs	AP	*E. coli O157: H7*	FL	10^2 -10^6 CFU mL^{-1}	10^2 CFU mL^{-1}	Selective, Long term stability, POC detection, In situ synthesis of photoluminescence-quenching nano paper	Lake water	[293]
Fe_3O_4 $NaYF_4$: Ce/ Tb NaGdF4: Eu	One-step solvothermal method synthesis, monodisperse, uniform, roughly spherical with 30 nm.	Ap	*S. Typhimurium & S. aureus*	FL	10^2 -10^5 CFU mL^{-1}	15, 20 CFU mL^{-1} *S. Typhimurium and S. aureus*		Milk	[294]
$NaYF_4$: Ce/Tb	$NaYF_4$: Ce/Tb 30 nm Solvothermal method 2-aminoethyl dihydrogen phosphate as a surfactant and capping agent.	Ap	*S.Typhimurium*	TR-FRET	10^2 -10^5 CFU mL^{-1}	25 CFU mL^{-1}	Selective, Good sensitivity	Chicken , Egg	[295]
$AuNPs_C$ GQD	AuNPs 15nm acceptor of FRET pair GQD 3nm donor of FRET pair dispersed fine in water solution because of the abundant oxygen-containing functional	Ap	*MecA gene sequence of S. aureus*	FL/FRET	1×10^{-9}-1×10^{-7} mol L^{-1}	1×10^{-9} mol L^{-1}	Selective, Sensitive PCR amplified product of S. aureus mecA gene		[296]
Ag@SiO_2	AgNPs 50 nm with 30nm silica shell (optimum thickness)	Ap	*Recombinant hemagglutinin (rHA) protein H5N1 influenza virus*	FL/MEF	2×10^{-6} -1×10^{-4} g L^{-1}	2×10^{-6}g L^{-1} Human serum3.5×10^{-6}	Selective, Fast, Ag@ SiO_2 increase the sensitivity 50 times, Recovery 105%	Human serum	[297]
Fe_3O_4-Ce6-Apt	Magnetic Fe_3O_4 nanoparticles were synthesized by thermal decomposition of the iron-oleate complex. Compared to micro-sized magnetic particles the nano-sized Fe_3O_4-Ce6-Apt has a higher surface to volume ratio exhibits a higher binding capacity to targets.Fe_3O_4-Ce6-Apt nanosystem	Ap	*S. aureus*	fluorescence microscopic	-	10 CFU mL^{-1}	Early sepsis diagnosis in mice (1.5h), Selective, Very good sensitivity, Fe_3O_4-Ce6-Apt 6 days of storage in blood, .No clear Potential toxicity of Fe_3O_4-Ce6-Apt toward red blood cells	Blood mice model	[148]
$MN^{2+}$$NaYF_4$:Yb, Tm UCNP Au Nanorode	$NaYF_4$: Yb, Tm UCNP spherical shape donor Au Nanorods Seed growth method acceptor	Ap	*S.Typhimurium*	LET	12-5×10^5 CFU mL^{-1}	11 CFU mL^{-1}	Selective, Recoveries85.7% 105.5%	Milk	[298]

Green and red QD Carbon particle		Ap	*V.parahaemolyticus &. S.Typhimurium*	FL/FRET	50-10^6 CFU m L^{-1}	6 *V.parahaemolyticus* 35 *S.Typhimurium* CFU m L^{-1}	Selective,	Shrimp Chicken breast	
CdSe/ZnS QD	MNP 20-150 nm CdSe/ZnS	Ap	*avian influenza virus (AIV) H5N1*	FL QCM	$2^{-1.2}$- 2^6 HAU 20μL^{-1}	0.4 HAU	Specific, Rapid, 96.6% Signal after 3 month		[299]
AgNCs	AgNCs synthesized reducing $AgNO_3$ with NaBH4 stabilized by the DNA template spherical in shape with the average size of about 2 nm	Ap	*S.Typhimurium*	FL	10^2 -10^7 CFU mL^{-1}	50 CFU mL^{-1}	Specific, detecting viable S. from heat-denatured, RSD 3% n=5	Chicken meat	[300]
Carbon nanotube	Gel green fluorescence ssDNA aptasensor based on carbon nanotubes for detection of anthrax protective antigen	Ap	recombinant protective antigen domain 4 (rPAD4) of *Bacillus anthracis*	FL	5-80×10^{-6} g L^{-1}	20 ×10^{-6} g L^{-1} 62.5 ×10^{-6} gL^{-1} purified and unpurified rPAD4 protein		Mouse serum sample	[301]
AuMNPs CdTe QD	AuNPs coated Maghemite nanoparticles maghemite 10 nm	DNA Probe		FL	5×10^{-8} - 2×10^{-4} mol L^{-1}	10^{-10} mol L^{-1}	Selective, immobilization of particles with bound targets using a force of the external magnetic field	Serum	[302]
MNPs& AuNPs	MNPs close to complete super paramagnetic. AuNPs citrate 15 nm	DNA probes *Shigella spp*		FL	10^2-10^7 CFU mL^{-1}	2.1 ng mL^{-1} or 90 CFU mL^{-1}	Selective		[303]
CdTe quantum dots (QDs)	Mono disparity & spherical morphology particle size of about 3.5 nm	DNA probe Human Papillomavirus 18 virus (HPV18) gene		FL/FRET	1.0×10^{-9} 5×10^{-8} mol L^{-1}	2×10^{-10} mol L^{-1}	Selective	DNA from positive patient	[304]
CdTe QDs	Red and green CdTe QDs were 8 ± 3 nm and 5± 2 QDs showed its fluorescence emission quantum yields up to 25%	antisense-*E6-HPV16 (HPV-* probe) Gag-HIV (HIV-probe) E6-HPV16 &Gag-HIV.		FL	2×10^{-10} -10^{-7} mol L^{-1}	5×10^{-11} mol L^{-1}	Simultaneous detection of HPV & HIV, Selective, The results were approved by PCR and electrochemistry	DNA sample of Patient	[305]
lysozyme-AuNCs	Microwave-assisted synthesis AuNCs 3-6nm green and facile one-pot microwave-assisted method red fluorescence gold nanocluster	lysozyme-*E.coli*		FL	2.4× 10^4 6.0 ×10^6 CFU mL^{-1}	2.0 ×10^4 CFU mL^{-1}	Green and facile one-pot microwave-assisted method for the synthesis of red fluorescence Au nanoclusters		[306]
Guanidine @UCNP	GDN@UCNPs have good environment adaptability UCNPs hexagonal size of around 20 nm.	-	*Shigella flexneri,/ Vibrio parahaemolyticus/ Staphylococcus aureus/ Listeria monocytogenes*	FL	10^3-10^8 CFU mL^{-1}	1.3× 10^2 CFU m L^{-1}	Facile, Low cost, Without the need for biomolecule	Tap water, Beef, Milk	[307]
Au nanocluster	AuNCs25 gold atom 2.29 nm	-	*E.coli*	FL	10^3-10^6 CFU mL^{-1}	89 CFU mL^{-1}	Selective, Fast		[308]
Au nanocluster	BSA-AuNCs, HSA-AuNCs &Lys-AuNCs	-	*Pseudomonas aeruginosa, Bacillus natto, E. coli,&Acetobacter aceti*	FL	-	-	5 different bacteria and 9 protein identified by the sensor array	-	[309]
Carbon dots	CD modified with vancomycin, CD synthesized with citric acid and urea and microwave treatment, spherical and well-dispersed 2.27 ±0.3 nm	-	*Gram positive Like S.aureus*	FL	3.18× 10^5-1.59×10^8 CFU mL^{-1}	9.40×10^4 CFU mL^{-1}	Low cost and easy to perform	Orange juice	[310]
Carbon dots	Green synthesis of QDs from papaya peel Water-soluble 2– 6 nm, and ethanol 8 –18 nm soluble CD with 18.98 and 18.39 %Quantum yield respectively, Water-soluble CDs better imaging compared ethanol because of smaller size and more quick entrance to cell	-	*E.coli*	FL	-	9.5×10^4 CFU mL^{-1}	Low cost and easy to perform Water CDs and ethanol-CDs are of low toxicity to HeLa cells	-	[311]
Carbon dots	CDs@ colistin well dispersed in water 2-5 nm the quantum yield of 7.56%.	-	*E.coli*	FL	3.18× 10^2-2.44×10^8 CFU mL^{-1}	578 CFU mL^{-1}	Simple, cheap, Selective	Urine, Apple juice, Tap water	[312]

collect the solution containing both nanoparticle and poly (ethylene glycol) in a pipette tip respectively. Poly (ethylene glycol) medium caused separation Pt/MNC- *E.coli O157: H7* nanoparticle from Free Pt/MNC nanoparticle. 10 CFU mL^{-1} E.*coli O157: H7* could detect by color change (oxidation TMB with nanoparticle) [136]. More colorimetric biosensors are presented in Table 2. Lateral flow and the immunochromatographic assays will discuss in a separate part in section 3.6.

3.3. Fluorescence biosensors

Fluorescence-based sensors have attracted great interest in presenting high sensitivity, low detection limit, rapid response, low signal-to-noise ratio, simple instrumentation, and cost-effectiveness. A variety of fluorescence nano-materials such as metal nanoparticles, quantum dots (QDs), carbon dots (CDs), graphene oxide, dye-doped silica nanobeads, nanotubes, and upconversion nanoparticle have been explored in sensing application [137]. Signal generation in fluorescence sensing has been carried out following a variety of strategies including fluorescence quenching ("turn-off"), fluorescence enhancement ("turn-on"), ratiometric(calculating intensity ratio of two or more fluorescence signal), fluorescence resonance energy transfer (FRET), photoinduced electron transfer (PET) and metal enhanced fluorescence(MEF) [138].

Specific separation and detection of *E. coli O157: H7* was reported with the use of a magnetic immunoassay and QDs labeling. The capture

of the bacteria was performed in a double layer quartz channel using the immune magnetic nanoparticle trapped on the channel wall by a high gradient magnetic field. Following labeling with QD, the formed sandwich complex was collected from the channel and the fluorescence intensity of the sample measured. This was shown to relate linearly with log concentration of bacteria in the range 8.9×10^{0}–8.9×10^{5} CFUmL^{-1} [139]. The schematic of this procedure is illustrated in Fig. 4A. Aptamer coated magnetic particles labeled with QD modified complementary DNA were used in a competitive assay for the detection of *S.Typhimurium.* In the presence of the target bacteria, the aptamer-DNA label duplex was cleaved due to the aptamer-target interaction resulting in free CdTe QD labeled DNA in solution. After magnetic separation, the QDs signal in solution was recorded and demonstrated to be linearly related to 10–10^{10} CFU mL^{-1} of log pathogen concentration [140]. Application of QD and upconversion nanoparticle (UCNP) modified, respectively, with *S.Typhimurim* and *S.aureus* aptamers allowed the simultaneous detection of these two food pathogens. After attachment of the two luminescent nanoparticles to the magnetic bead contains a partially complementary DNA sequence, the fluorescence emission spectra obtained at 500 nm for QD and 800 nm for UCNP was recorded; the addition of the target pathogens to the solution containing the sensing complex resulted in the loss of fluorescence labels with a subsequent decrease in the overall signal intensity of the magnetic beads (recorded after magnetic separation). The reduced signal correlated to the log concertation of the bacteria in the 50–10^{6} CFU mL^{-1} interval [141]. Liu and coworkers extracted *V. parahaemolyticus*-specific egg yolk antibody and used these to decorate AuNPs. Interaction of CdSe/ZnS QD which was decorated with 3-mercaptopropionic acid (carrying carboxylic acid group) and AuNPs, modulated by COOH groups in the QDs and Au^{0} atom in AgNps lead to fluorescence quenching of QD. A small amount of free AuNps was also added that enable a higher rate of quenching. In the presence of *V. parahaemolyticus* due to the interaction of bacteria and antibody, IgY-AuNPs aggregated freeing in this way the QDs and increasing the fluorescence response of them. The system was applied to the sensitive detection *V. parahaemolyticus* in food samples [142]. Composite of AuNPs, gallic acid-iron oxide nanoparticle, and graphene, modified with hemagglutinin (HA) antibody, was employed as an integrated magnetic and plasmonic surface for the capturing and detection of the influenza virus. The addition of QDs, also decorated with hemagglutinin (HA) antibody, caused the formation of a sandwich complex and the fluorescence of QD increased linearly with virus concentration. The detection limits of 7.27×10^{-12} g L^{-1} and 6.07×10^{-9} g L^{-1} were obtained in deionized water and Human serum respectively [143]. Quaternary alloyed CdZnSeTes QDs which can emit in the NIR range is an attractive option for the construction of low detection limit biosensor due to the low photonic-absorption of biological molecule in this area. 2 copies mL^{-1} of Influenza virus H1N1 RNA were detected with molecular beacons (MB) modified with the aforementioned QDs by fluorescence enhancement signal transduction mechanism. In the absence of the target sequence, QDs and MB in close proximity resulted in an efficient quenching of their IR signal. Hybridization of target viral RNA with the loop sequence of the MB probe formed DNA/RNA heteroduplex which enhanced the fluorescence of QD by inducing the separation of the two particles [144]. The schematic of this procedure is illustrated in Fig. 4.B. A FRET aptasensor consisting of AuNPs modified with aptamer (acceptor) and UCNPs conjugated with complementary DNA (donor) was designed for the ultrasensitive detection of *Escherichia coli ATCC 8739*, in food sample and water, down to 5 CFU mL^{-1}. Attachment of bacteria to aptamer led to the separation of the UCNP-CDNA from the AuNPs- Aptamer resulting in the loss of the FRET effect with subsequent recovery of the fluorescence signal of the donor [145]. Hollow silica nanospheres (HSNs) encapsulated with fluorescein and covered with polymer layers of poly (acrylic acid) and poly (dimethyldiallylammonium chloride) were synthesized and used in the development of a label in a sandwich magnetic immunoassay, following modification with Ab_2 antibodies, for the detection of *E.coli*.

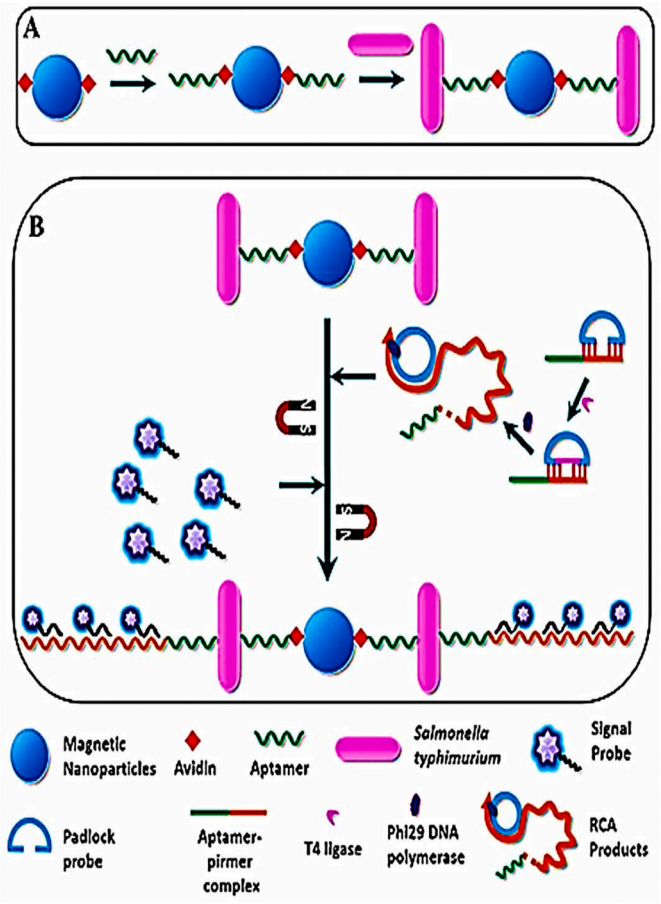

Fig. 5. The pattern of chemiluminescence biosensor A) Aptamer attachment and bacteria capturing B) Rolling circle amplification and Co^{2+}enhanced signal probes with permission ref [153].

Fe_3O_4@SiO_2@PAA-Ab_1 were used for the capture of the bacteria and the separation of the formed sandwich. Signal was generated, following the collection of the formed sandwich, by dissolution, with sodium hydroxide, of the HSNs label, and release of the internal fluorescein. The fluorescence intensity of the released fluorescein is related to the *E. coli O157: H7* concentration down to 4 CFUmL^{-1} [146]. FRET aptasensor based on AuNCs-Vancomycin and aptamer modified AuNPs as the energy donor and acceptor was developed for the sensitive detection of *S. aureus*. In the presence of *S.aureus* fluorescence intensity change ($\Delta F = F_0$-F) increased linearly with concentration 20-10^{8} of *S.aureus* [147]. Two main bacteria responsible for sepsis (*S. aureus*, *E. coli*) were separated and detected in mouse rat blood. In the presented work, Fe_3O_4 nanoparticles modified with chlorin e6 and *S.aureus and E.coli* aptamers were designed for the early and sensitive (10 CFUml^{-1}) detection of the two pathogens by fluorescence microscope. Moreover, chlorin e6, photosensitizers, applied and extracorporeal blood disinfection in mouse rats' blood was achieved with photodynamic therapy [148]. The schematic of this procedure is illustrated in Fig. 4C. A fluorometric aptasensor was fabricated by employing aptamer modified carbon nanoparticle and GO as fluorescent and quencher respectively for the sensitive detection of *P. aeruginosa.* In the presence of bacteria, the fluorescence signal was increased due to binding aptamer and bacteria that caused distance between the aptamer-carbon nanoparticle and Go, the recorded signal related linearly to 10^{1}-10^{7} CFUmL^{-1} concentration of bacteria with a LOD of 9 CFUmL^{-1} [149]. An Aptasensor consisting of MNP-Aptamer and UNCP-CDNA was developed to detect, low concentration (58 CFUmL^{-1}), *E.coli* in pork meat sample. MNP-Aptamer and UNCP-CDNA mixed and incubated for short time. Then, the addition of

Table 4
Chemiluminescence and photoluminescence biosensors, Abbriviation chemiluminesence (CL) [313–315].

Nanomaterial	Nanomaterial remark	Bio	Pathogen	Method	Linear range	LOD	Remark	Real sample	Ref
GO oxide/Fe_3O_4	Fe_3O_4 Co-precipitation	Ap	*E. coli O157:H7*	CL	10^4 – 10^7 CFU mL^{-1}.	4.5×10^3 CFU mL^{-1}.	Easy-to-use, Fast	Skim milk	[313]
Co^{2+}/N-(aminobutyl)-N-(ethylisoluminol) functional flowerlike gold Fe_3O_4-NH_2 MNP Fe_3O_4-NH_2 MNP 50nm AuNPs nm carrier for CL reagents & the catalyst to enhance CL intensity Good dispersibility and morphology with an		Ap	*S. Typhimurium*	CL	32–3.2×10^6 CFU mL^{-1}	10 CFU mL^{-1}	Selective	Pork samples	[151]
Co^{2+}/N-(aminobutyl)-N-(ethylisoluminol) functional flowerlike gold Fe_3O_4-NH_2 MNP,WS_2 Nanosheet Co^{2+}/N-(aminobutyl)-N-(ethylisoluminol) functional flowerlike gold as a donor & WS_2 Nanosheet acceptor		Ap	*Staphylococcus aureus*	CL	50-1.5×10^5 CFU mL^{-1}	15 CFU mL^{-1}	Recoveries of CL ranged from 94.7 to 102.0% 3.72% n =7	Pork paste	[153]
AuNPs	$AuNPs_C$ 20nm, Biotin, and Luminol attached to the surface of AuNPs	Ab	*Hepatitis B surface antigen*	CL	1.7×10^{-9}-1.92×10^{-6} g L^{-1}	3×10^{-10} g L^{-1}	Specific, Sensitive	Human Serum	[314]
AuCNTs, Cystamine coated CdTe QD	AuNPs 20nm	Ab	Influenza viruses H_3N_2	photoluminescence	50–10^5 $PFUmL^{-1}$	50 $PFUmL^{-1}$. 0.1 pg mL^{-1}	Selective, Sensitive	Clinical sample	[315]

E.coli release UNCP- CDNA particle due to the specific interaction of aptamer and target. Following the separation of *E.coli*-MNP-aptamer complex by the magnet, the fluorescence signal of the solution was recorded which was increased by increasing concentration of bacteria [150]. More fluorescence biosensors are demonstrated in table 3

3.4. Chemiluminechence and photoluminescence biosensors

Chemiluminescence (CL) takes advantage of the conversion of chemical energy into light. As a result, this method does not require sample radiation reducing in this way interfering phenomena such as light scattering, source instability, providing in this way high signal to noise ratio and high sensitivity; moreover, the readout instruments are less complicated than other optical systems [151,152].

Hao et al. reported on the steady-state Chemiluminescence aptasensor, based on the rolling circle amplification (RCA) method, for the sensitive detection of *S.Typhimurium*. In the proposed strategy target bacteria are captured using MNP immobilized aptamer; captured *S. Typhimurium* can then interact with the RCA product to form a sandwich complex. Finally, the formed sandwich was labeled using a Co^{+2} enhanced N- (aminobutyl)-N-(ethylisoluminol) (ABEI) functional flowerlike gold nanoparticles (AuNFs)-cDNA. Chemiluminescence signal was then generated by the addition of P-Indophenol and H_2O_2 applied to form ABEI- AuNFs-PIP-H_2O_2 Chemiluminescence system. The proposed sensor was shown to respond linearly in the concentration range between 3.2 and 3.2×10^6 CFU mL^{-1} [153]. The schematic of the presented assay was shown in Fig. 5. More examples of Chemiluminechence and photoluminescence methods are presented in Table 4.

3.5. Surface-enhanced Raman scattering (SERS) biosensors

Surface-enhanced Raman scattering is a powerful sensing tool; this presents several advantages including high sensitivity, reduced analysis time, portability as well as the ability for multiplex detection. SERS technology takes advantage of the enhancement of the Raman spectroscopy signal when performed at the surface of noble metal nanomaterials; signal enhancements of several orders of magnitude (10^7-10^{14}) were reported using this method. SERS is a fascinating method for the identification (fingerprinting) and detection of microorganisms because of its non-destructive nature. Nanomaterials like noble metal colloids, nanospheres, core-shell, gold-coated magnetic nanoparticle, nano aggregates, and bimetallic nanomaterial have been reported as promising materials for SERS detections using both labels (indirect) and label-free (direct) approaches. Labels (SERS reporters) are specific organic molecules like, Rhodamine B, 4-Nitrothiophenol 4-mercaptopurine (4-MPY), 4-amino thiophenol (4-ATP), 4-mercaptobenzoic acid and5,5-dithiobis-2-nitrobenzoic acid (DTNB) that are characterized by well-known Raman signals. Plasmonic nanoparticles decorated with Raman reporter molecules and biorecognition elements have been used to design SERS biosensors [154,155].

In a study reported by Wang et al. [156], positively charged polyethyleneimine was self-assembled on Fe_2O_4 magnetic nanoparticle; the surface of the MNP was modified, taking advantage of electrostatic interaction, with Au seeds that were then chemically grown to generate rough core/shell (Au/MNPs) label. To enable the selective capture of *S. aureus*, Au/MNPs were modified by the *S. aureus* antibody. On the other side, Au nanorods -DTNB modified with antibodies were used to complete the sandwich assay. SERS intensity at Raman peak of 1331 cm^{-1}showed a linear relationship with the logarithmic concentration of the bacteria in the range of 10^1- 10^5cells mL^{-1} [156]. Concanavalin A (Con A) is a lectin that presents the ability to specifically interact with the terminal α -D –mannosyl and α - D -glucosyl groups present on the surface of all bacteria. Kearns et al. reported on a SERS assay based on the use of Ag-MNPs core-shell system modified with Con A. The reported core-shell system enabled the capture and collection of bacteria from samples. With the help of three different SERS reporters, the authors demonstrated the multiplex detection of *S. Typhimurium, methicillin-resistant S. aureus,* and *E.coli* down to 10 $CFUmL^{-1}$ [157]. Zhou et al. carried out extensive studies on the design and fabrication of multifunctional nano-gapped nanoparticles (NNPs). In their works polydopamine (PDA) coating was used to deposit, in a controlled way (e.g. using PDA of different thicknesses), Au shells on a variety of core nanomaterials as spherical AuNPs, anisotropic Au nanorods (AuNRs), metal-organic frameworks (MOFs), and magnetic polymer nanoparticles (MAgNPs). The produced nanogap structures were reported as a carrier for Rhodamine-B or 4-nitrophenol Raman tags in bacteria sandwich assays; magnetic nanoparticle coated with PDA and 2 layers of 15 nm Au nanoshell and modified with 4- nitrophenol (Raman tag) enabled the sensitive detection of *E.coli O157: H7* down to concentration 100 CFU mL^{-1}. In the same work, the authors showed that the Raman signal could be significantly enhanced (ca. 5 folds) by the increase in the number of nanoshell layers (2 vs 1). The schematic of preparation nanogap structures is illustrated in Fig. 6A [158]. Thiol-poly adenine or Thiol-poly thymine was immobilized on the AuNps surface. Then, terminal deoxynucleotidyl transferase which was mediated incorporation of the chain of identical nucleotides utilized to synthesize nucleotide with different lengths due to change of elongation time (0 min −16 h). The prepared nanoconjugate worked as a nano seed to synthesis a gold

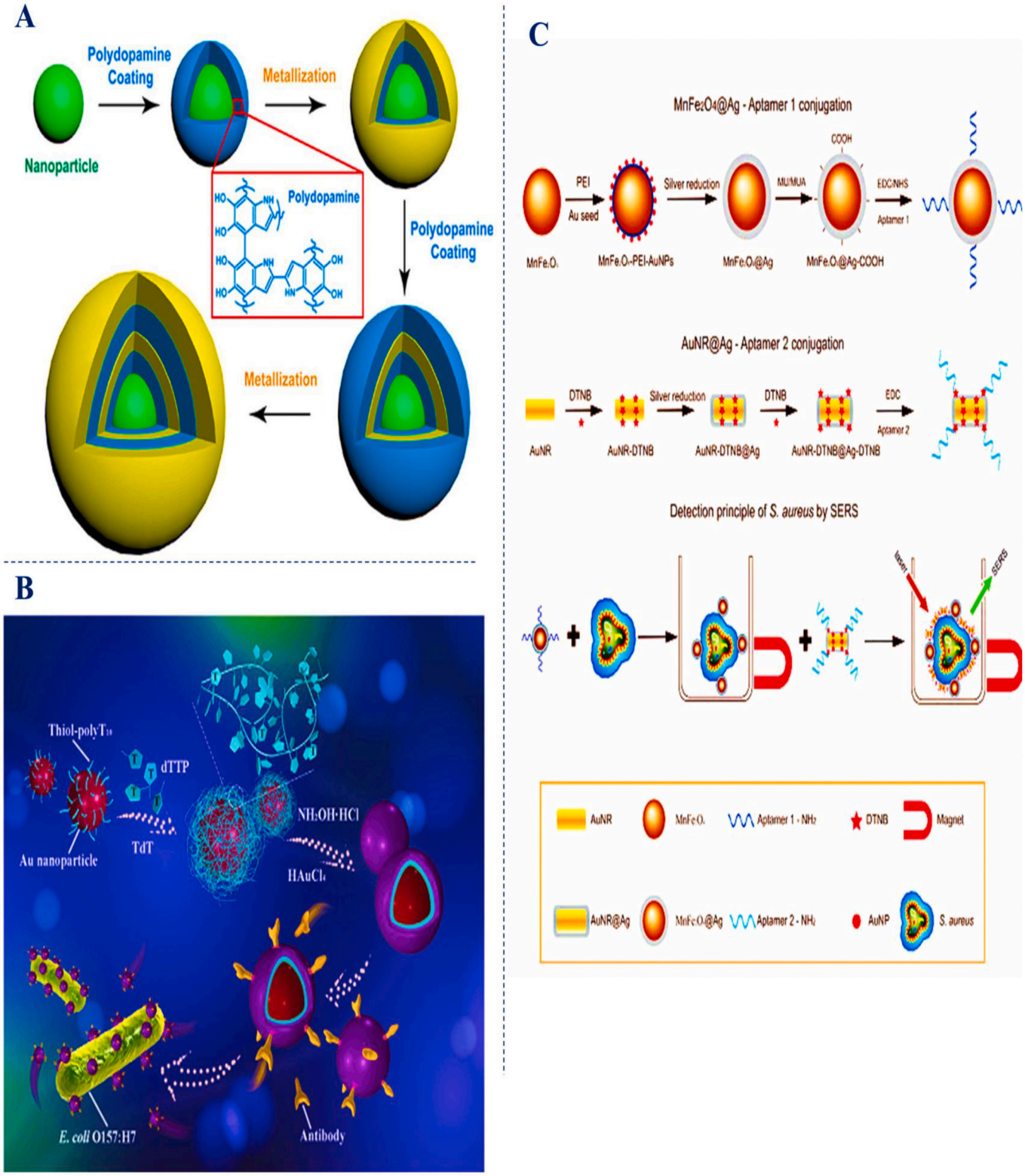

Fig. 6. A) Schematic of the synthesis nanogapped nanoparticles based on the polydopamine coating, B) Schematic of the synthetic sequence in producing hT-DENPs for recognition of E. coli O157: H7 C) Synthesis of silver-coated magnetic nanoparticles and their conjugation with aptamer 1, synthesis of core−shell plasmonic nanoparticles (AuNR− DTNB @Ag− DTNB) and their conjugation with aptamer 2 Operating principle for S. aureus detection.

layer to immobilize the antibody on it. Among different nanogap structures, the optimum one (16 h) with poly adenine was selected for the rest of the investigations. The so prepared particles were used as a Raman reporter in a bacteria immune assay that was shown to enable the detection of 2 CFU mL^{-1} of *E.coli* [159]. The schematic of the proposed immunosensor was illustrated in Fig. 6B. AuNPs decorated with 4, 4′-dipyridyl, and coated with silica layers were shown to allow bacterial detection in complex systems being stable for up to 50 h and not being prone to aggregation. The SERS immunosensor based on such nanoparticles was shown to detect 10 CFU mL^{-1} of *E.coli* [160].

Table 5
Surface-enhanced Raman scattering (SERS) biosensors, Abbreviation Loop-mediated isothermal amplification (LAMP), Membrane filter-assisted (MFA), Recombinase polymerase amplification (RPA) [316–340].

Nanoparticle	Nanoparticle performance	Biomolecule	Pathogen	method	Linear range	Detection limit	Remark	Real sample	Ref
AuNPs	distance between cy5 Raman tag less than 2 nm,	highly region within the gene	serovar - specific DNA Salmonella *Salmonella Enterica*	SERS/ LAMP	6.6×10^{0}-6.6×10^{6} CFU m L^{-1}	66 CFU m L^{-1}	Great selectivity	Milk	[316]
AuMNPs, Au nanorods	AuMNPs highly uniform in size and shape with good magnetic responsivity, stability, and high SERS activity, Superparamagnetic properties.	Ab	*S. aureus*	SERS	10^{1}-6.6×10^{5} cell mL^{-1}	10 cell mL^{-1}	Capture and fast separation of bacteria, Sonochemically assisted hydroxylamine seeding growth method for the facile synthesis of AuMNPs for the first time.		[156]
Functionalized polymeric MNPS, AuNPs	FPMNPs aqueous dispersion and storage stability up to one year at room temperature 140nm, AuNPs 31nm	Ab	*S. Typhimurium*	SERS	10^{1}-10^{7} cell mL^{-1}	10 cells mL^{-1}	Specific Good reproducibility	Cottage cheese Egg whit Juice	[317]
MNP@Ag@ ConA	MNP CO-precipitation method, Ag shell with the glucose reduction method	Ab	*S.Typhimurium, methicillin-resistant S. aureus E.coli*	SERS	10^{2}-10^{4} CFU mL^{-1}	10 CFU mL^{-1}	Easy to operate,3 different Raman reporter for simultaneous detection of 3 bacteria	-	[157]
MNP, AuNPs /SWCNT	MNP CO-precipitation method, 10-20nm	Ab	*E.coli*	SERS	10^{2}-10^{7} CFU mL^{-1}	10^{2} CFU mL^{-1}	Selective, AuNP@SWCNT photothermal killing effect	Water	[318]
Au shell	$AuNPs_C$ covered by poly adenine or thymine followed by Terminal deoxynucleotidyl transferase addition and Au Layer	Ab	*E. coli O157: H7*	SERS	10^{1}-10^{9} CFU mL^{-1}	2 CFU mL^{-1}	Specific	Apple juice	[159]
Multi shell plasmonic nanogap nanoparticle, AuNRs, MNPs	AuNRs seed-mediated method Magnetic particle co-precipitation method $AuNPs_C$ covered with polydopamine and Au shell, AuNPs covered with polydopamine and Rhodamine B	Ab	*E.coli O157:H7*	SERS	10^{2}-10^{8} CFU mL^{-1}	10^{2} CFU mL^{-1}	Selective, Adopted nanogap size by the thickness of Polydopamine, the photothermal killing effect	River water	[158]
AuNPs silica-coated	AuNPs 30nm silica shell 4 nm Magnetic beads 100nm	Ab	*E.coli O157: H7*	SERS	10-10^{8} CFU mL^{-1}	10 CFU mL^{-1}	Specific, AuNPs silica-coated stabilized signal 90 days	River water	[160]
AuMNPs, Au@MBA@ Van	Au citrate + MBA SERS tag +Vancomycin 52± 3 nm, Fe_3O_4@Au MNPs synthesized by a PEI-mediated seed growth method 200 ± 6 nm, Au shell 25 ± 5 nm 90-day stability, (MS)Fe3 O4@Au-aptamer MNPs are decreased bout 8.8% after aptamer coating	Ap	*S. aureus*	SERS	10-10^{7}cell mL^{-1}	3cell mL^{-1}	Selective, Vancomycin low price.	Milk, orange juice human blood	[163]
Spiny Gold Nps	The Spiny Gold Nps absorption peak red-shifted to 850 nm and the particle size was 200 ~120 nm	Ap	*S. Typhimurium*	SERS	10^{1}-10^{5} CFU m L^{-1}	4 CFU m L^{-1}	Excellent sensitivity, Selective, Recoveries 96.55% -105.45%	Pork	[164]
SiO_2@ Au core-shell	Silica Stöber method 200 ±19 nm	Ap	*Vibrio parahaemolyticus*	SERS	10^{1}-10^{6} CFU m L^{-1}	10 CFU mL^{-1}	Specific, cyanine dye Raman tag	Shrimp	[319]
GO oxide wrapped Fe_3O_4@Au	GO oxide wrapped Fe_3O_4@Au as separation source and SERS substrate $AuNPs_C$ 13 nm Fe_3O_4	Ap	*Vibrio parahaemolyticus*	SERS	1.4×10^{2}-1.4×10^{6} CFU m L^{-1}	14 CFU m L^{-1}	Selective	Salmon samples	[320]
$AuNPs_C$	$AuNPs_C$ 40 nm Capture DNA	Ap	*E.coli O157: H7*	SERS	10^{2}-10^{6} CFU m L^{-1}	10^{1} ground beef 10^{2}CFU mL^{-1}	Specific,10^{2}CFU mL^{-1} ground beef	Ground beef	[321]
AuNPs		Ap	*S. enteritidis*	SERS	1.4×10^{3}-1.4×10^{7} CFU m L^{-1}	10^{3} CFU m L^{-1}	Specific, Fast (3h)	Fresh spinach	[322]
MNPs, AuNPs	MNPs Co-precipitation method $AuNPs_C$ 15nm	Ap	*S. Typhimurium & S. aureus*	SERS	10^{2}-10^{7} CFU mL^{-1}	35& 15 CFU mL^{-1} *S. aureus & S. Typhimurium* Selective		Commercial pork	[323]
AgNPs	AgNPs $NaBH_4$	Ap	*S.aureus*	SERS	10^{1}-10^{7} CFU mL^{-1}	1.5 CFU mL^{-1}	Absence of Raman marker		[161]
$MnFe_2O_4$, AgMNPs, Au Nanorod	$MnFe_2O_4$ Superparamagnetic 170nm binary solvent Solvothermal AgMNPs 200nm DTNB-labeled inside-and-outside plasmonic NPs (DioPNPs) that exhibits high SERS conjugates with target recognition molecules (Ab or Ap)	Ap	*S. aureus*	SERS	10^{1}-10^{5} cells mL^{-1}	10 cells mL^{-1}	Specific, Raman signal of DioPNPs is 10 times		[162]
Ag@Au nanoshells	$AuNPs_C$ + $AgNO_3$+ Ascorbic acid AuNPs 15 nm+ Ag shell 4nm	Ap	*S. Typhimurium*	SERS	15-1.5×10^{6} CFU mL^{-1}	15 CFU mL^{-1}	Selective	Milk	[165]

MNP, AuNPs	Magnetic nanoparticles 15-20 nm co-precipitation method, $AuNPs_C$ MNP increased the Raman intensity due to thin Au shell surfaces, enabled the MGNPs to maintain their magnetic property but also obtain a much better dispersibility.	Ap	*S. Typhimurium*	SERS	10^1-10^7 CFU mL^{-1}	5 CFU mL^{-1}	Selective	Pork	[324]
Ag NRs	Ag NRs synthesized in a custom-built electron beam evaporator using the oblique angle deposition technique	Ap	*S. Typhimurium*	SERS	-	10^8 CFU mL^{-1}	Label-free	-	[325]
MNP, AuNPs	MNP 30 nm	Ab	*E.coli O157: H7,*	SERS/ MFA	10-500 CFU mL^{-}	10 CFU mL^{-1}	Selective	Ground beef	[326]
Fe_3O_4@Au nanoparticle, Fe_3O_4@AuVan	Fe_3O_4@Au nanoparticle uniform in size and morphology, with 250 nm, 25 nm Au shell Fe_3O_4@AuVan ,Vancomycin layer 1.5nm	Ap	*E. coli & S. aureus*	SERS	50- 10^5 *E.coli* 20- 10^5 *S. aureus* cell mL^{-1}	20 and 50 cells mL−1 for S. aureus &*E. Coli*	Selective, Rapid capture of bacteria, Fe_3O_4@Au effectively capture bacteria in comparisonFe_3O_4@Au	Urine	[327]
AuNPs, AuNds	AuNds 35 nm DNA carrier, AuNPs 15 nm asymmetric gold nanodimers uniform & monodisperse stabilized SERS activity	Ap	*S. Typhimurium*	SERS	10^2-10^7 CFU mL^{-1}	35 CFU mL^{-1}	Selective,	Milk	[328]
Silica Encapsulated Nanotags, MNP	Raman reporter +Au layer+ Silica shell 1015nm, SERS nanotags with shielding shells to avoid the leaching of Raman reporters and capture biomolecules as well as to	Ab	*West Nile virus* (WNV) *envelope (E) protein, Rift Valley fever virus (RVFV) nucleocapsid (N) protein, Capsular antigen fraction 1 (F1) Yersinia pestis*	SERS	10^{-8}– 10^{-5}g L^{-1}	10^{-11}g mL^{-1} in 20% fetal bovine serum	The thickness of the silica shell is important, Simultaneous detection	Fetal bovine serum	[329]
MNPs/SiO_2 AuNPs	Large $AuNPs_C$ 51 nm+ MBA MNPs CO-participation	DNA tags	target bacterial DNA sequence	SERS/ PCR	10^{-20}-10^{-12} mole	zeptomole (4.1×10^{-11}) g/L	Excellent sensitivity	-	[330]
Fe_3O_4@Ag-Van MNPs, Au@Ag core–shell	Superparamagnetic Fe_3O_4particles ~200 nm vancomycin-modified Ag capture agent and SERS substrate,30 s separation Au@Ag core-shell NPs 60 nm	*E. coli BL21, S. aureus , &MRS aureus*		SERS	5×10^2 Cell m L^{-1}	5×10^2 Cell mL^{-1}	11mercaptoundecanoic acid Raman Tag bifunctional linker thiol and carboxylic acid	Milk Blood	[331]
AgNPs	Microwave heating method,50-70 nm AgNPs greatly enhanced the SERS signal of bacteria	*- E.coli O157: H7,S.aureus Salmonella*		SERS	-	10^7 CFU mL^{-1}	Without the need for biomolecule	-	[332]
AgNPs	AgNPs Hydroxylamine in basic solution	*E.coli*		SERS	1×10^5- 1×10^7 Cell mL^{-1}	10^5 Cell m L^{-1}	Without the need for biomolecule	-	[333]

Fe_3O_4@PEI @Au, Fe_3O_4@Au@ PEI, Au@AgNPs	Fe_3O_4 300nm solvothermal, Au shell 3 nm super-paramagnetic, Au@AgNPs 60 nm better SERS activity, The Au@Ag–bacteria complexes showed an improvement about 1.5 and 3.2 times stronger than 60 nm Au NPs and50 nm Au NPs	*E. coli & S. aureus*	10^3-10^7 cells mL^{-1}	Rapid, Simple operation		Tap water, Milk	[334]
AgNPs		*S. enterica and Listeria monocytogenes*	3.5×10^4 3.5×10^7 CFU mL^{-1}	10^2 CFU mL^{-1}	3-mercaptophenylboronic acid capture and reporter for bacteria		[335]
Ag collides	Synthesis of AgNPs within a bacterial culture with $NaBH_4$	*P. aeruginosa, L.mono cytogenes & L. innocua and MRSA-86, MRSA-35*	*L. innocua* 10^3- 10^5 CFU mL^{-1}	Pre-treatment of cells with Triton X-100 considerably enhanced the sensitivity			[336]
AgNPs	In situ synthesis of Ag nanoparticles with close contact with the bacterial membrane.	*E. coli, M. morganii, E. lactis, L. casei*	SERS	Rapid, Low cost, single-cell detection			[337]
AgNPs, AuNPs	$AgNPs_C$	*E.coli, Shewanella putrefaciens Pseudomonas aeruginosa*	SERS	Discriminate between the three yeast species			[338]
AgNPs	$AgNPs_C$100nm	*Yeast, Saccharomycescerevisiae, Dekkera bruxellensis Wickerhamomyceanomalus*	SERS	Discriminate between the three yeast species		Beer	[339]
Au@Ag	Au@Ag self-assembled mussel shell AgNPs 40 ± 12.5 nm with 5nm shell	*E. coli, S.aureus, & P. aeruginosa*	SERS	Discriminate between the three bacteria			[340]

Label-free detection of *S.aureus* was performed by the use of specific aptamers and by in situ synthesis, using the aptamer as a template, on AgNPs. The SERS spectra of *S.aureus*-aptamer/AgNPs were shown to be significantly higher than those recorded in the absence of the aptamer. The system was reported to have a low LOD of 1.5 CFU mL^{-1} [161]. Ag coated magnetic nanoparticle (AgMNPs) and AuNR –DTNB@Ag-DTNB (DioPNP) as SERS tags were reported in single-cell detection of *S.aureus*. These were modified with aptamer 1 and 2, respectively, to form a dual sandwich structure; the Raman signal of DioPNPs was shown to be 10 times stronger than those of the AuNR−DTNB due to double-layer DTNB [162]. The schematic of preparation nanoparticle and bacteria detection was shown in Fig. 6C. Dual enhancement SERS aptasensor was developed by Pang et al. and applied to the detection of *S.aureus;* Fe_3O_4@Au –Aptamer nanoparticles were used for the specific recognition/capture of the target bacteria with SERS signal, due to the captured target, generated at the Au layer. The second element of the assay was AuNPs modified with-4 mercaptobenzoic acid (Raman label) and vancomycin (for bacteria capturing). The proposed biosensor was shown to allow detection of the pathogen in a wide range of concentrations (10-10^7 $CFUmL^{-1}$) with a LOD of 3$CFUmL^{-1}$ [163]. Ma et al. developed a sensitive aptasensor with the aid of pointy-like AuNPs that have unique field enhancement especially at the tip of the branches. The pointy-like AuNPs were used, following functionalization with 4- mercaptobezoeic acid and thiolated aptamer, as SERS label in ELISA plate-based aptamer assay. ELISA plates were modified with biotinylated aptamer used to capture *S.Typhimurium*. The proposed detection approach was shown to detect down to 10 CFU mL^{-1} of *S.Typhimurium* [164]. Duan et al. reported on an aptasensor for the detection of *S.Typhimurium;* this was based on the use of an Au@Ag core-shell nanoparticle modified with aptamer 1 as a signal enhancer and of aptamer2-X-rhodamine as SERS label. The fabricated biosensor enables sensitive detection of *S.Typhimurim* down to 15 $CFUmL^{-1}$ [165]. More example of SERS bio/sensor are summerized in Table 5.

3.6. Lateral flow-based biosensors

Lateral-flow immunoassay (LFIA) also known as lateral-flow immunochromatographic (LF- ICA) tests are simple, rapid, and portable systems which enable qualitative, non-invasive point of care detection (POC) with wider applications in medical diagnostic [166].

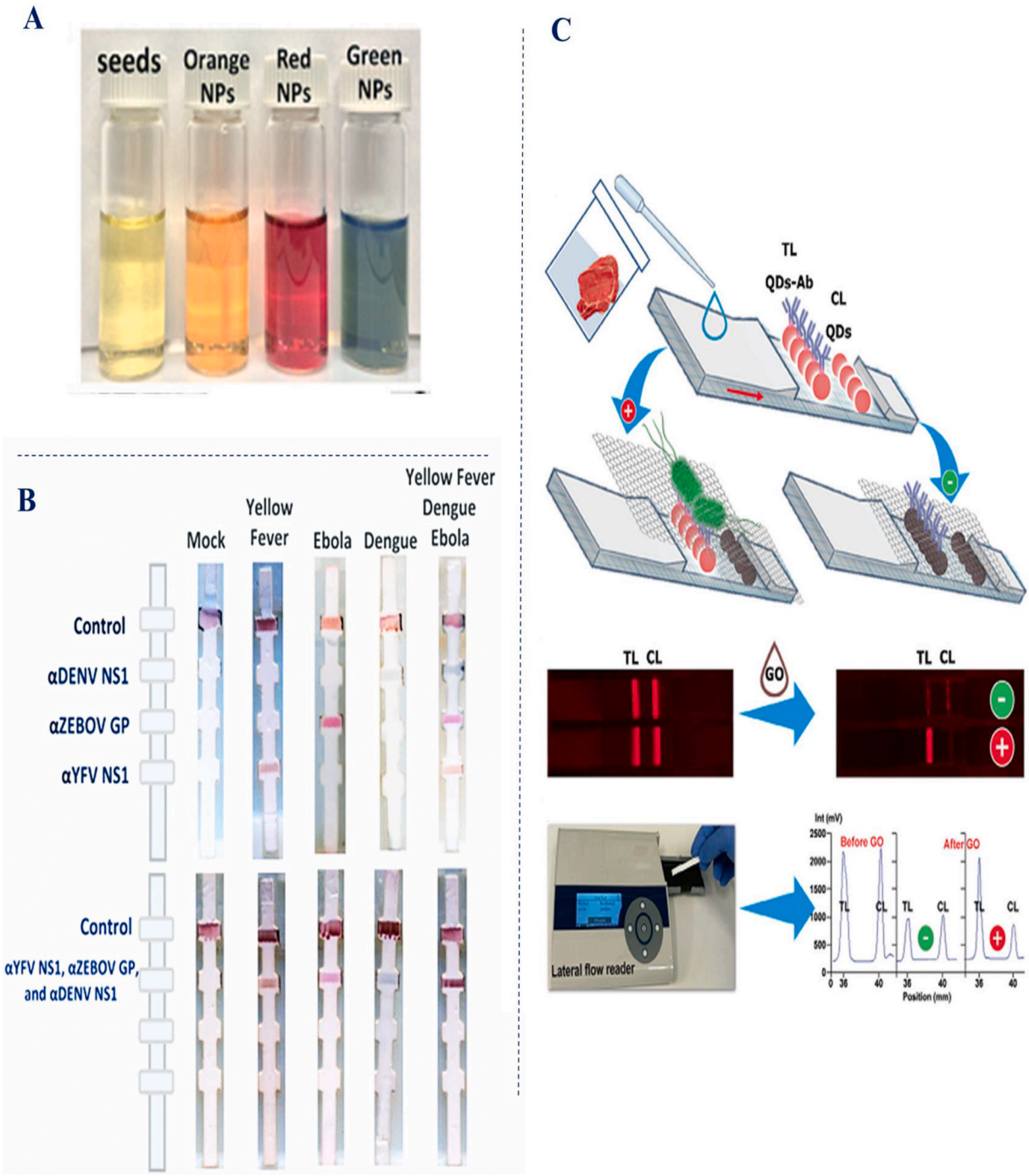

Fig. 7. A) AgNPs for multiplexed detection, B) Multiplex detection of dengue, yellow fever, and Ebola viruses with permission ref [173] C) Fluorescent lateral flow immunoassay ref [177]. (For interpretation of the references to color in this figure legend, the reader is referred to the Web version of this article.)

Conventional LFA system suffers from low sensitivity; nevertheless, in recent times several approaches for the improvement of LFA have reported including gold enhancement, enzyme labeling, increased loading of antibody, and use of various nanomaterials like QD, UCNP, peroxidase-like nanoparticle, and graphene oxide. Besides coupling LFIA systems with instrumental reading (fluorescence, colorimetric, SERS, and magnetic focus) enabled to obtain more reliable and quantitative data [167,168].

An innovative approach, combining gold-coated Fe_3O_4 magnetic nanoparticle (Au/MNCs) and lateral flow filters, was shown to allow the detection of 10^3 CFUmL^{-1} *Salmonella* from milk samples. In the proposed assay *Salmonella* was captured in milk samples using antibody fragment modified Au/MNCs; the formed complex following separation was resuspended in a buffer solution. The assay was then performed by immersing one end of the lateral stripe in the solution; if on one end the free Au/MNCs were able to move in the LFI strip and accumulating in the test line, the *Salmonella*-Au/MNCs were remained in the solution because of their big size; pressing of the nitrocellulose membrane was key factor in the success of the proposed assay. The colour of the test line decreased with increasing pathogen concentration because of a decrease in free Au/MNCs nanoparticle [169]. The same author also developed a similar strategy for the visual detection of *E.coli O157: H7* (10^3 CFU mL^{-1}) [170]. Cho et al. developed the lateral-flow immunochromatographic LF-ICA system based on AuNP-biotin and streptavidin -HRP

complex. A mixture of tetramethylbenzidine and H_2O_2, applied in the cross-flow direction of the antigen-antibodies complex, was used as a reagent for the generation of the colorimetric signal; the proposed assay allowed the naked eyes detection of *Cronobacter sakazakii* down to 10^2 CFU mL^{-1} [171]. The size and uniformity in the shape of AuNPs were shown to influence the sensitivity of LFIA. Cui and co-workers investigated the effect of size and uniformity of AuNPs and pre-incubation of AuNPs/antibody/*E. coli O157: H7* on the visual and instrumental reading of a colorimetric test strip. The authors synthesized AuNPs with size 20, 28, 35, 43, 54 nm; AuNPs of 35 nm showed the best results. If on one end smaller nanoparticles, due to their smaller steric hindrance, interacted more effectively with bacteria, larger ones offered better optical signal, and the 35 nm nanoparticles had plasmonic resonance wavelength 525 which was the same as the wavelength light of light source in the reader. Nanoparticles with lower polydispersity indices (PDI) provide a superior limit of detection [172]. Yen et al. synthesized AgNPs with different size and colour modified with *dengue* virus *(DENV) NS1* protein, *Yellow Fever Virus (YFV) NS1* protein, and *Zaire strain Ebola* virus glycoprotein *(ZEBOV)* for single and multiplex detection of these viruses. The visual detection of the three viruses demonstrates to be possible down to 150 $ngmL^{-1}$ [173]. Different AgNPs with the prepared stripe is depicted in Fig. 7A. Jin et al. investigated 15 different AuNps decorated polystyrene microparticle (Au-Ps) with different sizes (0.1.0.3,0.46) μm and Au coverage (5, 10, 25, 50, 75%) to find the nanoparticle with the highest sensitivity for visual detection of *E.coli O157: H7*. The optical density of the different nanoparticles was used as the physical parameter to discriminate between the manufactured particles and to select the best one. According to the optical density values, the UV–vis spectrums, and the TEM images, (50Au-0.46 PS) was expected to provide the better result nevertheless average grayscale analysis by image J software showed that lower LOD could be achieved with the (10Au-0.46 PS) nanoparticle. The same authors also studied the effect of signal enhancement by reduction of $HAuCl_4$ with hydroxylamine; this enhancement step lowered the LOD down to 100 $CFUmL^{-1}$and average 1.44 folds improvement for each concentration [174]. Eu (III) doped polystyrene nanoparticles were demonstrated in immunochromatographic assay for detection of *E .Coli O157: H7*. EuNP-6 carbon chain (CC), EuNP-200CC, EuNP-1000CC and EuNP-streptavidin were compared; EuNP-Streptavidin, due to their better ability to load antibodies, showed better sensitivity and wider linear range [175]. Ren et al. reported on the combination of Fe_3O_4/Au core-shell and HRP signal enhancement for the detection of pathogens. The use of the described system, in combination with an external magnet to slow down the movement of the labeled target which enabled the interaction of pathogens and antibody more readily, allowed detection limits of 25$CFUmL^{-1}$ E. *coli O157: H7* or *S. Typhimurium* [176]. A fluorescence lateral flow immunosensor was designed by taking advantage of the quenching properties of GO (acceptor) and the fluorescence ability of QDs (donor). In the proposed assay the test line contained CdSe@ZnS QDs/anti-*E. coli O157:H7* antibody while the control line only had bare QDs. In the absence of target bacteria, addition of GO resulted in the quenching of the fluorescence of the QDs in both the test and the control lines. By contrast, capturing of *E. coli O157: H7* with antibody, increase the distance between QD and GO, therefore reducing the ability of GO to quench the QDs; the intensity of the residual fluorescence was shown to be proportional to the pathogen concentration in the range 50–10^5 CFU mL^{-1} with LOD 57 CFU mL^{-1} [177]. The schematic of the assay was showed in Fig. 7B. Surface positive nitrogen-rich carbon nanoparticle (pNC), prepared from urea by calcination and etching reaction, were shown to have a good ability to adsorb/capturing bacteria. In the proposed LFIA monoclonal antibodies present on the test line were used to capture the complex made between the pNC and the bacteria; the intensity of back color of the test line was shown to relate to the concentration of *S. enteritidis* in the 10^2–10^8 CFU mL^{-1} interval [178]. Plasmonic LFIA with improved performances based on the AuNPs aggregation induced by polyethyleneimine (BPEI) released from liposome was reported by Ren et al. for the sensitive detection of *E. coli O157: H7*. Targeted bacteria were incubated with AuNPs modified with an antibody; following a certain time BPEI-loaded liposomes were added to the solution. The obtained mixture was added to the strip followed by the addition of free-AuNPs. The added nanoparticles were then captured at the test line by the BPEI present on the surface of the bacteria/AuNPs complex resulting in the generation of a colorimetric signal due to the aggregation effect. The proposed immunosensor could detect 100 $CFUmL^{-1}$ *of E. coli O157: H7* [179].

The peroxidase activities of some nanomaterials lead to select them as a prominent candidate for use in LFIA with improved sensitivity. For example, the peroxidases activity of Pt-AuNPs modified with antibody were explored to generate, upon reaction with TMB, a colored band in correspondence of the test line. The proposed assay enabled the detection of 10^2 $CFUmL^{-1}$ *E. coli O157: H7* [180]. Mesoporous core-shell Pd@Pt with the help of TMB and H_2O_2 was used for the simultaneous detection of *S.enteritidis* and *E. coli O157: H7* with LFIA and smartphone detection down to 20 and 34 $CFUmL^{-1}$ of *S. enteritidis and E. coli O157: H7* while the detection limit of the system for both pathogens was 10^6 $CFUmL^{-1}$ in the absence of TMB and H_2O_2 system. AuNR@Pt with peroxidase activity toward TMB and H_2O_2 and also SERS properties with 4-mercaptobezoic acid Raman reporter were explored for dual recognition, LFIA and SERS methods; the two methods allowed, respectively, the detection of *C. jejuni* in the 10^2–10^6 and 10^2–5×10^6 CFU mL^{-1} concentration ranges [181]. Use of Fe_3O_4 MNP as a nano-enzyme probe was reported by Han et al. for the LIFIA detection of the glycoprotein of the *Ebola* virus. The ability of the MNPs to catalyze the conversion of 3, 3′-Diaminobenzidine (DAB) in the presence of H_2O_2 allowed the detection of the glycoprotein at 1 ng mL^{-1} concentration which is 100 times lower than that achievable with the standard strip method (1 ng mL^{-1}) [182]. Bimetallic Pd-Pt nanoparticles were also explored as nano-enzyme for the conversion of TMB and H_2O_2 in LFIA for the detection of *E.coli O157: H7;* the proposed assay showed LOD of 10^2 $CFUmL^{-1}$ [183]. Fe_3O_4/Au- polyethyleneimine nanoparticles-casein-antibody complex were applied to capture *E. coli*, followed by cleavage of casein by rennet enzyme to release *E.coli*. Released bacteria were loaded on strip modified with DTNB labeled AuNPs and AuNPs modified with the antibody on the conjugate pad and test line respectively. The intensity of the test line was recorded which was increased with concentration 10^1–10^7 CFU mL^{-1} *E. coli* with LOD 0.52 CFU mL^{-1} [184]. Luo et al. compared 4 different nanoparticles including AuNPs, QD, Fluorescent nanoparticles (FNP), and Eu(III) chelate nanoparticles for application in the immunochromatographic assay for the detection of *E.coli O157: H7*. The EuNP showed the highest fluorescence intensity, larger Stokes shift, and sharpest emission profile, therefore the EuNP showed the highest sensitivity and fluorescent nanoparticles and EuNP provided the wider linear range. It needs to be noted that fluorescent nanoparticles were shown to require less antibody per strip [185]. Aptamer mediated strand displacement approach was reported for the sensitive detection of *E. coli O157: H7*. In the reported assay a reporting aptamer and a capture probe, modified with biotin, were used. Target bacteria were incubated with the two aptamers and extracted using streptavidin magnetic beads. After the separation of the magnetic complex, the reporting aptamer was amplified with the isothermal strand displacement amplification method and detected with LFIA. This method enabled visual detection of 10 $CFUmL^{-1}$ E. *coli O157: H7* [186]. Mesoporous silica nanoparticles, embedded with TMB and covered with amin-aptamer gate sequence, were employed for the sensitive detection of *L. monocytogenes*. The addition of bacteria caused the release of TBM due to their specific interaction with the aptamers. Released TMB interact with HRP enzymes trapped in the test line to produce the visible blue color. The aptasensor could obtain LOD of 53 cells in 1 mL sample [187]. AuNPs modified with 4-mercaptobenzoic acid (as a Raman tag), Ag layer, streptavidin and BSA were used as a label for the detection of *L.monocytogenes* and *S. enterica* DNA sequences. In the proposed assay the targeted DNA sequences were amplified, before their LFIA detection, using recombinase polymerase amplification method. The proposed assay allowed the visual and SERS detection of the targeted sequences with LOD of 27 and 19 $CFUmL^{-1}$. Visual qualitative detection was made possible via the aggregation of the

Table 6
Lateral flow-based biosensor detection Lateral flow immunoassay (LFIA) immunochromatographic immunoassay (ICA) Fluorescence Lateral flow immunoassay (FLFIA), Immunomagneticseparation (IMS), Polymerase chain reaction (PCR), Strand displacement amplification (SDA) [341–374].

Nanomaterial	Nanomaterial remark	Bio		Method	Linear range	LOD	Remark	Real sample	Ref
$AuNPs_C$	$AuNPs_C$ 30nm	Ab	*Pseudomonas syringaepv. maculicola*	LFIA	10^3- 10^7 CFU mL^{-1}	10^3CFU mL^{-1}	Broccoli and radish seeds, the IC strips sensitivity of 5×10^5& 10^6 CFU mL^{-1}	Broccoli & Radish seeds	[341]
$AuNPs_C$	$AuNPs_C$ average diameter 35 nm	Ab	*Cronobacter sakazakii*	LFIA	10^7-10^3 CFU mL^{-1}	10^3 CFU mL^{-1}	Specific, Enhancement 100 times in LOD and 3h in enrichment time by increasing the amount of Ab by conjugating with concentrated AuNPs in the test line	Powdered infant formula	[167]
$AuNPs_C$	$AuNPs_C$ 24nm in diameter	Ab	*E.coli O157:H7*	LFIA	1.65×10^4 - 3.3×10^6 CFU mL^{-1}	1.58×10^4 CFU mL^{-1}	Selective, Simultaneous detection of *E.coli O157:H7*& *Aflatoxin M*1	Milk	[342]
$AuNPs_C$	15nm	Ab	*Listeria*	LFIA	10^3 -10^4 CFU mL^{-1}	10^3 CFU mL^{-}	Selective, Sensitivity enhance 1order of magnitude by strip reader 1–9 CFU mL^{-1}after 8h	Milk	[343]
$AuNPs_C$	$AuNPs_C$ 15 nm	Ab	*Listeria monocytogenes*	LFIA	-	3.7×10^6 CFU mL^{-1}	Specific, 8- 12 h enrichment for Milk sample	Milk	[344]
Au/MNCs	MNC synthesized with the hydrothermal method, MNCs and Au/MNCs 160 and 180 nm, $AuNPs_C$ 14nm	Ab	*E.coli O157:H7*	Size-sortig LFIA	10^3 -10^6 CFU mL^{-1}	10^3 CFU mL^{-1}	Selective, Novel strategy by squeezing a nitrocellulose membrane to reduce its thickness	Milk	[170]
Au/MNCs	MNC synthesized with the hydrothermal method, MNCs and Au/MNCs 160 and 180 nm, $AuNPs_C$ 14nm	Ab	*Salmonella*	Size-sorting LFIA	10^3-10^5 CFU mL^{-1}	10^3 CFU mL^{-1}	Selective, Novel strategy by squeezing a nitrocellulose membrane to reduce its thickness	Milk	[169]
AuNPs	AuNPs Size 40 nm	Ab	*E.coli O157:H7*	LF-ICA	10^3 -10^6 CFU mL^{-1}	10^3 Visual CFU mL^{-1}	Selective, Applying AuNP-Avidin and biotin-HRP complex. HRP catalyzes TMB oxidation	Ground beef	[171]
AuNPs	$AuNPs_C$ solutions with different PDI and size 20,28,35,43,54	Ab	*E.coli O157:H7*	LFIA	10^3-10^7CFU mL^{-1}	10^3CFU mL^{-}	Uniform size AuNPs size and separated incubation of AuNPs/antibody/E. coli O157:H7 complex to improve sensitivity 35nm best 10^3CFU mL^{1} Specific reader10^2CFU mL^{-1}	-	[172]
MNPs	MNPs hydrothermal method	Ab	*glycoprotein (GP) of the Ebola Virus*	LFIA	10^{-6} – 10^{-3}g L^{-1}	10^{-6}g L^{-1} 240 PFU mL^{-1} pseudo-EBOV	Selective,100 fold increase in sensitivity with help MNPs intrinsic peroxidase-like activity feature & DAB	Clinical sample	[182]
Au magnetic bifunctional nanobeads	30 nm	Ab	*Salmonella choleraesuis*	ICT	1×10^8 5×10^5 CFU mL^{-1}	5×10^5 CFU mL^{-1}	Selective	Milk	[345]
AuNPs	$AuNPs_C$ 20 nm	Ab	*Salmonella*	LFIA	10^4-10^8 CFU mL^{-1}	10^4 CFU mL^{-1}	Selective	River water	[346]
$AuNPs_C$	Fe_3O_4 $AuNPs_C$ 30 nm	Ab	*Enterobacter cloacae*	IMS/ ICT	10^3-10^7 CFU mL^{-1}	10^2 CFU mL^{-1}	With the use of Immunomagnetic beads, the target bacteria were separated and enriched, Selective,10 times higher than that obtained by direct detection with ICTS	Water	[347]
AuNPs	AuNPs 15 nm	Ab	*Shigella boydii & (E . coli O157:H7*	ICA	10^6-10^8 CFU mL^{-1}	10^6 CFU mL^{-1}	With pre-incubation 4CFU mL^{-1}	Bread Milk Jelly	[348]
AuNPs	A 28 nm and 45 nm with spherical shape were demonstrated to be the optimal dual pair	Ab	*E.coli O157: H7*	LFIA	10^3-10^3 CFU mL^{-1}	1.14×10^3 CFU mL^{-1}	Comparing 4 nanoparticles with size 18,28,45,80 as dual pair.	Reduced-fat milk	[349]
AuNPs, QD, FNP, EuNps	AuNPs, QD,FNP, EuNps size 21, 11, 182, 155 nm EuNP had the highest fluorescence intensity	Ab	*E.coli O157: H7*	LF-ICA	1.0×10^4- 1.0×10^6 2.5×10^3 - 1.0×10^6 2.5×10^2 - 2.5×10^5 2.5×10^2 -2.5×10^5 For GNP-ICA, QD-ICA, FNP-ICA EuNP-ICA	2.5×10^4 5×10^3 1.0×10^3 5.0×10^2 CFU mL^{-1} For GNP-ICA, QD-ICA, FNP-ICA, EuNP-ICA	Specific, Comparing 4 nanoparticle The EuNP-ICA showed the highest sensitivity, FNP-ICA need the least Ab per strip, The FNP-ICA, and EuNP-IC broader linear range FNP-ICA and EuNP-ICA better resistance in the milk sample	Milk	[185]
Au-decorated polystyrene particles (Au-PS)	AuNPsC Mixing AuNPs With PS and boiling them to 100 ° C AuNPs 20 nm diameter size dispersed on PS particle surface	Ab	*E. O157: H 7*	LFIA	5×10^2- 1×10^6 CFU·mL^{-1}	500 CFU·mL^{-1}	Selective, lowered LOD 1×10^2CFU·mL^{-1} with signal amplification with1 w t% $HAuCl_4$ and10mMNH_2OH·HCl 1:10, Au- PS particles with0. 46 μm PS with 50% Au coverage has maximum OD but the one with 10% coverage has better LOD	Ground beef	[174]

AgNPs	Three AgNPs by seed-mediated growth method, Size: orange30 ± 7 nm, Red 41 ± 6 nm, green= 47 ± 8 nm	A b	*Dengue, Yellow Fever protein, and Ebola viruses glycoprotein*	LFIA	150-500 $\times 10^{-6}$ g L^{-1}	150 $\times 10^{-6}$ g L^{-1}	Multiplex detection with three different AgNPs, Selective	Human serum	[173]
Carboxyl functionalized superparamagnetic beads	140 nm	A b	*Listeria monocytogenes*	LFIA/ Magnetic assay reader	10^4-10^8 CFU mL^{-1}	10^4 CFU mL^{-1}	Specific	Food samples	[350]
Core-shell red silica nanoparticle	Monodispersed SiO_2 covered reactive red 126 NPs were prepared by Stöber methods spherical morphology and good dispersity diameter 216 nm	A b	*E.coli O157: H7*	LFIA	4.5 $\times 10^4$ -4.5 $\times 10^5$ CFU mL^{-1}	4.5×10^5 CFU m L^{-1}	Specific 4.5 $\times 10^6$ –CFU mL^{-1} Milk and pork sample	Pork and milk sample	[351]
Nanobeads	Magnetic nanobeads	A b	*E.coli O157: H7*	FLFIA	Selective, Stroger signal with magnetic nanobeads Detect 1,5, 25, and 125 CFU of in 25 mL milk in 8, 7, 6, and 5 h.			Milk	[352]
Eu (III)-doped polystyrene nanoparticle	EuNP & EuNP-linker size 158 , 159 , 158 , 161,159 nm,	A b	*E. O157: H7*	FICA	8×10^1-1.59×10^5 CFU·mL^{-1}	1.08×10^2 CFU·mL^{-1}	Selective, carboxyl-modified EuNPs with 4 linkers. EuNP-SA-ICA best result	Milk	[175]
EuNPs	EuNPs 103 nm ± 1.4 nm, EuNP-McAb 114 nm ± 1.7 nm	A b	E. coli O157:H7	FLFIA	10^4-10^7	Strip& quantitative detection was 10^4 & 5 × 10^2 CFU mL^{-1} with the test-strip reader	Specific, Pre-incubation for 8 h in meat and 6 h Milk LOD1CFU mL^{-1}	Beef, Pork, Chicken	[353]
Fe_3O_4/Au core-shell AuNPs.	Au core-shell nano-35-50 nm AuNP40 nm.	A b	*E. coli O157:H7, S.Typhimurium*	LFIA/ Magnetic focus	0-10^2 CFU mL^{-1}	25 CFU mL^{-1}	Specific	Pineapple juice	[176]
CdSe/ZnS-COOH	Water-soluble QD Spherical 3nm	A b	*E. coli O157: H7*	FLFIA	10^4-10^9 CFU mL^{-1}	10^4 CFU mL^{-1}	Specific, 35-day stability, fast detection time 12 min	Milk	[354]
GO & r GO	GO, rGO and conjugated rGO sheets 1 μm,rGo produce higher color intensity	A b	*E. coli O157: H7*	LFIA	10^5-10^7 CFU mL^{-1}	10^5 CFU mL^{-1}	Specific, rGO10^6 Drinking water 10^7 Milk CFU mL^{-1}	Milk Drinking water	[355]
Go, CdSe@ZnS	CdSe@ZnS QDs, of size14 ± 2 nm & maximum emission wavelength at ≈665 nm	A b	*E. coli O157: H7*	FLFIA	50 to 10^5 CFU mL^{-1}	57 CFU mL^{-1}	Selective,178 and 133 CFU g^{-1}or mL^{-1} real sample, The single Antibody approach reduced the assay cost to 60% less,	Minced beef Water	[177]
GO, CdSe@ZnS	Optimal QDs concentration be 1.5 nM The optimum GO concentration was determined to be 90 μg mL	A b	*E. coli*	FLFIA	10-10^5 CFU mL^{-1}	10 CFU mL^{-1}	10 CFU mL^{-1}in standard buffer and 100 CFU mL^{-1}in bottled water and milk	Bottled water Milk	[356]
MoS_2 & GO	MoS_2& Go nanosheets well defined laminar morphology with a uniform size of around 200 and 500 nm	A b	*Salmonella enteritidis*	LFIA/ICT	MoS_2 10^3-10^8 GO 10^4-10^8 CFU mL^{-1}	MoS_2 10^3 GO 10^4 CFU mL^{-1}	Specific	Drinking water Watermelon juice	[357]
CdSe/ZnSQDs /Fe_3O_4 .	carboxyl-poly styrene/acrylamide copolymer nanospheres 250 nm coated with Fe_3O_4 and QDs repeatedly and with an outer silica layer	A b	*S.Typhimurium*	LFIA/ FL Magnetic reader	1.88×10^4 - 1.88 × 10^7 CFU mL^{-1} FL	1.88 × 10^4 CFU mL^{-1} Typhi, 3.75× 10^3 a magnetic assay reader, range of 1.88	Selective, Simple	Tap water Milk, Fetal bovine serum Whole blood	[358]
Streptavidin AuNPs	40nm	A b	*Salmonella and E.coli Amplicon*	Quadruple tagging PCR/NAFA	*E.coli* 7×10^{-6}g L^{-1} Salmonella 9.5×10^{-5}g L^{-1}	-	Simultaneous detection, Selective 6.6×10^{-7}g L^{-1}gL-^{1}for *E.coli* (in presence of high concentrations of *Salmonella*), 1.17×10^{-6}L^{-1}For salmonella (in presence of High concentration of E.coli		[359]
Surface positively charged nitrogen-rich Carbon nanoparticles(g-C_3N_4)	g-C_3N_4 pNC generate a signal and capture Bacteria	A b	*Salmonella enteritidis*	LFIA	10^2-10^8 CFU mL^{-1}	10^2 CFU mL^{-1}	Good sensitivity, Broad linear range, Specific, Single Ab, Recoveries ranging from 85% - 110%.	Potable water, Coleslaw cabbage Salad, watermelon juice Purple cabbage	[178]
$NaYF_4$:Yb^{3+}/Er^{3+}	50 nm	A b	*E. coil O157: H7 S. parayphi A S. parayphi B, S. parayphi C, S. enteritidis, S. Typhi, S. choleraesuis, V. cholera O1,*	LFIA	10^4 -10^8 CFU mL^{-1}	10^4 or 10^5 CFU mL^{-1} Enrichment 10 CFU mL^{-1}	Simultaneous detection of 10 pathogens	Dairy products Marine products Beverages Snacks Meats	[360]

			V. cholera O139, V. parahaemolyticus						
Pd-Pt nanoparticles	Pd-Pt nanoparticles size 40 nm	A b	*E.coli O157: H7*	LFIA	10^2-10^6 CFU mL^{-1} 10^3-10^6 CFU mL^{-1}	1×10^2 CFU mL^{-1} PBS 9×10^2 CFU mL^{-1} in Milk	Selective, Amplifying signal With peroxidase-like catalytic activities of Pd-Pt NP& TMB & H_2O_2	Milk	[183]
Au-Pt bimetallic	Porous 50 nm.	A b	*E. coli O157: H7*	ICA	10^2–10^8 CFU mL^{-1}	10^2 CFU mL^{-1}	Amplifying signal With peroxidase-like catalytic activities of Au-Pt NP& TMB & H_2O_2	-	[180]
Pd@Pt	Pd@Pt mesoporous core-shell l35 nm	A b	*S.enteritidis& E. coli O157:H7*	LFIA/ Smartphone		10^2 CFU mL^{-1}	Selective, Simultaneous, 30 day stability,10^6 CFU mL^{-1} without TMB & H_2O_2	Milk Ice cream	[361]
MNPs, AuNPs	MNPs 180 nm AuNPs 13 nm	Ab DNA probe	*Listeria monocytogenes*	IMS/LFIA	10^3–10^7 CFU mL^{-1}	3.5×10^3 CFU mL^{-1} 3.5×10^4 CFU g^{-1} Lettuce	Selective, Eliminate dead cell, Less amount of Ab, based on biotin exposure strategy	lettuce samples	[362]
Magnetic beads	1000, 500, 200 , 130 nm size	A b	*E.coli*	Visual/ CO/ LFIA	10^5–10^7 CFU mL^{-1}	10^5 CFU mL^{-1}	Selective, 6-month stability	River water	[363]
AuNR@Pt	AuNR@Pt length & diameter of around 65 and 15 nm, with Pt layer with the spiky shape	A b	*Campylobacter jejuni*	SERS/ LFIA	10^2–10^6 CFU mL^{-1} and 10^2 –5×10^6 CFU mL^{-1}	75 CFU mL^{-1} and 50 CFU mL^{-1}	Selective, Easy operation, Rapid	Milk Chicken	[181]
Casein modified Fe_3O_4 /Au-PEI	$AuNPs_C$ 2-6 nm	A b	*E. coli*	SERS/ LFIA	10^1–10^7 CFU mL^{-1}	LOD 0.52 and LOQ = 1.57 CFU mL^{-1}	Selective, Wide linear range	Urine Milk	[184]
AuNPs	AuNPs 25nm	A b	*S.Typhimurium*	ICA/ELISA	1.3×10^5-2×10^6 CFU mL^{-1}	1.25×10^5 Milk 1.25×10^5 CFU mL^{-1}	Specific, Comparison 10 different antibody	Milk	[364]
carboxylate-modified CdSe/ZnS core@shell, Fe_3O_4, Fe_3O_4@SiO_2, Fe_3O_4@SiO_2@ NH_2, Fe_3O_4@SiO_2@QD	QD 10 nm, Fe_3O_4solvothermal method spherical 100 nm Fe_3O_4@SiO2 @NH_2 250 nm,Fe_3O_4@SiO2@QD Stöber255 nm	A b	*E. coli O157: H7*	FLFIA /IMS	2.5×10^2-5×10^5 CFU mL^{-1} Visual	2.5×10^3 Visual 2.39×10^2 CFU mL^{-1} FL	Specific, Optimization of QD amount and MNP, Silica layer have NH_2 functional group and separated QDs from MNBs and decrease the	Milk	[365]
AuNPs	$AuNPS_C$ decorated with Raman label, $AuNPS_C$ 21.56± 4.52, for Antibody interaction pH 9 is optimum	A b	*E. coli ATCC 35218*	LFIA/ SERS/ CL	10^3-10^8 CFU mL^{-1} CL 10^3-10^6 CFU mL^{-1} SERS	78CO 45 SERS CFU mL^{-1}	10 mm Pore size had a slightly higher intensity. DTNB better than Glutathione as Raman label	Urine Blood	[366]
AuNPs	AuNPs 20nm	A b	*E. coliO157:H7, S. Typhimurium, S. aureus , Bacillus cereus*	LFIA	10^4-10^6 CFU mL^{-1}	10^5,10^6,10^5 10^5 *E.coliO157:H7, S.Typhimurium, S. aureus, Bacillus cereus* CFU mL^{-1}	Rotary type device1.87×10^4CFU of *E. coli O157: H7* $1.47\times 10^4$of *S. Typhimurium*, 1 CFU g^{-1}*E. Coli O157: H7 and S. Typhimurium* after 6 h preconcentration	Lettuce	[367]
UCP($NaYF4:Yb^{3+}$),Er^{3+}	Stable optical property	A b	*Francisella tularensis*	LFIA	10^4-10^9CFU mL^{-1}	10^4CFU mL^{-1}	Selective, pH 2–13, high ion strengths , high viscosities, high concentrations of bio macromolecules showed little influence	Seven powders and Eight viscera	[368]
AuNPs	$AuNPs_C$	A b	*Salmonella serogroups*	LFIA/ CO	-	-	Arrangement of five Salmonella serogroups. Three test line	Feces Anal swab	[369]
Hierarchical flowerlike AuNPs	20 nm AuNPs as seeds &polyelectrolyte PDDA as polymer capping agent to synthesize hierarchical flowerlike Au particles, AuNPs 20,40 nm	A b	*E. coli O157: H7*	LFIA/ CO	10^3-10^7CFU mL^{-1}	10^3CFU mL^{-1}	Comparing 5 different nanoparticles, diverse shaped AuNPs showed better sensitivity 2 order of magnitude better than spherical AuNPs 20 nm	-	[370]

AuNPs	$AuNPs_C$ 18 nm	A b *E. coli O157: H7*	pLFIA	100-600 CFU mL^{-1}	100 CFU mL^{-}	Colorimetric signal improved by utilizing liposome encapsulating polyethyleneimine to activate the aggregation of gold nanoparticles 1000 fold better sensitivity, 600 $CFUmL^{-1}$*E. coli O157: H7* in cranberry juice	Cranberry juice	[179]
QD	-	A p *E.coli*	FLFA	-	15-150 Viable cell	Specific, Test 7 Big aptamer sequence	-	[371]
AuNPs Magnetic bead	AuNPs 15 nm citrate	A p *E. coli O157: H7*	SDA/LFA	$10–10^6$ CFU mL^{-1}	10 CFU mL^{-1}		Milk powder, Water, Apple juice	[186]
AuNPs		A p *Vibrio parahaemolyticus*	SDA/LFA	$10–10^7$ CFU mL^{-1}	10 CFU mL^{-1}	Selective, 200 CFU mL^{-1} in Oyster	Oyster	[372]
Au^{MBA}@Ag core-shell nanoparticles	Au^{MBA}@Ag core the the diameter of 23.58 nm shell thickness 8.48 adding MBA solution to the AuNPs solution followed by ascorbic acid reduction of silver nitrate	DNA probe *L. monocytogenes & S.enterica*	RPA/LFA/SERS	1.9×10^1-1.9×10^6 2.7×10^1-2.7×10^6 CFU mL^{-1} *L. monocytogenes &S.enterica*	19 & 27 for CFU mL^{-1} *L. monocytogenes &S.enterica*	Specific	Milk, Chicken breast, Beef	[188]
$AuNPs_C$	$AuNPs_C$ 30 – 40 nm	DNA probe *HIV-1 viruses*	SERS/LFA	10^{-8}-10^{-4} gL^{-1}	8×10^{-9} mL^{-1}, Naked eye8 $\times10^{-8}$ gL^{-1}	Specific	-	[373]
Mesoporous silica nano-particles	Silica nanoparticle prepared with sol-gel method hexagonal pore structure 2.4 nm mesopores	A p *Listeria monocytogenes*	LFA/Apgated release	3×10^1–3×10^6 CFU mL^{-1}	53 cells mL^{-1}	Selective	Minced Chicken meat	[187]
$AuNPs_C$	$AuNPs_C$ 20 nm, Polystyrene beads -Au-PEI particles	A p *E. coli O157: H7*	LFA/digital camera	$10–10^3$ CFU mL^{-1}	25 CFU mL^{-1}, 253 CFU mL^{-1} Naked eye, 233 CFU mL^{-1} Ground beef	Specific, Novel modification Carboxyl functionalized DNA aptamers to effectively graft the aptamer on the label particles surface, Inkjet printer fabrication for patterning of aptameric ink	Ground beef	[374]

nanoparticle in the two test lines containing specific capturing probes while the SERS signal of test lines was measured for quantitative detection of bacteria. SERS signal was shown to be linear with target concentration in the 1.9×10^1–1.9×10^6 and 2.7×10^1–2.7×10^6 interval for *L.monocytogenes* and *S. enterica* respectively [188]. More examples of lateral flow based biosensor are available in Table 6.

4. Conclusion and future prospective

In this review, various nanomaterials and their application in different detection systems for infectious agents covered. Nanomaterials as magnetic nanoparticles alone and in combination with Ag or Au coatings, bimetallic nanoparticles, peroxidase-like nanomaterials, and newly designed nanomaterials have been described and their widespread application in electrochemical and optical biosensing discussed. Applications as separation materials, materials for improving conductivity, and elements for biomolecules grafting have been described. Besides, their application in colorimetric, fluorometric, and SERS detection methods was also reported. Finally, we demonstrated the advantage of the usage of these materials to enhance the sensitivity of the lateral flow strip test. Although some authors illustrated comparative data to highlight the benefits of the usage of nanomaterials, there is still the need for more investigation to understand the real effect and advantages of exploiting nanomaterials in various sensing applications. In the future, we expect novel functional biomimetic and bimetallic nanomaterial or bionanocomposite with fascinating features will be introduced. Moreover, innovative designs strategies with the help of biochemical pathways to shorten the analysis time, to obtain the results of the molecular techniques such as PCR and LAMP and to produce efficient and rapid POC devices to be used in the field will report. Nanoenzye material may replace natural recognition receptors to produce more durable biosensors. One of the biggest challenge for the nanomaterials are their work in various real-samples matrices such as blood, serum, urine or stool in biomedical or various food matrices or for example sewage water in case of environmental samples. Therefore we expect a lot of attention will be directed towards the development of more efficient nanomaterials characteristics with minimum non-specific binding and low false positive signals. We also expect much attention will be paid in the future towards the development of multifunctional nanomaterials where it integrates for example specific analyte fishing or preconcentration tool as well as sensing platform. Despite the numerous proposed biosensors, there is still a crucial need for developing new biosensors for on-site monitoring of infectious diseases to prevent epidemic and economic loss.

Declaration of competing interest

The authors declare that they have no known competing financial interests or personal relationships that could have appeared to influence the work reported in this paper.

References

[1] H.J. Lim, T. Saha, B.T. Tey, W.S. Tan, C.W. Ooi, Quartz crystal microbalance-based biosensors as rapid diagnostic devices for infectious diseases, Biosens. Bioelectron. 168 (2020), 112513.

[2] F.S. World Health Organization, 2015 http://www.who.int/, mediacentre/factsheets/fs399/en/.

[3] R.M. Renuka, J. Achuth, H.R. Chandan, M. Venkataramana, K. Kadirvelu, A fluorescent dual aptasensor for the rapid and sensitive onsite detection of E. coli O157: H7 and its validation in various food matrices, News J. Chem42 (2018) 10807–10817.

[4] J. Zhang, J. Wang, X. Zhang, F. He, Rapid detection of Escherichia coli based on 16S rDNA nanogap network electrochemical biosensor, Biosens. Bioelectron. 118 (2018) 9–15.

[5] D.E. Bloom, D. Cadarette, Infectious disease threats in the twenty-first century: strengthening the global response, Front. Immunol. (2019).

[6] N. Reta, C.P. Saint, A. Michelmore, B. Prieto-Simon, N.H. Voelcker, Nanostructured electrochemical biosensors for label-free detection of water- and food-borne pathogens, ACS Appl. Mater. Interfaces 10 (2018) 6055–6072.

[7] E. Sheikhzadeh, S. Eissa, A. Ismail, M. Zourob, Diagnostic techniques for COVID-19 and new developments, Talanta 220 (2020), 121392.

[8] S. Mehmood, R. Ciancio, E. Carlino, A.S. Bhatti, Role of Au(NPs) in the enhanced response of Au(NPs)-decorated MWCNT electrochemical biosensor, Int. J. Nanomed. 13 (2018) 2093–2106.

[9] L. Peng, B.L. Li, C.W. Zhou, N.B. Li, M.I. Setyawati, H.L. Zou, "Naked-eye" recognition: emerging gold nano-family for visual sensing, Appl. Mater. Today 11 (2018) 166–188.

[10] M. Miernicki, T. Hofmann, I. Eisenberger, F. von der Kammer, A. Praetorius, Legal and practical challenges in classifying nanomaterials according to regulatory definitions, Nat. Nanotechnol. 14 (2019) 208–216.

[11] J. Jeevanandam, A. Barhoum, Y.S. Chan, A. Dufresne, M.K. Danquah, Review on nanoparticles and nanostructured materials: history, sources, toxicity and regulations, Beilstein J. Nanotechnol. 9 (2018) 1050–1074.

[12] P.T. Snee, Semiconductor quantum dot FRET: untangling energy transfer mechanisms in bioanalytical assays, TrAC Trends Anal. Chem. (Reference Ed.) 123 (2020), 115750.

[13] S. Liu, B. Yu, S. Wang, Y. Shen, H. Cong, Preparation, surface functionalization and application of Fe3O4 magnetic nanoparticles, Adv. Colloid Interface Sci. 281 (2020), 102165.

[14] T.A.P. Rocha-Santos, Sensors and biosensors based on magnetic nanoparticles, TrAC Trends Anal. Chem. (Reference Ed.) 62 (2014) 28–36.

[15] R. Bonnet, C. Farre, L. Valera, L. Vossier, F. Léon, T. Dagland, A. Pouzet, N. Jaffrézic-Renault, J. Fareh, C. Fournier-Wirth, C. Chaix, Highly labeled methylene blue-ds DNA silica nanoparticles for signal enhancement of immunoassays: application to the sensitive detection of bacteria in human platelet concentrates, Analyst 143 (2018) 2293–2303.

[16] Q. Li, C.W. Kartikowati, S. Horie, T. Ogi, T. Iwaki, K. Okuyama, Correlation between particle size/domain structure and magnetic properties of highly crystalline Fe3O4 nanoparticles, Sci. Rep. 7 (2017) 9894.

[17] O.A. Noqta, A.A. Aziz, I.A. Usman, M. Bououdina, Recent advances in iron oxide nanoparticles (IONPs): synthesis and surface modification for biomedical applications, J. Supercond. Nov. Magnetism 32 (2019) 779–795.

[18] S. Tong, H. Zhu, G. Bao, Magnetic iron oxide nanoparticles for disease detection and therapy, Mater. Today 31 (2019) 86–99.

[19] S. Gul, S.B. Khan, I.U. Rehman, M.A. Khan, M.I. Khan, A comprehensive review of magnetic nanomaterials modern day theranostics, Front. Mater. 6 (2019).

[20] F. Sharifianjazi, M. Moradi, N. Parvin, A. Nemati, A. Jafari Rad, N. Sheysi, A. Abouchenari, A. Mohammadi, S. Karbasi, Z. Ahmadi, A. Esmaeilkhanian, M. Irani, A. Pakseresht, S. Sahmani, M. Shahedi Asl, Magnetic CoFe2O4 nanoparticles doped with metal ions: a review, Ceram Int46 (11, Part B) (2020) 18391–18412.

[21] K. Zhou, X. Zhou, J. Liu, Z. Huang, Application of magnetic nanoparticles in petroleum industry: a review, J. Petrol. Sci. Eng. 188 (2020), 106943.

[22] T. Xiao, J. Huang, D. Wang, T. Meng, X. Yang, Au and Au-Based nanomaterials: synthesis and recent progress in electrochemical sensor applications, Talanta 206 (2020) 120210.

[23] J. Fei, W. Dou, G. Zhao, A sandwich electrochemical immunosensor for Salmonella pullorum and Salmonella gallinarum based on a screen-printed carbon electrode modified with an ionic liquid and electrodeposited gold nanoparticles, Microchim. Acta 182 (13–14) (2015) 2267–2275.

[24] A. Güner, E. Çevik, M. Şenel, L. Alpsoy, An electrochemical immunosensor for sensitive detection of Escherichia coli O157:H7 by using chitosan, MWCNT, polypyrrole with gold nanoparticles hybrid sensing platform, Food Chem. 229 (2017) 358–365.

[25] Z. Khoshbin, M.R. Housaindokht, A. Verdian, M.R. Bozorgmehr, Simultaneous detection and determination of mercury (II) and lead (II) ions through the achievement of novel functional nucleic acid-based biosensors, Biosens. Bioelectron. 116 (2018) 130–147.

[26] W. Phanchai, U. Srikulwong, A. Chompoosor, C. Sakonsinsiri, T. Puangmali, Insight into the molecular mechanisms of AuNP-based aptasensor for colorimetric detection: a molecular dynamics approach, Langmuir 34 (2018) 6161–6169.

[27] Y. Lu, S. Xu, J. Lou, Gold nanorods, in: B. Bhushan (Ed.), Encyclopedia of Nanotechnology, Springer Netherlands, Dordrecht, 2014, pp. 1–9.

[28] M. Gorbunova, V. Apyari, S. Dmitrienko, Y. Zolotov, Gold nanorods and their nanocomposites: synthesis and recent applications in Anal. Chem, TrAC Trends Anal. Chem. (Reference Ed.) (2020), 115974.

[29] L. Yu, Z. Song, J. Peng, M. Yang, H. Zhi, H. He, Progress of gold nanomaterials for colorimetric sensing based on different strategies, TrAC Trends Anal. Chem. (Reference Ed.) 127 (2020) 115880.

[30] A. Onaciu, C. Braicu, A.-A. Zimta, A. Moldovan, R. Stiufiuc, M. Buse, C. Ciocan, S. Buduru, I. Berindan-Neagoe, Gold nanorods: from anisotropy to opportunity. An evolution update, Nanomedicine 14 (2019) 1203–1226.

[31] X. Qu, Y. Li, L. Li, Y. Wang, J. Liang, J. Liang, Fluorescent gold nanoclusters: synthesis and recent biological application, J. Nanomater. (2015), 784097.

[32] M. Liu, F. Tang, Z. Yang, J. Xu, X. Yang, Recent progress on gold-nanocluster-based fluorescent probe for environmental analysis and biological sensing, J. Anal. Methods Chem. (2019), 1095148.

[33] T. Kawawaki, Y. Negishi, Gold nanoclusters as electrocatalysts for energy conversion, Nanomaterials (Basel) 10 (2020) 238.

[34] Y. Zhang, C. Zhang, C. Xu, X. Wang, C. Liu, G.I.N. Waterhouse, Y. Wang, H. Yin, Ultrasmall Au nanoclusters for biomedical and biosensing applications: a mini-review, Talanta 200 (2019) 432–442.

[35] A. Loiseau, V. Asila, G. Boitel-Aullen, M. Lam, M. Salmain, S. Boujday, Silver-based plasmonic nanoparticles for and their use in biosensing, Biosensors (Basel) 9 (2019).

[36] M. Sabela, S. Balme, M. Bechelany, J.-M. Janot, K. Bisetty, A review of gold and silver nanoparticle-based colorimetric sensing assays, Adv. Eng. Mater. 19 (2017) 1700270.

[37] H.S. Lee, B.-H. Jun, Silver nanoparticles: synthesis and application for nanomedicine, Int. J. Mol. Sci. 20 (2019).

[38] G. Sharma, A. Kumar, S. Sharma, M. Naushad, R. Prakash Dwivedi, Z. A. Alothman, G.T. Mola, Novel development of nanoparticles to bimetallic nanoparticles and their composites: a review, J. King Saud Univ. Sci. 31 (2019) 257–269.

[39] P. Srinoi, Y.-T. Chen, V. Vittur, M.D. Marquez, T.R. Lee, Bimetallic nanoparticles: enhanced magnetic and optical properties for emerging biological applications, Appl. Sci. 8 (2018) 1106.

[40] Z. Dehghani, M. Hosseini, J. Mohammadnejad, B. Bakhshi, A.H. Rezayan, Colorimetric aptasensor for Campylobacter jejuni cells by exploiting the peroxidase like activity of Au@Pd nanoparticles, Microchim. Acta 185 (2018) 448.

[41] R. Mandal, A. Baranwal, A. Srivastava, P. Chandra, Evolving trends in bio/chemical sensor fabrication incorporating bimetallic nanoparticles, Biosens. Bioelectron. 117 (2018) 546–561.

[42] N. Arora, K. Thangavelu, G.N. Karanikolos, Bimetallic nanoparticles for antimicrobial applications, Front. Chem. 8 (2020).

[43] K. Loza, M. Heggen, M. Epple, Synthesis, structure, properties, and applications of bimetallic nanoparticles of noble metals, Adv. Funct. Mater. 30 (2020), 1909260.

[44] F. Ma, C.-c. Li, C.-y. Zhang, Development of quantum dot-based biosensors: principles and applications, J. Mater. Chem. B 6 (2018) 6173–6190.

[45] K. Mokwebo, O. Oluwafemi, O. Arotiba, An electrochemical cholesterol biosensor based on A CdTe/CdSe/ZnSe quantum dots—poly (propylene imine) dendrimer nanocomposite immobilisation layer, Sensors 18 (2018) 3368.

[46] H. Liu, X. Wang, H. Wang, R. Nie, Synthesis and biomedical applications of graphitic carbon nitride quantum dots, J. Mater. Chem. B 7 (2019) 5432–5448.

[47] V.G. Reshma, P.V. Mohanan, Quantum dots: applications and safety consequences, J. Lumin. 205 (2019) 287–298.

[48] J.C. Bonilla, F. Bozkurt, S. Ansari, N. Sozer, J.L. Kokini, Applications of quantum dots in Food Science and biology, Trends Food Sci. Technol. 53 (2016) 75–89.

[49] X. Bo, M. Zhou, L. Guo, Electrochemical sensors and biosensors based on less aggregated graphene, Biosens. Bioelectron. 89 (2017) 167–186.

[50] Y. Du, S. Guo, S. Dong, E. Wang, An integrated sensing system for detection of DNA using new parallel-motif DNA triplex system and graphene–mesoporous silica–gold nanoparticle hybrids, Biomaterials 32 (2011) 8584–8592.

[51] A.T. Dideikin, A.Y. Vul, Graphene oxide and derivatives: the place in graphene family, Front. Physiol. 6 (149) (2019).

[52] L. Wang, A. Wu, G. Wei, Graphene-based aptasensors: from molecule–interface interactions to sensor design and biomedical diagnostics, Analyst 143 (2018) 1526–1543.

[53] C. Punckt, F. Muckel, S. Wolff, I.A. Aksay, C.A. Chavarin, G. Bacher, W. Mertin, The effect of degree of reduction on the electrical properties of functionalized graphene sheets, Appl. Phys. Lett. 102 (2) (2013), 023114.

[54] S. Muniandy, I.J. Dinshaw, S.J. Teh, C.W. Lai, F. Ibrahim, K.L. Thong, B.F. Leo, Graphene-based label-free electrochemical aptasensor for rapid and sensitive detection of foodborne pathogen, Anal. Bioanal. Chem. 409 (2017) 6893–6905.

[55] S. Taniselass, M.K.M. Arshad, S.C.B. Gopinath, Graphene-based electrochemical biosensors for monitoring noncommunicable disease biomarkers, Biosens. Bioelectron. 130 (2019) 276–292.

[56] P.T. Yin, S. Shah, M. Chhowalla, K.-B. Lee, Design, synthesis, and characterization of graphene–nanoparticle hybrid materials for bioapplications, Chem. Rev. 115 (2015) 2483–2531.

[57] N.-F. Chiu, C.-T. Kuo, C.-Y. Chen, High-affinity carboxyl-graphene oxide-based SPR aptasensor for the detection of hCG protein in clinical serum samples, Int. J. Nanomed. 14 (2019) 4833.

[58] S.J. Rowley-Neale, E.P. Randviir, A.S. Abo Dena, C.E. Banks, An overview of recent applications of reduced graphene oxide as a basis of electroanalytical sensing platforms, Appl. Mater. Today 10 (2018) 218–226.

[59] P. Gholami, A. Khataee, R.D.C. Soltani, A. Bhatnagar, A Review on Carbon-Based Materials for Heterogeneous Sonocatalysis: Fundamentals, Properties and Applications, Ultrason. Sonochem, 2019, 104681.

[60] M. Sireesha, V. Jagadeesh Babu, A.S. Kranthi Kiran, S. Ramakrishna, A review on carbon nanotubes in biosensor devices and their applications in medicine, Nanocomposites 4 (2018) 36–57.

[61] N. Anzar, R. Hasan, M. Tyagi, N. Yadav, J. Narang, Carbon nanotube - a review on Synthesis, Properties and plethora of applications in the field of biomedical science, Sens. Int. 1 (2020), 100003.

[62] C. Xia, S. Zhu, T. Feng, M. Yang, B. Yang, Evolution and synthesis of carbon dots: from carbon dots to carbonized polymer dots, Adv. Sci. 6 (2019), 1901316.

[63] X. Luo, Y. Han, X. Chen, W. Tang, T. Yue, Z. Li, Carbon dots derived fluorescent nanosensors as versatile tools for food quality and safety assessment: a review, Trends Food Sci. Technol. 95 (2020) 149–161.

[64] A. Cayuela, M.L. Soriano, C. Carrillo-Carrión, M. Valcárcel, Semiconductor and carbon-based fluorescent nanodots: the need for consistency, Chem.Commun. 52 (2016) 1311–1326.

[65] X. Wang, Y. Feng, P. Dong, J. Huang, A mini review on carbon quantum dots: preparation, properties, and electrocatalytic application, Front. Chem. 7 (2019).

[66] C. Testa, A. Zammataro, A. Pappalardo, G. Trusso Sfrazzetto, Catalysis with carbon nanoparticles, RSC Adv. 9 (2019) 27659–27664.

[67] J.F.-C. Loo, Y.-H. Chien, F. Yin, S.-K. Kong, H.-P. Ho, K.-T. Yong, Upconversion and downconversion nanoparticles for biophotonics and nanomedicine, Coord. Chem. Rev. 400 (2019), 213042.

[68] Z. Zhang, S. Shikha, J. Liu, J. Zhang, Q. Mei, Y. Zhang, Upconversion nanoprobes: recent advances in sensing applications, Anal. Chem. 91 (2019) 548–568.

[69] R. Rafique, S.K. Kailasa, T.J. Park, Recent advances of upconversion nanoparticles in theranostics and bioimaging applications, TrAC Trends Anal. Chem. (Reference Ed.) 120 (2019), 115646.

[70] Q. Sun, G. Zhao, W. Dou, An optical and rapid sandwich immunoassay method for detection of Salmonella pullorum and Salmonella gallinarum based on immune blue silica nanoparticles and magnetic nanoparticles, Sensor. Actuator. B Chem. 226 (2016) 69–75.

[71] Q. Sun, G. Zhao, W. Dou, A nonenzymatic optical immunoassay strategy for detection of Salmonella infection based on blue silica nanoparticles, Anal. Chim. Acta 898 (2015) 109–115.

[72] H. Zhu, G. Zhao, S.Q. Wang, W. Dou, Photometric sandwich immunoassay for Salmonella pullorum and Salmonella gallinarum using horseradish peroxidase and magnetic silica nanoparticles, Microchim. Acta 184 (2017) 1873–1880.

[73] A.F. Moreira, C.F. Rodrigues, C.A. Reis, E.C. Costa, I.J. Correia, Gold-core silica shell nanoparticles application in imaging and therapy: a review, Microporous Mesoporous Mater. 270 (2018) 168–179.

[74] E. Sheikhzadeh, M. Chamsaz, A.P.F. Turner, E.W.H. Jager, V. Beni, Label-free impedimetric biosensor for Salmonella Typhimurium detection based on poly [pyrrole-co-3-carboxyl-pyrrole] copolymer supported aptamer, Biosens. Bioelectron. 80 (2016) 194–200.

[75] N.A.M.R. Housaindokht, E. Sheikhzadeh, Design of a disposable solid state potentiometric sensor for codeine content control in pharmaceutical preparations, Sens. Lett. 12 (2014) 1341–1346.

[76] S. Eissa, N. Alshehri, A.M.A. Rahman, M. Dasouki, K.M. Abu-Salah, M. Zourob, Electrochemical immunosensors for the detection of survival motor neuron (SMN) protein using different carbon nanomaterials-modified electrodes, Biosens. Bioelectron. 101 (2018) 282–289.

[77] J. Fei, W. Dou, G. Zhao, Amperometric immunoassay for the detection of Salmonella pullorum using a screen - printed carbon electrode modified with gold nanoparticle-coated reduced graphene oxide and immunomagnetic beads, Microchim. Acta 183 (2016) 757–764.

[78] F. Zhu, G. Zhao, W. Dou, Electrochemical sandwich immunoassay for Escherichia coli O157:H7 based on the use of magnetic nanoparticles and graphene functionalized with electrocatalytically active Au@Pt core/shell nanoparticles, Microchim. Acta 185 (2018).

[79] F. Zhu, G. Zhao, W. Dou, A non-enzymatic electrochemical immunoassay for quantitative detection of Escherichia coli O157:H7 using Au@Pt and graphene, Anal. Biochem. 559 (2018) 34–43.

[80] Z. Wang, Z. Chen, N. Gao, J. Ren, X. Qu, Transmutation of personal glucose meters into portable and highly sensitive microbial pathogen detection platform, Small 11 (2015) 4970–4975.

[81] Y. Wang, E.C. Alocilja, Gold nanoparticle-labeled biosensor for rapid and sensitive detection of bacterial pathogens, J. Biol. Eng. 9 (2015).

[82] M. Xu, R. Wang, Y. Li, An electrochemical biosensor for rapid detection of: E. coli O157:H7 with highly efficient bi-functional glucose oxidase-polydopamine nanocomposites and Prussian blue modified screen-printed interdigitated electrodes, Analyst 141 (2016) 5441–5449.

[83] D. Brandão, S. Liébana, S. Campoy, S. Alegret, M.I. Pividori, Immunomagnetic separation of Salmonella with tailored magnetic micro and nanocarriers. A comparative study, Talanta 143 (2015) 198–204.

[84] L. Ye, G. Zhao, W. Dou, An electrochemical immunoassay for Escherichia coli O157:H7 using double functionalized Au@Pt/SiO_2 nanocomposites and immune magnetic nanoparticles, Talanta 182 (2018) 354–362.

[85] F. Huang, H. Zhang, L. Wang, W. Lai, J. Lin, A sensitive biosensor using double-layer capillary based immunomagnetic separation and invertase-nanocluster based signal amplification for rapid detection of foodborne pathogen, Biosens. Bioelectron. 100 (2018) 583–590.

[86] H. Huang, G. Zhao, W. Dou, Portable and quantitative point-of-care monitoring of Escherichia coli O157:H7 using a personal glucose meter based on immunochromatographic assay, Biosens. Bioelectron. 107 (2018) 266–271.

[87] L. Ye, G. Zhao, W. Dou, An ultrasensitive sandwich immunoassay with a glucometer readout for portable and quantitative detection of Cronobacter sakazakii, Anal.Methods 9 (2017) 6286–6292.

[88] D. Jiang, L. Zhang, F. Liu, C. Liu, L. Liu, X. Pu, An electrochemiluminescence sensor with dual signal amplification of $Ru(bpy)_3^{2+}$ based on PtNPs and glucose dehydrogenase for diagnosis of gas gangrene, RSC Adv. 6 (2016) 19676–19685.

[89] M. Zhu, W. Liu, H. Liu, Y. Liao, J. Wei, X. Zhou, D. Xing, Construction of Fe3O4/vancomycin/PEG magnetic nanocarrier for highly efficient pathogen enrichment and gene sensing, ACS Appl. Mater. Interfaces 7 (2015) 12873–12881.

[90] J. Fei, W. Dou, G. Zhao, A sandwich electrochemical immunoassay for Salmonella pullorum and Salmonella gallinarum based on a AuNPs/SiO2Fe3O4 adsorbing antibody and 4 channel screen printed carbon electrode electrodeposited gold nanoparticles, RSC Adv. 5 (2015) 74548–74556.

[91] X. Hu, W. Dou, G. Zhao, Electrochemical immunosensor for Enterobacter sakazakii detection based on electrochemically reduced graphene oxide–gold nanoparticle/ionic liquid modified electrode, J. ElectroAnal. Chem. 756 (2015) 43–48.

[92] X. Mo, Z. Wu, J. Huang, G. Zhao, W. Dou, A sensitive and regenerative electrochemical immunosensor for quantitative detection of: Escherichia coli O157:H7 based on stable polyaniline coated screen-printed carbon electrode and rGO-NR-Au@Pt, Anal.Methods 11 (2019) 1475–1482.

[93] A. Singh, M. Choudhary, M.P. Singh, H.N. Verma, S.P. Singh, K. Arora, DNA functionalized direct electro-deposited gold nanoaggregates for efficient detection of Salmonella typhi, Bioelectrochemistry 105 (2015) 7–15.

[94] D. Lin, R.G. Pillai, W.E. Lee, A.B. Jemere, An impedimetric biosensor for E. coli O157:H7 based on the use of self-assembled gold nanoparticles and protein G, Microchim, Acta 186 (2019).

[95] D. Lin, T. Tang, D. Jed Harrison, W.E. Lee, A.B. Jemere, A regenerating ultrasensitive electrochemical impedance immunosensor for the detection of adenovirus, Biosens. Bioelectron. 68 (2015) 129–134.

[96] E.Y. Ariffin, Y.H. Lee, D. Futra, L.L. Tan, N.H.A. Karim, N.N.N. Ibrahim, A. Ahmad, An ultrasensitive hollow-silica-based biosensor for pathogenic Escherichia coli DNA detection, Anal. Bioanal. Chem. 410 (2018) 2363–2375.

[97] Y. Ye, Y. Liu, S. He, X. Xu, X. Cao, Y. Ye, H. Zheng, Ultrasensitive electrochemical DNA sensor for virulence invA gene of Salmonella using silver nanoclusters as signal probe, Sensor. Actuator. B Chem. 272 (2018) 53–59.

[98] X. Zhang, Y. Jiang, C. Huang, J. Shen, X. Dong, G. Chen, W. Zhang, Functionalized nanocomposites with the optimal graphene oxide/Au ratio for amplified immunoassay of E. coli to estimate quality deterioration in dairy product, Biosens. Bioelectron. 89 (2017) 913–918.

[99] S. Ranjbar, S. Shahrokhian, F. Nurmohammadi, Nanoporous gold as a suitable substrate for preparation of a new sensitive electrochemical aptasensor for detection of Salmonella typhimurium, Sensor. Actuator. B Chem. 255 (2018) 1536–1544.

[100] Y. Guo, Y. Wang, S. Liu, J. Yu, H. Wang, M. Cui, J. Huang, Electrochemical immunosensor assay (EIA) for sensitive detection of E. coli O157:H7 with signal amplification on a SG–PEDOT–AuNPs electrode interface, Analyst 140 (2015) 551–559.

[101] T. Lee, S.Y. Park, H. Jang, G.-H. Kim, Y. Lee, C. Park, M. Mohammadniaei, M.-H. Lee, J. Min, Fabrication of electrochemical biosensor consisted of multi-functional DNA structure/porous au nanoparticle for avian influenza virus (H5N1) in chicken serum, Mater. Sci. Eng. C 99 (2019) 511–519.

[102] M. Roushani, M. Sarabaegi, F. Pourahmad, Impedimetric aptasensor for Pseudomonas aeruginosa by using a glassy carbon electrode modified with silver nanoparticles, Microchim. Acta 186 (2019) 725.

[103] C. Xiang, R. Li, B. Adhikari, Z. She, Y. Li, H.-B. Kraatz, Sensitive electrochemical detection of Salmonella with chitosan–gold nanoparticles composite film, Talanta 140 (2015) 122–127.

[104] D. Lu, G. Pang, J. Xie, A new phosphothreonine lyase electrochemical immunosensor for detecting Salmonella based on horseradish peroxidase/GNPs-thionine/chitosan, Biomed. Microdevices 19 (2017).

[105] D. Vijian, S.V. Chinni, L.S. Yin, B. Lertanantawong, W. Surareungchai, Non-protein coding RNA-based genosensor with quantum dots as electrochemical labels for attomolar detection of multiple pathogens, Biosens. Bioelectron. 77 (2016) 805–811.

[106] L. Liu, X. Wang, Q. Ma, Z. Lin, S. Chen, Y. Li, L. Lu, H. Qu, X. Su, Multiplex electrochemiluminescence DNA sensor for determination of hepatitis B virus and hepatitis C virus based on multicolor quantum dots and Au nanoparticles, Anal. Chim. Acta916 (2016) 92–101.

[107] H. Hao, S. Hao, H. Hou, G. Zhang, Y. Hou, Z. Zhang, J. Bi, S. Yan, A Novel Label-free Photoelectrochemical Immunosensor Based on CdSe Quantum Dots Sensitized Ho^{3+}/Yb^{3+}-TiO2 for the Detection of Vibrio Parahaemolyticus, Methods, 2019.

[108] Y. Hu, Y. Huang, Y. Wang, C. Li, W. Wong, X. Ye, D. Sun, A photoelectrochemical immunosensor based on gold nanoparticles/ZnAgInS quaternary quantum dots for the high-performance determination of hepatitis B virus surface antigen, Anal. Chim. Acta (2018) 136–145.

[109] Y. Luo, W. Dou, G. Zhao, Rapid electrochemical quantification of Salmonella Pullorum and Salmonella Gallinarum based on glucose oxidase and antibody-modified silica nanoparticles, Anal. Bioanal. Chem. 409 (2017) 4139–4147.

[110] H. Huang, W. Bai, C. Dong, R. Guo, Z. Liu, An ultrasensitive electrochemical DNA biosensor based on graphene/Au nanorod/polythionine for human papillomavirus DNA detection, Biosens. Bioelectron. 68 (2015) 442–446.

[111] C. Xiang, R. Li, B. Adhikari, Z. She, Y. Li, H.B. Kraatz, Sensitive electrochemical detection of Salmonella with chitosan-gold nanoparticles composite film, Talanta 140 (2015) 122–127.

[112] A. Valipour, M. Roushani, Using silver nanoparticle and thiol graphene quantum dots nanocomposite as a substratum to load antibody for detection of hepatitis C virus core antigen: electrochemical oxidation of riboflavin was used as redox probe, Biosens. Bioelectron. 89 (2017) 946–951.

[113] C.M. Pandey, I. Tiwari, V.N. Singh, K.N. Sood, G. Sumana, B.D. Malhotra, Highly sensitive electrochemical immunosensor based on graphene-wrapped copper oxide-cysteine hierarchical structure for detection of pathogenic bacteria, Sensor. Actuator. B Chem. 238 (2017) 1060–1069.

[114] J. Bhardwaj, S. Devarakonda, S. Kumar, J. Jang, Development of a paper-based electrochemical immunosensor using an antibody-single walled carbon nanotubes bio-conjugate modified electrode for label-free detection of foodborne pathogens, Sensor. Actuator. B Chem. 253 (2017) 115–123.

[115] N. Jaiswal, C.M. Pandey, A. Soni, I. Tiwari, M. Rosillo-Lopez, C.G. Salzmann, B. D. Malhotra, G. Sumana, Electrochemical genosensor based on carboxylated graphene for detection of water-borne pathogen, Sensor. Actuator. B Chem. 275 (2018) 312–321.

[116] A. Abbaspour, F. Norouz-Sarvestani, A. Noori, N. Soltani, Aptamer-conjugated silver nanoparticles for electrochemical dual-aptamer-based sandwich detection of staphylococcus aureus, Biosens. Bioelectron. 68 (2015) 149–155.

[117] M. Zhong, L. Yang, H. Yang, C. Cheng, W. Deng, Y. Tan, Q. Xie, S. Yao, An electrochemical immunobiosensor for ultrasensitive detection of Escherichia coli O157:H7 using CdS quantum dots-encapsulated metal-organic frameworks as signal-amplifying tags, Biosens. Bioelectron. 126 (2019) 493–500.

[118] N. Hao, X. Zhang, Z. Zhou, R. Hua, Y. Zhang, Q. Liu, J. Qian, H. Li, K. Wang, AgBr nanoparticles/3D nitrogen-doped graphene hydrogel for fabricating all-solid-state luminol-electrochemiluminescence Escherichia coli aptasensors, Biosens. Bioelectron. 97 (2017) 377–383.

[119] R. Hua, N. Hao, J. Lu, J. Qian, Q. Liu, H. Li, K. Wang, A sensitive Potentiometric resolved ratiometric Photoelectrochemical aptasensor for Escherichia coli detection fabricated with non-metallic nanomaterials, Biosens. Bioelectron. 106 (2018) 57–63.

[120] L. Russo, J. Leva Bueno, J.F. Bergua, M. Costantini, M. Giannetto, V. Puntes, A. De La Escosura-Muñiz, A. Merkoçi, Low-cost strategy for the development of a rapid

electrochemical assay for bacteria detection based on AuAg nanoshells, ACS Omega 3 (2018) 18849–18856.
[121] J. Xu, S. Wu, Chapter 4 - other nanomaterials, in: G. Li (Ed.), Nano-Inspired Biosensors for Protein Assay with Clinical Applications, Elsevier, 2019, pp. 91–111.
[122] G.A.R.Y. Suaifan, S. Alhogail, M. Zourob, Rapid and low-cost biosensor for the detection of Staphylococcus aureus, Biosens. Bioelectron. 90 (2017) 230–237.
[123] G.A.R.Y. Suaifan, S. Alhogail, M. Zourob, Paper-based magnetic nanoparticle-peptide probe for rapid and quantitative colorimetric detection of Escherichia coli O157:H7, Biosens. Bioelectron 92 (2017) 702–708.
[124] S. Alhogail, G.A.R.Y. Suaifan, S. Bizzarro, W.E. Kaman, F.J. Bikker, K. Weber, D. Cialla-May, J. Popp, M. Zourob, On site visual detection of Porphyromonas gingivalis related periodontitis by using a magnetic-nanobead based assay for gingipains protease biomarkers, Microchim. Acta 185 (2018) 149.
[125] S. Alhogail, G.A.R.Y. Suaifan, M. Zourob, Rapid colorimetric sensing platform for the detection of Listeria monocytogenes foodborne pathogen, Biosens. Bioelectron. 86 (2016) 1061–1066.
[126] M.-P.N. Bui, S. Ahmed, A. Abbas, Single-digit pathogen and attomolar detection with the naked eye using liposome-amplified plasmonic immunoassay, Nano Lett. 15 (2015) 6239–6246.
[127] R. Chen, X. Huang, H. Xu, Y. Xiong, Y. Li, Plasmonic enzyme-linked immunosorbent assay using nanospherical brushes as a catalase container for colorimetric detection of ultralow concentrations of Listeria monocytogenes, ACS Appl. Mater. Interfaces 7 (2015) 28632–28639.
[128] S.M. Shawky, A.M. Awad, W. Allam, M.H. Alkordi, S.F. El-Khamisy, Gold aggregating gold: a novel nanoparticle biosensor approach for the direct quantification of hepatitis C virus RNA in clinical samples, Biosens. Bioelectron. 92 (2017) 349–356.
[129] P. Singh, R. Gupta, M. Choudhary, A.K. Pinnaka, R. Kumar, V. Bhalla, Drug and nanoparticle mediated rapid naked eye water test for pathogens detection, Sensor. Actuator. B Chem. 262 (2018) 603–610.
[130] S.R. Ahmed, J. Kim, V.T. Tran, T. Suzuki, S. Neethirajan, J. Lee, E.Y. Park, In situ self-assembly of gold nanoparticles on hydrophilic and hydrophobic substrates for influenza virus-sensing platform, Sci. Rep. 7 (2017) 44495, 44495.
[131] J.Y. Park, H.Y. Jeong, M.I. Kim, T.J. Park, Colorimetric detection system for Salmonella typhimurium based on peroxidase-like activity of magnetic nanoparticles with DNA aptamers, J. Nanomater. 2015 (2015).
[132] R. Das, B. Chaterjee, A. Kapil, T.K. Sharma, Aptamer-NanoZyme Mediated Sensing Platform for the Rapid Detection of Escherichia coli in Fruit Juice, Sensing and Bio-Sensing Research, 2019, 100313.
[133] Y. Liu, J. Wang, C. Zhao, X. Guo, X. Song, W. Zhao, S. Liu, K. Xu, J. Li, A multicolorimetric assay for rapid detection of Listeria monocytogenes based on the etching of gold nanorods, Anal. Chim. Acta 1048 (2019) 154–160.
[134] S. Wu, N. Duan, Y. Qiu, J. Li, Z. Wang, Colorimetric aptasensor for the detection of Salmonella enterica serovar typhimurium using ZnFe2O4-reduced graphene oxide nanostructures as an effective peroxidase mimetics, Int. J. Food Microbiol. 261 (2017) 42–48.
[135] S.R. Ahmed, J. Kim, T. Suzuki, J. Lee, E.Y. Park, Enhanced catalytic activity of gold nanoparticle-carbon nanotube hybrids for influenza virus detection, Biosens. Bioelectron. 85 (2016) 503–508.
[136] D. Kwon, S. Lee, M.M. Ahn, I.S. Kang, K.H. Park, S. Jeon, Colorimetric detection of pathogenic bacteria using platinum-coated magnetic nanoparticle clusters and magnetophoretic chromatography, Anal. Chim. Acta883 (2015) 61–66.
[137] N. Bhardwaj, S.K. Bhardwaj, M.K. Nayak, J. Mehta, K.-H. Kim, A. Deep, Fluorescent nanobiosensors for the targeted detection of foodborne bacteria, TrAC Trends Anal. Chem. (Reference Ed.) 97 (2017) 120–135.
[138] Y. Li, Z. Wang, L. Sun, L. Liu, C. Xu, H. Kuang, Nanoparticle-based sensors for food contaminants, TrAC Trends Anal. Chem. (Reference Ed.) 113 (2019) 74–83.
[139] L. Xue, L. Zheng, H. Zhang, X. Jin, J. Lin, An ultrasensitive fluorescent biosensor using high gradient magnetic separation and quantum dots for fast detection of foodborne pathogenic bacteria, Sensor. Actuator. B Chem. 265 (2018) 318–325.
[140] J. Ren, G. Liang, Y. Man, A. Li, X. Jin, Q. Liu, L. Pan, Aptamer-based fluorometric determination of Salmonella Typhimurium using Fe3O4 magnetic separation and CdTe quantum dots, PloS One 14 (2019) e0218325-e0218325.
[141] H. Kurt, M. Yüce, B. Hussain, H. Budak, Dual-excitation upconverting nanoparticle and quantum dot aptasensor for multiplexed food pathogen detection, Biosens. Bioelectron. 81 (2016) 280–286.
[142] Y. Liu, C. Zhao, K. Fu, X. Song, K. Xu, J. Wang, J. Li, Selective turn-on fluorescence detection of Vibrio parahaemolyticus in food based on charge-transfer between CdSe/ZnS quantum dots and gold nanoparticles, Food Contr. 80 (2017) 380–387.
[143] J. Lee, K. Takemura, E.Y. Park, Plasmonic/magnetic graphene-based magnetofluoro-immunosensing platform for virus detection, Sensor. Actuator. B Chem. 276 (2018) 254–261.
[144] O. Adegoke, T. Kato, E.Y. Park, An ultrasensitive alloyed near-infrared quinternary quantum dot-molecular beacon nanodiagnostic bioprobe for influenza virus RNA, Biosens. Bioelectron. 80 (2016) 483–490.
[145] B. Jin, S. Wang, M. Lin, Y. Jin, S. Zhang, X. Cui, Y. Gong, A. Li, F. Xu, T.J. Lu, Upconversion nanoparticles based FRET aptasensor for rapid and ultrasenstive bacteria detection, Biosens. Bioelectron. 90 (2017) 525–533.
[146] R.-R. Hu, Z.-Z. Yin, Y.-B. Zeng, J. Zhang, H.-Q. Liu, Y. Shao, S.-B. Ren, L. Li, A novel biosensor for Escherichia coli O157:H7 based on fluorescein-releasable biolabels, Biosens. Bioelectron. 78 (2016) 31–36.
[147] M. Yu, H. Wang, F. Fu, L. Li, J. Li, G. Li, Y. Song, M.T. Swihart, E. Song, Dual-recognition Förster resonance energy transfer based platform for one-step sensitive detection of pathogenic bacteria using fluorescent vancomycin–gold nanoclusters and aptamer–gold nanoparticles, Anal. Chem. 89 (2017) 4085–4090.
[148] J. Wang, H. Wu, Y. Yang, R. Yan, Y. Zhao, Y. Wang, A. Chen, S. Shao, P. Jiang, Y.-Q. Li, Bacterial species-identifiable magnetic nanosystems for early sepsis diagnosis and extracorporeal photodynamic blood disinfection, Nanoscale 10 (2018) 132–141.
[149] H. Wang, Z. Chi, Y. Cong, Z. Wang, F. Jiang, J. Geng, P. Zhang, P. Ju, Q. Dong, C. Liu, Development of a fluorescence assay for highly sensitive detection of Pseudomonas aeruginosa based on an aptamer-carbon dots/graphene oxide system, RSC Adv. 8 (2018) 32454–32460.
[150] H. Li, W. Ahmad, Y. Rong, Q. Chen, M. Zuo, Q. Ouyang, Z. Guo, Designing an aptamer based magnetic and upconversion nanoparticles conjugated fluorescence sensor for screening Escherichia coli in food, Food Contr. 107 (2020) 106761.
[151] L. Hao, H. Gu, N. Duan, S. Wu, X. Ma, Y. Xia, H. Wang, Z. Wang, A chemiluminescent aptasensor based on rolling circle amplification and Co2+/N-(aminobutyl)-N-(ethylisoluminol) functional flowerlike gold nanoparticles for Salmonella typhimurium detection, Talanta 164 (2017) 275–282.
[152] J. Deng, M. Yang, J. Wu, W. Zhang, X. Jiang, A self-contained chemiluminescent lateral flow assay for point-of-care testing, Anal. Chem. 90 (2018) 9132–9137.
[153] L. Hao, H. Gu, N. Duan, S. Wu, X. Ma, Y. Xia, Z. Tao, Z. Wang, An enhanced chemiluminescence resonance energy transfer aptasensor based on rolling circle amplification and WS2 nanosheet for Staphylococcus aureus detection, Anal. Chim. Acta959 (2017) 83–90.
[154] Y. Liu, H. Zhou, Z. Hu, G. Yu, D. Yang, J. Zhao, Label and label-free based surface-enhanced Raman scattering for pathogen bacteria detection: a review, Biosens. Bioelectron. 94 (2017) 131–140.
[155] X. Zhao, M. Li, Z. Xu, Detection of foodborne pathogens by surface enhanced Raman spectroscopy, Front. Microbiol. 9 (2018) 1236.
[156] J. Wang, X. Wu, C. Wang, Z. Rong, H. Ding, H. Li, S. Li, N. Shao, P. Dong, R. Xiao, S. Wang, Facile synthesis of Au-coated magnetic nanoparticles and their application in bacteria detection via a SERS method, ACS Appl. Mater. Interfaces 8 (2016) 19958–19967.
[157] H. Kearns, R. Goodacre, L.E. Jamieson, D. Graham, K. Faulds, SERS detection of multiple antimicrobial-resistant pathogens using nanosensors, Anal. Chem. 89 (2017) 12666–12673.
[158] J. Zhou, Q. Xiong, J. Ma, J. Ren, P.B. Messersmith, P. Chen, H. Duan, Polydopamine-enabled approach toward tailored plasmonic nanogapped nanoparticles: from nanogap engineering to multifunctionality, ACS Nano 10 (2016) 11066–11075.
[159] Y. Zhou, W. Fang, K. Lai, Y. Zhu, X. Bian, J. Shen, Q. Li, L. Wang, W. Zhang, J. Yan, Terminal deoxynucleotidyl transferase (TdT)-catalyzed homo-nucleotides-constituted ssDNA: inducing tunable-size nanogap for core-shell plasmonic metal nanostructure and acting as Raman reporters for detection of Escherichia coli O157:H7, Biosens. Bioelectron. 141 (2019) 111419.
[160] T. Zhu, Y. Hu, K. Yang, N. Dong, M. Yu, N. Jiang, A novel SERS nanoprobe based on the use of core-shell nanoparticles with embedded reporter molecule to detect E. coli O157:H7 with high sensitivity, Microchim. Acta 185 (2017) 30.
[161] W. Gao, B. Li, R. Yao, Z. Li, X. Wang, X. Dong, H. Qu, Q. Li, N. Li, H. Chi, B. Zhou, Z. Xia, Intuitive label-free SERS detection of bacteria using aptamer-based in situ silver nanoparticles synthesis, Anal. Chem. 89 (2017) 9836–9842.
[162] J. Wang, X. Wu, C. Wang, N. Shao, P. Dong, R. Xiao, S. Wang, Magnetically assisted surface-enhanced Raman spectroscopy for the detection of Staphylococcus aureus based on aptamer recognition, ACS Appl. Mater. Interfaces 7 (2015) 20919–20929.
[163] Y. Pang, N. Wan, L. Shi, C. Wang, Z. Sun, R. Xiao, S. Wang, Dual-recognition surface-enhanced Raman scattering(SERS)biosensor for pathogenic bacteria detection by using vancomycin-SERS tags and aptamer-Fe3O4@Au, Anal. Chim. Acta1077 (2019) 288–296.
[164] X. Ma, X. Xu, Y. Xia, Z. Wang, SERS aptasensor for Salmonella typhimurium detection based on spiny gold nanoparticles, Food Contr. 84 (2018) 232–237.
[165] N. Duan, B. Chang, H. Zhang, Z. Wang, S. Wu, Salmonella typhimurium detection using a surface-enhanced Raman scattering-based aptasensor, Int. J. Food Microbiol. 218 (2016) 38–43.
[166] K.M. Koczula, A. Gallotta, Lateral flow assays, Essays Biochem. 60 (2016) 111–120.
[167] R. Pan, Y. Jiang, L. Sun, R. Wang, K. Zhuang, Y. Zhao, H. Wang, M.A. Ali, H. Xu, C. Man, Gold nanoparticle-based enhanced lateral flow immunoassay for detection of Cronobacter sakazakii in powdered infant formula, Int. J. Dairy Sci. 101 (2018) 3835–3843.
[168] W.C. Mak, V. Beni, A.P.F. Turner, Lateral-flow technology: from visual to instrumental, TrAC Trends Anal. Chem. (Reference Ed.) 79 (2016) 297–305.
[169] J. Hwang, D. Kwon, S. Lee, S. Jeon, Detection of: Salmonella bacteria in milk using gold-coated magnetic nanoparticle clusters and lateral flow filters, RSC Adv. 6 (2016) 48445–48448.
[170] H. Lee, J. Hwang, Y. Park, D. Kwon, S. Lee, I. Kang, S. Jeon, Immunomagnetic separation and size-based detection of Escherichia coli O157 at the meniscus of a membrane strip, RSC Adv. 8 (2018) 26266–26270.
[171] I.-H. Cho, A. Bhunia, J. Irudayaraj, Rapid pathogen detection by lateral-flow immunochromatographic assay with gold nanoparticle-assisted enzyme signal amplification, Int. J. Food Microbiol. 206 (2015) 60–66.
[172] X. Cui, Y. Huang, J. Wang, L. Zhang, Y. Rong, W. Lai, T. Chen, A remarkable sensitivity enhancement in a gold nanoparticle-based lateral flow immunoassay for the detection of Escherichia coli O157:H7, RSC Adv. 5 (2015) 45092–45097.
[173] C.-W. Yen, H. de Puig, J.O. Tam, J. Gómez-Márquez, I. Bosch, K. Hamad-Schifferli, L. Gehrke, Multicolored silver nanoparticles for multiplexed disease

diagnostics: distinguishing dengue, yellow fever, and Ebola viruses, Lab Chip 15 (2015) 1638–1641.
[174] S.A. Jin, Y. Heo, L.K. Lin, A.J. Deering, G.T.C. Chiu, J.P. Allebach, L.A. Stanciu, Gold decorated polystyrene particles for lateral flow immunodetection of Escherichia coli O157:H7, Microchim. Acta 184 (2017) 4879–4886.
[175] K.-Y. Xing, J. Peng, D.-F. Liu, L.-M. Hu, C. Wang, G.-Q. Li, G.-G. Zhang, Z. Huang, S. Cheng, F.-F. Zhu, N.-M. Liu, W.-H. Lai, Novel immunochromatographic assay based on Eu (III)-doped polystyrene nanoparticle-linker-monoclonal antibody for sensitive detection of Escherichia coli O157:H7, Anal. Chim. Acta 998 (2018) 52–59.
[176] W. Ren, I.-H. Cho, Z. Zhou, J. Irudayaraj, Ultrasensitive detection of microbial cells using magnetic focus enhanced lateral flow sensors, Chem. Commun. 52 (2016) 4930–4933.
[177] A.H.A. Hassan, J.F. Bergua, E. Morales-Narváez, A. Mekoçi, Validity of a single antibody-based lateral flow immunoassay depending on graphene oxide for highly sensitive determination of E. coli O157:H7 in minced beef and river water, Food Chem. 297 (2019), 124965.
[178] Z. Wang, X. Yao, R. Wang, Y. Ji, T. Yue, J. Sun, T. Li, J. Wang, D. Zhang, Label-free strip sensor based on surface positively charged nitrogen-rich carbon nanoparticles for rapid detection of Salmonella enteritidis, Biosens. Bioelectron. 132 (2019) 360–367.
[179] W. Ren, D.R. Ballou, R. FitzGerald, J. Irudayaraj, Plasmonic enhancement in lateral flow sensors for improved sensing of E. coli O157:H7, Biosens. Bioelectron 126 (2019) 324–331.
[180] T. Jiang, Y. Song, T. Wei, H. Li, D. Du, M.-J. Zhu, Y. Lin, Sensitive detection of Escherichia coli O157:H7 using Pt–Au bimetal nanoparticles with peroxidase-like amplification, Biosens. Bioelectron. 77 (2016) 687–694.
[181] D. He, Z. Wu, B. Cui, E. Xu, Z. Jin, Establishment of a dual mode immunochromatographic assay for Campylobacter jejuni detection, Food Chem. 289 (2019) 708–713.
[182] D. Duan, K. Fan, D. Zhang, S. Tan, M. Liang, Y. Liu, J. Zhang, P. Zhang, W. Liu, X. Qiu, G.P. Kobinger, G. Fu Gao, X. Yan, Nanozyme-strip for rapid local diagnosis of Ebola, Biosens. Bioelectron 74 (2015) 134–141.
[183] J. Han, L. Zhang, L. Hu, K. Xing, X. Lu, Y. Huang, J. Zhang, W. Lai, T. Chen, Nanozyme-based lateral flow assay for the sensitive detection of Escherichia coli O157:H7 in milk, Int. J. Dairy Sci. 101 (2018) 5770–5779.
[184] H. Ilhan, B. Guven, U. Dogan, H. Torul, S. Evran, D. Çetin, Z. Suludere, N. Saglam, İ.H. Boyaci, U. Tamer, The coupling of immunomagnetic enrichment of bacteria with paper-based platform, Talanta 201 (2019) 245–252.
[185] K. Luo, L. Hu, Q. Guo, C. Wu, S. Wu, D. Liu, Y. Xiong, W. Lai, Comparison of 4 label-based immunochromatographic assays for the detection of Escherichia coli O157:H7 in milk, Int. J. Dairy Sci. 100 (7) (2017) 5176–5187.
[186] W. Wu, S. Zhao, Y. Mao, Z. Fang, X. Lu, L. Zeng, A sensitive lateral flow biosensor for Escherichia coli O157:H7 detection based on aptamer mediated strand displacement amplification, Anal. Chim. Acta861 (2015) 62–68.
[187] B.B. Taşbasi, B.C. Guner, M. Sudagidan, S. Ucak, M. Kavruk, V.C. Ozalp, Label-free lateral flow assay for Listeria monocytogenes by aptamer-gated release of signal molecules, Anal. Biochem. 587 (2019) 113449.
[188] H.B. Liu, X.J. Du, Y.X. Zang, P. Li, S. Wang, SERS-based lateral flow strip biosensor for simultaneous detection of Listeria monocytogenes and Salmonella enterica serotype enteritidis, J. Agric. Food Chem. 65 (2017) 10290–10299.
[189] C.H. Gayathri, P. Mayuri, K. Sankaran, A.S. Kumar, An electrochemical immunosensor for efficient detection of uropathogenic E. Coli based on thionine dye immobilized chitosan/functionalized-MWCNT modified electrode, Biosens. Bioelectron. 82 (2016) 71–77.
[190] M. Mathelié-Guinlet, T. Cohen-Bouhacina, I. Gammoudi, A. Martin, L. Béven, M. H. Delville, C. Grauby-Heywang, Silica nanoparticles-assisted electrochemical biosensor for the rapid, sensitive and specific detection of Escherichia coli, Sensor. Actuator. B Chem. (2019) 314–320.
[191] S. Shukla, Y. Haldorai, V.K. Bajpai, A. Rengaraj, S.K. Hwang, X. Song, M. Kim, Y. S. Huh, Y.-K. Han, Electrochemical coupled immunosensing platform based on graphene oxide/gold nanocomposite for sensitive detection of Cronobacter sakazakii in powdered infant formula, Biosens. Bioelectron. 109 (2018) 139–149.
[192] F. Zhu, G. Zhao, W. Dou, Voltammetric sandwich immunoassay for Cronobacter sakazakii using a screen-printed carbon electrode modified with horseradish peroxidase, reduced graphene oxide, thionine and gold nanoparticles, Microchim. Acta 185 (2018).
[193] A.S. Afonso, C.V. Uliana, D.H. Martucci, R.C. Faria, Simple and rapid fabrication of disposable carbon-based electrochemical cells using an electronic craft cutter for sensor and biosensor applications, Talanta 146 (2016) 381–387.
[194] J. Bhardwaj, S. Devarakonda, S. Kumar, J. Jang, Development of a paper-based electrochemical immunosensor using an antibody-single walled carbon nanotubes bio-conjugate modified electrode for label-free detection of foodborne pathogens, Sensor. Actuator. B Chem. 253 (2017) 115–123.
[195] X. Zhang, F. Zhang, H. Zhang, J. Shen, E. Han, X. Dong, Functionalized gold nanorod-based labels for amplified electrochemical immunoassay of E. coli as indicator bacteria relevant to the quality of dairy product, Talanta 132 (2015) 600–605.
[196] R. Jijie, K. Kahlouche, A. Barras, N. Yamakawa, J. Bouckaert, T. Gharbi, S. Szunerits, R. Boukherroub, Reduced graphene oxide/polyethylenimine based immunosensor for the selective and sensitive electrochemical detection of uropathogenic Escherichia coli, Sensor. Actuator. B Chem. 260 (2018) 255–263.
[197] Y. Zou, J. Liang, Z. She, H.B. Kraatz, Gold nanoparticles-based multifunctional nanoconjugates for highly sensitive and enzyme-free detection of E.coli K12, Talanta 193 (2019) 15–22.
[198] Y. Guo, Y. Wang, S. Liu, J. Yu, H. Wang, M. Cui, J. Huang, Electrochemical immunosensor assay (EIA) for sensitive detection of E. coli O157:H7 with signal amplification on a SG-PEDOT-AuNPs electrode interface, Analyst 140 (2) (2015) 551–559.
[199] X. Zhang, J. Shen, H. Ma, Y. Jiang, C. Huang, E. Han, B. Yao, Y. He, Optimized dendrimer-encapsulated gold nanoparticles and enhanced carbon nanotube nanoprobes for amplified electrochemical immunoassay of E. coli in dairy product based on enzymatically induced deposition of polyaniline, Biosens. Bioelectron. 80 (2016) 666–673.
[200] D.Q. Nguyen, K. Ishiki, H. Shiigi, Single cell immunodetection of Escherichia coli O157:H7 on an indium-tin-oxide electrode by using an electrochemical label with an organic-inorganic nanostructure, Microchim. Acta 185 (2018).
[201] Y. Li, Y. Xiong, L. Fang, L. Jiang, H. Huang, J. Deng, W. Liang, J. Zheng, An electrochemical strategy using multifunctional nanoconjugates for efficient simultaneous detection of escherichia coli O157: H7 and vibrio cholerae O1, Theranostics 7 (2017) 935–944.
[202] D. Zhou, M. Wang, J. Dong, S. Ai, A novel electrochemical immunosensor based on mesoporous graphitic carbon nitride for detection of subgroup J of avian leukosis viruses, Electrochim. Acta 205 (2016) 95–101.
[203] J. Huang, Z. Xie, Z. Xie, S. Luo, L. Xie, L. Huang, Q. Fan, Y. Zhang, S. Wang, T. Zeng, Silver nanoparticles coated graphene electrochemical sensor for the ultrasensitive analysis of avian influenza virus H7, Anal. Chim. Acta913 (2016) 121–127.
[204] Z. Wu, C.-H. Zhou, J.-J. Chen, C. Xiong, Z. Chen, D.-W. Pang, Z.-L. Zhang, Bifunctional magnetic nanobeads for sensitive detection of avian influenza A (H7N9) virus based on immunomagnetic separation and enzyme-induced metallization, Biosens. Bioelectron. 68 (2015) 586–592.
[205] Y.-S. Fang, X.-J. Huang, L.-S. Wang, J.-F. Wang, An enhanced sensitive electrochemical immunosensor based on efficient encapsulation of enzyme in silica matrix for the detection of human immunodeficiency virus p24, Biosens. Bioelectron. 64 (2015) 324–332.
[206] M. Veerapandian, R. Hunter, S. Neethirajan, Dual immunosensor based on methylene blue-electroadsorbed graphene oxide for rapid detection of the influenza A virus antigen, Talanta 155 (2016) 250–257.
[207] Q. Chen, J. Lin, C. Gan, Y. Wang, D. Wang, Y. Xiong, W. Lai, Y. Li, M. Wang, A sensitive impedance biosensor based on immunomagnetic separation and urease catalysis for rapid detection of Listeria monocytogenes using an immobilization-free interdigitated array microelectrode, Biosens. Bioelectron. 74 (2015) 504–511.
[208] N.F.D. Silva, J.M.C.S. Magalhães, M.T. Oliva-Teles, C. Delerue-Matos, A potentiometric magnetic immunoassay for rapid detection of Salmonella typhimurium, Anal.Methods 7 (9) (2015) 4008–4011.
[209] M. Martín, P. Salazar, C. Jiménez, M. Lecuona, M.J. Ramos, J. Ode, J. Alcoba, R. Roche, R. Villalonga, S. Campuzano, J.M. Pingarrón, J.L. González-Mora, Rapid Legionella pneumophila determination based on a disposable core-shell Fe_3O_4@poly(dopamine) magnetic nanoparticles immunoplatform, Anal. Chim. Acta887 (2015) 51–58.
[210] A.-R.H.A.-A. Hassan, A. de la Escosura-Muñiz, A. Merkoçi, Highly sensitive and rapid determination of Escherichia coli O157:H7 in minced beef and water using electrocatalytic gold nanoparticle tags, Biosens. Bioelectron. 67 (2015) 511–515.
[211] R. Wang, J. Lum, Z. Callaway, J. Lin, W. Bottje, Y. Li, A label-free impedance immunosensor using screen-printed interdigitated electrodes and magnetic nanobeads for the detection of E. coli O157:H7, Biosensors 5 (2015) 791–803.
[212] R. Mutreja, M. Jariyal, P. Pathania, A. Sharma, D.K. Sahoo, C.R. Suri, Novel surface antigen based impedimetric immunosensor for detection of Salmonella typhimurium in water and juice samples, Biosens. Bioelectron. 85 (2016) 707–713.
[213] D.G.A. Cabral, E.C.S. Lima, P. Moura, R.F. Dutra, A label-free electrochemical immunosensor for hepatitis B based on hyaluronic acid–carbon nanotube hybrid film, Talanta 148 (2016) 209–215.
[214] Y. Wang, P.A. Fewins, E.C. Alocilja, Electrochemical immunosensor using nanoparticle-based signal enhancement for Escherichia coli O157:H7 detection, IEEE Sensor. J. 15 (2015) 4692–4699.
[215] F. Moghtader, G. Congur, H.M. Zareie, A. Erdem, E. Piskin, Impedimetric detection of pathogenic bacteria with bacteriophages using gold nanorod deposited graphite electrodes, RSC Adv. 6 (100) (2016) 97832–97839.
[216] Y. Zhou, A. Marar, P. Kner, R.P. Ramasamy, Charge-directed immobilization of bacteriophage on nanostructured electrode for whole-cell electrochemical biosensors, Anal. Chem. 89 (11) (2017) 5734–5741.
[217] C.A.S. Andrade, J.M. Nascimento, I.S. Oliveira, C.V.J. de Oliveira, C.P. de Melo, O.L. Franco, M.D.L. Oliveira, Nanostructured sensor based on carbon nanotubes and clavanin A for bacterial detection, Colloids Surf. B Biointerfaces 135 (2015) 833–839.
[218] K.F. Low, P. Rijiravanich, K.K.B. Singh, W. Surareungchai, C.Y. Yean, An electrochemical genosensing assay based on magnetic beads and gold nanoparticle-loaded latex microspheres for vibrio cholerae detection, J. Biomed. Nanotechnol. 11 (2015) 702–710.
[219] W. Sun, X. Wang, Y. Lu, S. Gong, X. Qi, B. Lei, Z. Sun, G. Li, Electrochemical deoxyribonucleic acid biosensor based on electrodeposited graphene and nickel oxide nanoparticle modified electrode for the detection of salmonella enteritidis gene sequence, Mater. Sci. Eng. C 49 (2015) 34–39.
[220] Y. Ye, W. Yan, Y. Liu, S. He, X. Cao, X. Xu, H. Zheng, S. Gunasekaran, Electrochemical detection of Salmonella using an invA genosensor on polypyrrole-reduced graphene oxide modified glassy carbon electrode and AuNPs-horseradish peroxidase-streptavidin as nanotag, Anal. Chim. Acta1074 (2019) 80–88.

[221] D. Ozkan-Ariksoysal, Y.U. Kayran, F.F. Yilmaz, A.A. Ciucu, I.G. David, V. David, M. Hosgor-Limoncu, M. Ozsoz, DNA-wrapped multi-walled carbon nanotube modified electrochemical biosensor for the detection of Escherichia coli from real samples, Talanta 166 (2017) 27–35.
[222] Y. Chen, S. Guo, M. Zhao, P. Zhang, Z. Xin, J. Tao, L. Bai, Amperometric DNA biosensor for Mycobacterium tuberculosis detection using flower-like carbon nanotubes-polyaniline nanohybrid and enzyme-assisted signal amplification strategy, Biosens. Bioelectron. 119 (2018) 215–220.
[223] I. Tiwari, M. Singh, C.M. Pandey, G. Sumana, Electrochemical genosensor based on graphene oxide modified iron oxide-chitosan hybrid nanocomposite for pathogen detection, Sensor. Actuator. B Chem. 206 (2015) 276–283.
[224] A. de la Escosura-Muñiz, L. Baptista-Pires, L. Serrano, L. Altet, O. Francino, A. Sánchez, A. Merkoçi, Magnetic bead/gold nanoparticle double-labeled primers for electrochemical detection of isothermal amplified leishmania DNA, Small 12 (2) (2016) 205–213.
[225] R. Chand, Y.L. Wang, D. Kelton, S. Neethirajan, Isothermal DNA amplification with functionalized graphene and nanoparticle assisted electroanalysis for rapid detection of Johne's disease, Sensor. Actuator. B Chem. 261 (2018) 31–37.
[226] C. Singhal, A. Ingle, D. Chakraborty, A.K. Pn, C.S. Pundir, J. Narang, Impedimetric genosensor for detection of hepatitis C virus (HCV1) DNA using viral probe on methylene blue doped silica nanoparticles, Int. J. Biol. Macromol. 98 (2017) 84–93.
[227] P.K. Pathania, J.K. Saini, S. Vij, R. Tewari, P. Sabherwal, P. Rishi, C.R. Suri, Aptamer functionalized MoS2-rGO nanocomposite based biosensor for the detection of Vi antigen, Biosens. Bioelectron. 122 (2018) 121–126.
[228] C. Ge, R. Yuan, L. Yi, J. Yang, H. Zhang, L. Li, W. Nian, G. Yi, Target-induced aptamer displacement on gold nanoparticles and rolling circle amplification for ultrasensitive live Salmonella typhimurium electrochemical biosensing, J. ElectroAnal. Chem. 826 (2018) 174–180.
[229] E. Hamidi-Asl, F. Dardenne, S. Pilehvar, R. Blust, K. De Wael, Unique properties of core shell Ag@Au nanoparticles for the aptasensing of bacterial cells, Chemosensors 4 (2016) 16.
[230] G. Dai, Z. Li, F. Luo, S. Ai, B. Chen, Q. Wang, Electrochemical determination of Salmonella typhimurium by using aptamer-loaded gold nanoparticles and a composite prepared from a metal-organic framework (type UiO-67) and graphene, Mikrochim. Acta (2019) 620.
[231] J.N. Appaturi, T. Pulingam, K.L. Thong, S. Muniandy, N. Ahmad, B.F. Leo, Rapid and sensitive detection of Salmonella with reduced graphene oxide-carbon nanotube based electrochemical aptasensor, Anal. Biochem. 589 (2020) 113489.
[232] S. Muniandy, S.J. Teh, J.N. Appaturi, K.L. Thong, C.W. Lai, F. Ibrahim, B.F. Leo, A reduced graphene oxide-titanium dioxide nanocomposite based electrochemical aptasensor for rapid and sensitive detection of Salmonella enterica, Bioelectrochemistry 127 (2019) 136–144.
[233] X. Li, H. Fu, Y. He, Q. Zhai, J. Guo, K. Qing, G. Yi, Electrochemical aptasensor for rapid and sensitive determination of Salmonella based on target-induced strand displacement and gold nanoparticle amplification, Anal. Lett. 49 (15) (2016) 2405–2417.
[234] I.J. Dinshaw, S. Muniandy, S.J. Teh, F. Ibrahim, B.F. Leo, K.L. Thong, Development of an aptasensor using reduced graphene oxide chitosan complex to detect Salmonella, J. ElectroAnal. Chem. 806 (2017) 88–96.
[235] A.V.M.R. Housaindokht, E. Sheikhzadeh, P. Pordeli, Z. Rouhbakhsh Zaeri, F. Janati-Fard, M. Nosrati, M. Mashreghi, A.R. Haghparast, A. Nakhaeipour, A. A. Esmaeili, S. Solimani, A sensitive electrochemical aptasensor based on single wall carbon nanotube modified screen printed electrode for detection of Escherichia coli O157:H7, Adv. Mater. Lett. 9 (2018) 369–373.
[236] Y.H. Haixia Peng, Rong Ren, Bini Wang, Shuanghong Song, Yaping He, Fuxin Zhang, A sensitive electrochemical aptasensor based on MB-anchored GOfor the rapid detection of Cronobacter sakazaki, J. Solid State Electrochem. (2019).
[237] S. Karash, R. Wang, L. Kelso, H. Lu, T.J. Huang, Y. Li, Rapid detection of avian influenza virus H5N1 in chicken tracheal samples using an impedance aptasensor with gold nanoparticles for signal amplification, J. Virol. Methods 236 (2016) 147–156.
[238] J.N. Appaturi, T. Pulingam, S. Muniandy, I.J. Dinshaw, L.B. Fen, M.R. Johan, Supported cobalt nanoparticles on graphene oxide/mesoporous silica for oxidation of phenol and electrochemical detection of H2O2 and Salmonella spp, Mater. Chem. Phys. 232 (2019) 493–505.
[239] F. Jia, N. Duan, S. Wu, R. Dai, Z. Wang, X. Li, Impedimetric Salmonella aptasensor using a glassy carbon electrode modified with an electrodeposited composite consisting of reduced graphene oxide and carbon nanotubes, Microchim. Acta 183 (2016) 337–344.
[240] M.R. Hasan, T. Pulingam, J.N. Appaturi, A.N. Zifruddin, S.J. Teh, T.W. Lim, F. Ibrahim, B.F. Leo, K.L. Thong, Carbon nanotube-based aptasensor for sensitive electrochemical detection of whole-cell Salmonella, Anal. Biochem. 554 (2018) 34–43.
[241] S.L. Burrs, M. Bhargava, R. Sidhu, J. Kiernan-Lewis, C. Gomes, J.C. Claussen, E. S. McLamore, A paper based graphene-nanocauliflower hybrid composite for point of care biosensing, Biosens. Bioelectron. 85 (2016) 479–487.
[242] H. Kaur, M. Shorie, M. Sharma, A.K. Ganguli, P. Sabherwal, Bridged Rebar Graphene functionalized aptasensor for pathogenic E. coli O78:K80:H11 detection, Biosens. Bioelectron. 98 (2017) 486–493.
[243] S. Ranjbar, S. Shahrokhian, Design and fabrication of an electrochemical aptasensor using Au nanoparticles/carbon nanoparticles/cellulose nanofibers nanocomposite for rapid and sensitive detection of Staphylococcus aureus, Bioelectrochemistry 123 (2018) 70–76.
[244] K. Ghanbari, M. Roushani, A. Azadbakht, Ultra-sensitive aptasensor based on a GQD nanocomposite for detection of hepatitis C virus core antigen, Anal. Biochem. 534 (2017) 64–69.
[245] D. Han, Y. Yan, J. Wang, M. Zhao, X. Duan, L. Kong, H. Wu, W. Cheng, X. Min, S. Ding, An enzyme-free electrochemiluminesce aptasensor for the rapid detection of Staphylococcus aureus by the quenching effect of MoS2-PtNPs-vancomycin to S2O82−/O2 system, Sensor. Actuator. B Chem. 288 (2019) 586–593.
[246] H. Yue, Y. Zhou, P. Wang, X. Wang, Z. Wang, L. Wang, Z. Fu, A facile label-free electrochemiluminescent biosensor for specific detection of Staphylococcus aureus utilizing the binding between immunoglobulin G and protein A, Talanta 153 (2016) 401–406.
[247] Y. Sha, X. Zhang, W. Li, W. Wu, S. Wang, Z. Guo, J. Zhou, X. Su, A label-free multi-functionalized graphene oxide based electrochemiluminscence immunosensor for ultrasensitive and rapid detection of Vibrio parahaemolyticus in seawater and seafood, Talanta 147 (2016) 220–225.
[248] S. Alamer, S. Eissa, R. Chinnappan, P. Herron, M. Zourob, Rapid colorimetric lactoferrin-based sandwich immunoassay on cotton swabs for the detection of foodborne pathogenic bacteria, Talanta 185 (2018) 275–280.
[249] Y. You, S. Lim, J. Hahn, Y.J. Choi, S. Gunasekaran, Bifunctional linker-based immunosensing for rapid and visible detection of bacteria in real matrices, Biosens. Bioelectron. 100 (2018) 389–395.
[250] J. Hahn, E. Kim, Y.S. You, S. Gunasekaran, S. Lim, Y.J. Choi, A switchable linker-based immunoassay for ultrasensitive visible detection of Salmonella in tomatoes, J. Food Sci. 82 (10) (2017) 2321–2328.
[251] J. Chen, Z. Jiang, J.D. Ackerman, M. Yazdani, S. Hou, S.R. Nugen, V.M. Rotello, Electrochemical nanoparticle–enzyme sensors for screening bacterial contamination in drinking water, Analyst 140 (2015) 4991–4996.
[252] X. Xu, Y. Yuan, G. Hu, X. Wang, P. Qi, Z. Wang, Q. Wang, X. Wang, Y. Fu, Y. Li, H. Yang, Exploiting pH-regulated dimer-tetramer transformation of concanavalin A to develop colorimetric biosensing of bacteria, Sci. Rep. 7 (2017), 1452-1452.
[253] W. Ren, W. Liu, J. Irudayaraj, A net fishing enrichment strategy for colorimetric detection of E. coli O157:H7, Sensor. Actuator. B Chem. 247 (2017) 923–929.
[254] S. Yang, H. Ouyang, X. Su, H. Gao, W. Kong, M. Wang, Q. Shu, Z. Fu, Dual-recognition detection of Staphylococcus aureus using vancomycin-functionalized magnetic beads as concentration carriers, Biosens. Bioelectron. 78 (2016) 174–180.
[255] Y. Liu, J. Wang, X. Song, K. Xu, H. Chen, C. Zhao, J. Li, Colorimetric immunoassay for Listeria monocytogenes by using core gold nanoparticles, silver nanoclusters as oxidase mimetics, and aptamer-conjugated magnetic nanoparticles, Microchim. Acta 185 (2018) 360.
[256] Y. Liu, L. Zhang, W. Wei, H. Zhao, Z. Zhou, Y. Zhang, S. Liu, Colorimetric detection of influenza A virus using antibody-functionalized gold nanoparticles, Analyst 140 (2015) 3989–3995.
[257] Y.-H. Hou, J.-J. Wang, Y.-Z. Jiang, C. Lv, L. Xia, S.-L. Hong, M. Lin, Y. Lin, Z.-L. Zhang, D.-W. Pang, A colorimetric and electrochemical immunosensor for point-of-care detection of enterovirus 71, Biosens. Bioelectron 99 (2018) 186–192.
[258] J.-J. Wang, Y. Lin, Y.-Z. Jiang, Z. Zheng, H.-Y. Xie, C. Lv, Z.-L. Chen, L.-H. Xiong, Z.-L. Zhang, H. Wang, D.-W. Pang, Multifunctional cellular beacons with in situ synthesized quantum dots make pathogen detectable with the naked eye, Anal. Chem. 91 (2019) 7280–7287.
[259] H.-S. Kim, Y.-J. Kim, J.-W. Chon, D.-H. Kim, J.-H. Yim, H. Kim, K.-H. Seo, Two-stage label-free aptasensing platform for rapid detection of Cronobacter sakazakii in powdered infant formula, Sensor. Actuator. B Chem. 239 (2017) 94–99.
[260] Y.-J. Kim, H.-S. Kim, J.-W. Chon, D.-H. Kim, J.-Y. Hyeon, K.-H. Seo, New colorimetric aptasensor for rapid on-site detection of Campylobacter jejuni and Campylobacter coli in chicken carcass samples, Anal. Chim. Acta1029 (2018) 78–85.
[261] R. Das, A. Dhiman, A. Kapil, V. Bansal, T.K. Sharma, Aptamer-mediated colorimetric and electrochemical detection of Pseudomonas aeruginosa utilizing peroxidase-mimic activity of gold NanoZyme, Anal. Bioanal. Chem. 411 (2019) 1229–1238.
[262] L. Zhang, R. Huang, W. Liu, H. Liu, X. Zhou, D. Xing, Rapid and visual detection of Listeria monocytogenes based on nanoparticle cluster catalyzed signal amplification, Biosens. Bioelectron. 86 (2016) 1–7.
[263] J. Feng, Q. Shen, J. Wu, Z. Dai, Y. Wang, Naked-eyes detection of Shigella flexneri in food samples based on a novel gold nanoparticle-based colorimetric aptasensor, Food Contr. 98 (2019) 333–341.
[264] L. Zhu, S. Li, X. Shao, Y. Feng, P. Xie, Y. Luo, K. Huang, W. Xu, Colorimetric detection and typing of E. coli lipopolysaccharides based on a dual aptamer-functionalized gold nanoparticle probe, Microchim. Acta 186 (2019) 111.
[265] L. Long, J. Liu, K. Lu, T. Zhang, Y. Xie, Y. Ji, X. Wu, Highly sensitive and robust peroxidase-like activity of Au–Pt core/shell nanorod-antigen conjugates for measles virus diagnosis, J. Nanobiotechnol. 16 (2018) 46.
[266] S. Wachiralurpan, T. Sriyapai, S. Areekit, P. Sriyapai, S. Augkarawaritsawong, S. Santiwatanakul, K. Chansiri, Rapid colorimetric assay for detection of Listeria monocytogenes in food samples using LAMP formation of DNA concatemers and gold nanoparticle-DNA probe complex, Front. Chem. 6 (90) (2018).
[267] A.S. Mohammed, R. Nagarjuna, M.N. Khaja, R. Ganesan, J.R. Dutta, Effects of free patchy ends in ssDNA and dsDNA on goldnanoparticles in a colorimetric gene sensor for Hepatitis C virus RNA, Microchim. Acta 186 (2019) 566.
[268] F. Li, F. Li, G. Yang, Z.P. Aguilar, W. Lai, H. Xu, Asymmetric polymerase chain assay combined with propidium monoazide treatment and unmodified gold nanoparticles for colorimetric detection of viable emetic Bacillus cereus in milk, Sensor. Actuator. B Chem. 255 (2018) 1455–1461.

[269] T.A.C.S. Ganareal, M.M. Balbin, J.J. Monserate, J.R. Salazar, C.N. Mingala, Gold nanoparticle-based probes for the colorimetric detection of Mycobacterium avium subspecies paratuberculosis DNA, Biochem. Biophys. Res. Commun. 496 (3) (2018) 988–997.
[270] J. Du, H. Singh, W.-j. Dong, Y.-h. Bai, T.-H. Yi, Colorimetric detection of Listeria monocytogenes using one-pot biosynthesized flower-shaped gold nanoparticles, Sensor. Actuator. B Chem. 265 (2018) 285–292.
[271] R. Shahbazi, M. Salouti, B. Amini, A. Jalilvand, E. Naderlou, A. Amini, A. Shams, Highly selective and sensitive detection of Staphylococcus aureus with gold nanoparticle-based core-shell nano biosensor, Mol. Cell. Probes 41 (2018) 8–13.
[272] F. Tanvir, A. Yaqub, S. Tanvir, W.A. Anderson, Colorimetric enumeration of bacterial contamination in water based on β-galactosidase gold nanoshell activity, Enzym. Microb. Technol. 99 (2017) 49–56.
[273] J. Huang, J. Sun, A.R. Warden, X. Ding, Colorimetric and photographic detection of bacteria in drinking water by using 4-mercaptophenylboronic acid functionalized AuNPs, Food Contr. 108 (2020) 106885.
[274] J. Chen, A.A. Jackson, V.M. Rotello, S.R. Nugen, Colorimetric detection of Escherichia coli based on the enzyme-induced metallization of gold nanorods, Small 12 (18) (2016) 2469–2475.
[275] Q. You, X. Zhang, F.-G. Wu, Y. Chen, Colorimetric and test stripe-based assay of bacteria by using vancomycin-modified gold nanoparticles, Sensor. Actuator. B Chem. 281 (2019) 408–414.
[276] L. Zheng, P. Qi, D. Zhang, A simple, rapid and cost-effective colorimetric assay based on the 4-mercaptophenylboronic acid functionalized silver nanoparticles for bacteria monitoring, Sensor. Actuator. B Chem. 260 (2018) 983–989.
[277] R. Chen, X. Huang, J. Li, S. Shan, W. Lai, Y. Xiong, A novel fluorescence immunoassay for the sensitive detection of Escherichia coli O157:H7 in milk based on catalase-mediated fluorescence quenching of CdTe quantum dots, Anal. Chim. Acta947 (2016) 50–57.
[278] Ü. Dogan, E. Kasap, D. Cetin, Z. Suludere, I.H. Boyaci, C. Türkyılmaz, N. Ertas, U. Tamer, Rapid detection of bacteria based on homogenous immunoassay using chitosan modified quantum dots, Sensor. Actuator. B Chem. 233 (2016) 369–378.
[279] B. Yin, Y. Wang, M. Dong, J. Wu, B. Ran, M. Xie, S.W. Joo, Y. Chen, One-step multiplexed detection of foodborne pathogens: combining a quantum dot-mediated reverse assaying strategy and magnetic separation, Biosens. Bioelectron. 86 (2016) 996–1002.
[280] F. Tang, D.-W. Pang, Z. Chen, J.-B. Shao, L.-H. Xiong, Y.-P. Xiang, Y. Xiong, K. Wu, H.-W. Ai, H. Zhang, X.-L. Zheng, J.-R. Lv, W.-Y. Liu, H.-B. Hu, H. Mei, Z. Zhang, H. Sun, Y. Xiang, Z.-Y. Sun, Visual and efficient immunosensor technique for advancing biomedical applications of quantum dots on Salmonella detection and isolation, Nanoscale 8 (8) (2016) 4688–4698.
[281] S. Shukla, G. Lee, X. Song, S. Park, M. Kim, Immunoliposome-based immunomagnetic concentration and separation assay for rapid detection of Cronobacter sakazakii, Biosens. Bioelectron. 77 (2016) 986–994.
[282] S. Bagdeli, A.H. Rezayan, R.A. Taheri, M. Kamali, M. Hosseini, FRET- based immunoassay using CdTe and AuNPs for the detection of OmpW antigen of Vibrio cholerae, J. Lumin. 192 (2017) 932–939.
[283] K. Takemura, O. Adegoke, N. Takahashi, T. Kato, T.-C. Li, N. Kitamoto, T. Tanaka, T. Suzuki, E.Y. Park, Versatility of a localized surface plasmon resonance-based gold nanoparticle-alloyed quantum dot nanobiosensor for immunofluorescence detection of viruses, Biosens. Bioelectron. 89 (2017) 998–1005.
[284] E.J. Kim, E.B. Kim, S.W. Lee, S.A. Cheon, H.-J. Kim, J. Lee, M.-K. Lee, S. Ko, T. J. Park, An easy and sensitive sandwich assay for detection of Mycobacterium tuberculosis Ag85B antigen using quantum dots and gold nanorods, Biosens. Bioelectron. 87 (2017) 150–156.
[285] X. Lv, Y. Huang, D. Liu, C. Liu, S. Shan, G. Li, M. Duan, W. Lai, Multicolor and ultrasensitive enzyme-linked immunosorbent assay based on the fluorescence hybrid chain reaction for simultaneous detection of pathogens, J. Agric. Food Chem. 67 (33) (2019) 9390–9398.
[286] Z.-Z. Chen, L. Cai, M.-Y. Chen, Y. Lin, D.-W. Pang, H.-W. Tang, Indirect immunofluorescence detection of E. coli O157:H7 with fluorescent silica nanoparticles, Biosens. Bioelectron. 66 (2015) 95–102.
[287] W. Pan, J. Zhao, Q. Chen, Fabricating upconversion fluorescent probes for rapidly sensing foodborne pathogens, J. Agric. Food Chem. 63 (36) (2015) 8068–8074.
[288] R. Chinnappan, S. AlAmer, S. Eissa, A.A. Rahamn, K.M. Abu Salah, M. Zourob, Fluorometric graphene oxide-based detection of Salmonella enteritis using a truncated DNA aptamer, Microchim. Acta 185 (2017) 61.
[289] B.A. Borsa, B.G. Tuna, F.J. Hernandez, L.I. Hernandez, G. Bayramoglu, M. Y. Arica, V.C. Ozalp, Staphylococcus aureus detection in blood samples by silica nanoparticle-oligonucleotides conjugates, Biosens. Bioelectron 86 (2016) 27–32.
[290] X. Meng, G. Yang, F. Li, T. Liang, W. Lai, H. Xu, Sensitive detection of Staphylococcus aureus with vancomycin-conjugated magnetic beads as enrichment carriers combined with flow cytometry, ACS Appl. Mater. Interfaces 9 (2017) 21464–21472.
[291] D. Cheng, M. Yu, F. Fu, W. Han, G. Li, J. Xie, Y. Song, M.T. Swihart, E. Song, Dual recognition strategy for specific and sensitive detection of bacteria using aptamer-coated magnetic beads and antibiotic-capped gold nanoclusters, Anal. Chem. 88 (2016) 820–825.
[292] D.O. Demirkol, S. Timur, A sandwich-type assay based on quantum dot/aptamer bioconjugates for analysis of E. Coli O157:H7 in microtiter plate format, Int. J. Polym. Mater. 65 (2016) 85–90.
[293] Y. Liu, G. Mao, W. Wang, S. Tian, X. Ji, M. Liu, Z. He, In situ synthesis of photoluminescence-quenching nanopaper for rapid and robust detection of pathogens and proteins, Chem. Commun. 55 (2019) 2660–2663.
[294] X. Wang, Y. Huang, S. Wu, N. Duan, B. Xu, Z. Wang, Simultaneous detection of Staphylococcus aureus and Salmonella typhimurium using multicolor time-resolved fluorescence nanoparticles as labels, Int. J. Food Microbiol. 237 (2016) 172–179.
[295] X. Wang, S. Niazi, H. Yukun, W. Sun, S. Wu, N. Duan, X. Hun, Z. Wang, Homogeneous time-resolved FRET assay for the detection of Salmonella typhimurium using aptamer-modified NaYF4:Ce/Tb nanoparticles and a fluorescent DNA label, Microchim. Acta 184 (2017) 4021–4027.
[296] J. Shi, C. Chan, Y. Pang, W. Ye, F. Tian, J. Lyu, Y. Zhang, M. Yang, A fluorescence resonance energy transfer (FRET) biosensor based on graphene quantum dots (GQDs) and gold nanoparticles (AuNPs) for the detection of mecA gene sequence of Staphylococcus aureus, Biosens. Bioelectron. 67 (2015) 595–600.
[297] Y. Pang, Z. Rong, J. Wang, R. Xiao, S. Wang, A fluorescent aptasensor for H5N1 influenza virus detection based-on the core–shell nanoparticles metal-enhanced fluorescence (MEF), Biosens. Bioelectron 66 (2015) 527–532.
[298] K. Cheng, J. Zhang, L. Zhang, L. Wang, H. Chen, Aptamer biosensor for Salmonella typhimurium detection based on luminescence energy transfer from Mn2+-doped NaYF4:Yb, Tm upconverting nanoparticles to gold nanorods, Spectrochim. Acta Mol. Biomol. Spectrosc. 171 (2017) 168–173.
[299] L. Xu, R. Wang, L.C. Kelso, Y. Ying, Y. Li, A target-responsive and size-dependent hydrogel aptasensor embedded with QD fluorescent reporters for rapid detection of avian influenza virus H5N1, Sensor. Actuator. B Chem. 234 (2016) 98–108.
[300] P. Zhang, H. Liu, X. Li, S. Ma, S. Men, H. Wei, J. Cui, H. Wang, A label-free fluorescent direct detection of live Salmonella typhimurium using cascade triple trigger sequences-regenerated strand displacement amplification and hairpin template-generated-scaffolded silver nanoclusters, Biosens. Bioelectron. 87 (2017) 1044–1049.
[301] F. Karimi, S. Dabbagh, Gel green fluorescence ssDNA aptasensor based on carbon nanotubes for detection of anthrax protective antigen, Int. J. Biol. Macromol. 140 (2019) 842–850.
[302] A.M. Jimenez Jimenez, M.A.M. Rodrigo, V. Milosavljevic, S. Krizkova, P. Kopel, Z. Heger, V. Adam, Gold nanoparticles-modified nanomaghemite and quantum dots-based hybridization assay for detection of HPV, Sensor. Actuator. B Chem. 240 (2017) 503–510.
[303] N. Elahi, M. Kamali, M.H. Baghersad, B. Amini, A fluorescence Nano-biosensors immobilization on Iron (MNPs) and gold (AuNPs) nanoparticles for detection of Shigella spp, Mater. Sci. Eng. C 105 (2019) 110113.
[304] M. Shamsipur, V. Nasirian, K. Mansouri, A. Barati, A. Veisi-Raygani, S. Kashanian, A highly sensitive quantum dots-DNA nanobiosensor based on fluorescence resonance energy transfer for rapid detection of nanomolar amounts of human papillomavirus 18, J. Pharm.Biomed. Anal. 136 (2017) 140–147.
[305] A.M. Jimenez Jimenez, A. Moulick, L. Richtera, L. Krejcova, L. Kalina, R. Datta, M. Svobodova, D. Hynek, M. Masarik, Z. Heger, V. Adam, Dual-color quantum dots-based simultaneous detection of HPV-HIV co-infection, Sensor. Actuator. B Chem. 258 (2018) 295–303.
[306] J. Liu, L. Lu, S. Xu, L. Wang, One-pot synthesis of gold nanoclusters with bright red fluorescence and good biorecognition Abilities for visualization fluorescence enhancement detection of E. coli, Talanta 134 (2015) 54–59.
[307] M. Yin, C. Wu, H. Li, Z. Jia, Q. Deng, S. Wang, Y. Zhang, Simultaneous sensing of seven pathogenic bacteria by guanidine-functionalized upconversion fluorescent nanoparticles, ACS Omega 4 (2019) 8953–8959.
[308] R. Yan, Z. Shou, J. Chen, H. Wu, Y. Zhao, L. Qiu, P. Jiang, X.-Z. Mou, J. Wang, Y.-Q. Li, On–off–on gold nanocluster-based fluorescent probe for rapid Escherichia coli differentiation, detection and bactericide screening, ACS Sustain. Chem. Eng. 6 (2018) 4504–4509.
[309] Y. Wu, B. Wang, K. Wang, P. Yan, Identification of proteins and bacteria based on a metal ion–gold nanocluster sensor array, Anal.Methods 10 (2018) 3939–3944.
[310] D. Zhong, Y. Zhuo, Y. Feng, X. Yang, Employing carbon dots modified with vancomycin for assaying Gram-positive bacteria like Staphylococcus aureus, Biosens. Bioelectron. 74 (2015) 546–553.
[311] N. Wang, Y. Wang, T. Guo, T. Yang, M. Chen, J. Wang, Green preparation of carbon dots with papaya as carbon source for effective fluorescent sensing of Iron (III) and Escherichia coli, Biosens. Bioelectron 85 (2016) 68–75.
[312] S. Chandra, T.K. Mahto, A.R. Chowdhuri, B. Das, S.k. Sahu, One step synthesis of functionalized carbon dots for the ultrasensitive detection of Escherichia coli and iron (III), Sensor. Actuator. B Chem. 245 (2017) 835–844.
[313] J. Khang, D. Kim, K.W. Chung, J.H. Lee, Chemiluminescent aptasensor capable of rapidly quantifying Escherichia Coli O157:H7, Talanta 147 (2016) 177–183.
[314] M. Shourian, H. Ghourchian, M. Boutorabi, Ultra-sensitive immunosensor for detection of hepatitis B surface antigen using multi-functionalized gold nanoparticles, Anal. Chim. Acta895 (2015) 1–11.
[315] J. Lee, S.R. Ahmed, S. Oh, J. Kim, T. Suzuki, K. Parmar, S.S. Park, J. Lee, E. Y. Park, A plasmon-assisted fluoro-immunoassay using gold nanoparticle-decorated carbon nanotubes for monitoring the influenza virus, Biosens. Bioelectron. 64 (2015) 311–317.
[316] M.S. Draz, X. Lu, Development of a loop mediated isothermal amplification (LAMP) - surface enhanced Raman spectroscopy (SERS) assay for the detection of Salmonella enterica serotype enteritidis, Theranostics 6 (2016) 522–532.
[317] S. Chattopadhyay, P.K. Sabharwal, S. Jain, A. Kaur, H. Singh, Functionalized polymeric magnetic nanoparticle assisted SERS immunosensor for the sensitive detection of S. typhimurium, Anal. Chim. Acta1067 (2019) 98–106.
[318] T.J. Ondera, A.T. Hamme Ii, Magnetic-optical nanohybrids for targeted detection, separation, and photothermal ablation of drug-resistant pathogens, Analyst 140 (2015) 7902–7911.
[319] N. Duan, Y. Yan, S. Wu, Z. Wang, Vibrio parahaemolyticus detection aptasensor using surface-enhanced Raman scattering, Food Contr. 63 (2016) 122–127.
[320] N. Duan, M. Shen, S. Wu, C. Zhao, X. Ma, Z. Wang, Graphene oxide wrapped Fe3O4@Au nanostructures as substrates for aptamer-based detection of Vibrio

parahaemolyticus by surface-enhanced Raman spectroscopy, Microchim. Acta 184 (2017) 2653–2660.
[321] S. Díaz-Amaya, L.-K. Lin, A.J. Deering, L.A. Stanciu, Aptamer-based SERS biosensor for whole cell analytical detection of E. coli O157:H7, Anal. Chim. Acta1081 (2019) 146–156.
[322] S. Gao, L. He, Development of a filtration-based SERS mapping platform for specific screening of Salmonella enterica serovar Enteritidis, Anal. Bioanal. Chem. 411 (2019) 7899–7906.
[323] H. Zhang, X. Ma, Y. Liu, N. Duan, S. Wu, Z. Wang, B. Xu, Gold nanoparticles enhanced SERS aptasensor for the simultaneous detection of Salmonella typhimurium and Staphylococcus aureus, Biosens. Bioelectron. 74 (2015) 872–877.
[324] X. Ma, Y. Liu, N. Zhou, N. Duan, S. Wu, Z. Wang, SERS aptasensor detection of Salmonella typhimurium using a magnetic gold nanoparticle and gold nanoparticle based sandwich structure, Anal.Methods 8 (2016) 8099–8105.
[325] J. Chen, B. Park, Y.-w. Huang, Y. Zhao, Y. Kwon, Label-free SERS detection of Salmonella Typhimurium on DNA aptamer modified AgNR substrates, J. Food Meas. Char. 11 (2017) 1773–1779.
[326] I.-H. Cho, P. Bhandari, P. Patel, J. Irudayaraj, Membrane filter-assisted surface enhanced Raman spectroscopy for the rapid detection of E. coli O157:H7 in ground beef, Biosens. Bioelectron 64 (2015) 171–176.
[327] C. Zhang, C. Wang, R. Xiao, L. Tang, J. Huang, D. Wu, S. Liu, Y. Wang, D. Zhang, S. Wang, X. Chen, Sensitive and specific detection of clinical bacteria via vancomycin-modified Fe3O4@Au nanoparticles and aptamer-functionalized SERS tags, J. Mater. Chem. B 6 (2018) 3751–3761.
[328] X. Xu, X. Ma, H. Wang, Z. Wang, Aptamer based SERS detection of Salmonella typhimurium using DNA-assembled gold nanodimers, Microchim. Acta 185 (7) (2018) 325.
[329] J. Neng, Y. Li, A.J. Driscoll, W.C. Wilson, P.A. Johnson, Detection of multiple pathogens in serum using silica-encapsulated nanotags in a surface-enhanced Raman scattering-based immunoassay, J. Agric. Food Chem. 66 (2018) 5707–5712.
[330] P. Drake, Y.-C. Chen, I. Lehmann, P.-S. Jiang, Nanoparticle labels for pathogen detection through nucleic acid amplification tests, Microfluid. Nanofluidics 19 (2) (2015) 299–305.
[331] C.W. Wang, B. Gu, Q.Q. Liu, Y.F. Pang, R. Xiao, S.Q. Wang, Combined use of vancomycin-modified Ag-coated magnetic nanoparticles and secondary enhanced nanoparticles for rapid surface-enhanced Raman scattering detection of bacteria, Int. J. Nanomed. 13 (2018) 1159–1178.
[332] C. Wei, M. Li, X. Zhao, Surface-enhanced Raman scattering (SERS) with silver nano substrates synthesized by microwave for rapid detection of foodborne pathogens, Front. Microbiol. (2018).
[333] D. Yang, H. Zhou, C. Haisch, R. Niessner, Y. Ying, Reproducible E. coli detection based on label-free SERS and mapping, Talanta 146 (2016) 457–463.
[334] C. Wang, J. Wang, M. Li, X. Qu, K. Zhang, Z. Rong, R. Xiao, S. Wang, A rapid SERS method for label-free bacteria detection using polyethylenimine-modified Au-coated magnetic microspheres and Au@Ag nanoparticles, Analyst 141 (22) (2016) 6226–6238.
[335] B. Pearson, P. Wang, A. Mills, S. Pang, L. McLandsborough, L. He, Innovative sandwich assay with dual optical and SERS sensing mechanisms for bacterial detection, Anal.Methods 9 (2017) 4732–4739.
[336] L. Chen, N. Mungroo, L. Daikuara, S. Neethirajan, Label-free NIR-SERS discrimination and detection of foodborne bacteria by in situ synthesis of Ag colloids, J. Nanobiotechnol. 13 (2015) 45.
[337] N.E. Dina, H. Zhou, A. Colniţă, N. Leopold, T. Szoke-Nagy, C. Coman, C. Haisch, Rapid single-cell detection and identification of pathogens by using surface-enhanced Raman spectroscopy, Analyst 142 (2017) 1782–1789.
[338] P.A. Mosier-Boss, K.C. Sorensen, R.D. George, A. Obraztsova, SERS substrates fabricated using ceramic filters for the detection of bacteria, Spectrochim. Acta A Mol. Biomol. Spectrosc. 153 (2016) 591–598.
[339] T. Lemma, J. Wang, K. Arstila, V.P. Hytönen, J.J. Toppari, Identifying yeasts using surface enhanced Raman spectroscopy, Spectrochim. Acta A Mol. Biomol. Spectrosc. 218 (2019) 299–307.
[340] K. Yuan, J. Zheng, D. Yang, B. Jurado Sánchez, X. Liu, X. Guo, C. Liu, N.E. Dina, J. Jian, Z. Bao, Z. Hu, Z. Liang, H. Zhou, Z. Jiang, Self-Assembly of Au@Ag nanoparticles on Mussel shell to form large-scale 3D supercrystals as natural SERS substrates for the detection of pathogenic bacteria, ACS Omega 3 (2018) 2855–2864.
[341] T. Bu, Q. Huang, L. Yan, L. Huang, M. Zhang, Q. Yang, B. Yang, J. Wang, D. Zhang, Ultra technically-simple and sensitive detection for Salmonella Enteritidis by immunochromatographic assay based on gold growth, Food Contr. 84 (2018) 536–543.
[342] C. Wang, J. Peng, D.-F. Liu, K.-Y. Xing, G.-G. Zhang, Z. Huang, S. Cheng, F.-F. Zhu, M.-L. Duan, K.-Y. Zhang, M.-F. Yuan, W.-H. Lai, Lateral flow immunoassay integrated with competitive and sandwich models for the detection of aflatoxin M1 and Escherichia coli O157:H7 in milk, Int. J. Dairy Sci. 101 (2018) 8767–8777.
[343] W. Wang, L. Liu, S. Song, L. Xu, J. Zhu, H. Kuang, Gold nanoparticle-based paper sensor for multiple detection of 12 Listeria spp. by P60-mediated monoclonal antibody, Food Agric. Immunol. 28 (2017) 274–287.
[344] W. Wang, L. Liu, S. Song, L. Xu, H. Kuang, J. Zhu, C. Xu, Identification and quantification of eight Listeria monocytogene serotypes from Listeria spp. using a gold nanoparticle-based lateral flow assay, Microchim. Acta 184 (2017) 715–724.
[345] S. Xia, Z. Yu, D. Liu, C. Xu, W. Lai, Developing a novel immunochromatographic test strip with gold magnetic bifunctional nanobeads (GMBN) for efficient detection of Salmonella choleraesuis in milk, Food Contr. 59 (2016) 507–512.
[346] J. Singh, S. Sharma, S. Nara, Nanogold based lateral flow assay for the detection of Salmonella typhi in environmental water samples, Anal.Methods 7 (2015) 9281–9288.
[347] X. Zhang, J. Zhou, C. Zhang, D. Zhang, X. Su, Rapid detection of Enterobacter cloacae by immunomagnetic separation and a colloidal gold-based immunochromatographic assay, RSC Adv. 6 (2016) 1279–1287.
[348] C. Song, Development of a lateral flow colloidal gold immunoassay strip for the simultaneous detection of Shigella boydii and Escherichia coli O157:H7 in bread, milk and jelly samples, Food Contr. 59 (2016) 345–351.
[349] M. Chen, Z. Yu, D. Liu, T. Peng, K. Liu, S. Wang, Y. Xiong, H. Wei, H. Xu, W. Lai, Dual gold nanoparticle lateflow immunoassay for sensitive detection of Escherichia coli O157:H7, Anal. Chim. Acta876 (2015) 71–76.
[350] L. Shi, F. Wu, Y. Wen, F. Zhao, J. Xiang, L. Ma, A novel method to detect Listeria monocytogenes via superparamagnetic lateral flow immunoassay, Anal. Bioanal. Chem. 407 (2015) 529–535.
[351] C. Zhu, G. Zhao, W. Dou, Core-shell red silica nanoparticles based immunochromatographic assay for detection of Escherichia coli O157:H7, Anal. Chim. Acta1038 (2018) 97–104.
[352] Z. Huang, X. Cui, Q.-Y. Xie, D.-F. Liu, W.-H. Lai, Short communication: a novel method using immunomagnetic separation with a fluorescent nanobeads lateral flow assay for the rapid detection of low-concentration Escherichia coli O157:H7 in raw milk, Int. J. Dairy Sci. 99 (2016) 9581–9585.
[353] Q. Wang, M. Long, C. Lv, S. Xin, X. Han, W. Jiang, Lanthanide-labeled fluorescent-nanoparticle immunochromatographic strips enable rapid and quantitative detection of Escherichia coli O157:H7 in food samples, Food Contr. 109 (2020), 106894.
[354] J. Yu, J. Su, J. Zhang, X. Wei, A. Guo, CdTe/CdS quantum dot-labeled fluorescent immunochromatography test strips for rapid detection of Escherichia coli O157:H7, RSC Adv. 7 (2017) 17819–17823.
[355] V. Shirshahi, S.N. Tabatabaei, S. Hatamie, R. Saber, Functionalized reduced graphene oxide as a lateral flow immuneassay label for one-step detection of Escherichia coli O157:H7, J. Pharm. Biomed. 164 (2019) 104–111.
[356] E. Morales-Narváez, T. Naghdi, E. Zor, A. Merkoçi, Photoluminescent lateral-flow immunoassay revealed by graphene oxide: highly sensitive paper-based pathogen detection, Anal. Chem. 87 (2015) 8573–8577.
[357] T. Bu, J. Wang, L. Huang, L. Dou, B. Zhao, T. Li, D. Zhang, New functional tracer—two-dimensional nanosheet-based immunochromatographic assay for Salmonella enteritidis detection, J. Agric. Food Chem. 67 (23) (2019) 6642–6649.
[358] J. Hu, Y.Z. Jiang, M. Tang, L.L. Wu, H.Y. Xie, Z.L. Zhang, D.W. Pang, Colorimetric-fluorescent-magnetic nanosphere-based multimodal assay platform for Salmonella detection, Anal. Chem. 91 (2019) 1178–1184.
[359] A. Ben Aissa, J.J. Jara, R.M. Sebastián, A. Vallribera, S. Campoy, M.I. Pividori, Comparing nucleic acid lateral flow and electrochemical genosensing for the simultaneous detection of foodborne pathogens, Biosens. Bioelectron. 88 (2017) 265–272.
[360] Y. Zhao, H. Wang, P. Zhang, C. Sun, X. Wang, X. Wang, R. Yang, C. Wang, L. Zhou, Rapid multiplex detection of 10 foodborne pathogens with an up-converting phosphor technology-based 10-channel lateral flow assay, Sci. Rep. 6 (2016) 21342.
[361] N. Cheng, Y. Song, M.M.A. Zeinhom, Y.-C. Chang, L. Sheng, H. Li, D. Du, L. Li, M.-J. Zhu, Y. Luo, W. Xu, Y. Lin, Nanozyme-mediated dual immunoassay integrated with smartphone for use in simultaneous detection of pathogens, ACS Appl. Mater. Interfaces 9 (2017) 40671–40680.
[362] F. Li, F. Li, D. Luo, W. Lai, Y. Xiong, H. Xu, Biotin-exposure-based immunomagnetic separation coupled with nucleic acid lateral flow biosensor for visibly detecting viable Listeria monocytogenes, Anal. Chim. Acta1017 (2018) 48–56.
[363] Y. Chen, Y. Xianyu, J. Sun, Y. Niu, Y. Wang, X. Jiang, One-step detection of pathogens and cancer biomarkers by the naked eye based on aggregation of immunomagnetic beads, Nanoscale 8 (2016) 1100–1107.
[364] W. Wang, L. Liu, S. Song, L. Tang, H. Kuang, C. Xu, A highly sensitive ELISA and immunochromatographic strip for the detection of Salmonella typhimurium in milk samples, Sensors (Basel) 15 (2015) 5281–5292.
[365] Z. Huang, J. Peng, J. Han, G. Zhang, Y. Huang, M. Duan, D. Liu, Y. Xiong, S. Xia, W. Lai, A novel method based on fluorescent magnetic nanobeads for rapid detection of Escherichia coli O157:H7, Food Chem. 276 (2019) 333–341.
[366] A. Gumustas, M.G. Caglayan, M. Eryilmaz, Z. Suludere, E. Acar Soykut, B. Uslu, I. H. Boyaci, U. Tamer, Paper based lateral flow immunoassay for the enumeration of Escherichia coli in urine, Anal.Methods 10 (2018) 1213–1218.
[367] J.H. Shin, J. Hong, H. Go, J. Park, M. Kong, S. Ryu, K.-P. Kim, E. Roh, J.-K. Park, Multiplexed detection of foodborne pathogens from contaminated lettuces using a handheld multistep lateral flow assay device, J. Agric. Food Chem. 66 (2018) 290–297.
[368] F. Hua, P. Zhang, F. Zhang, Y. Zhao, C. Li, C. Sun, X. Wang, R. Yang, C. Wang, A. Yu, L. Zhou, Development and evaluation of an up-converting phosphor technology-based lateral flow assay for rapid detection of Francisella tularensis, Sci. Rep. 5 (2015) 17178.
[369] G. Li, Y. Huang, M. Duan, K. Xing, X. You, H. Zhou, Y. Liu, C. Liu, D. Liu, W. Lai, Biosensing multiplexer based on immunochromatographic assay for rapid and high-throughput classification of Salmonella serogroups, Sensor. Actuator. B Chem. 282 (2019) 317–321.
[370] L. Zhang, Y. Huang, J. Wang, Y. Rong, W. Lai, J. Zhang, T. Chen, Hierarchical flowerlike gold nanoparticles labeled immunochromatography test strip for highly sensitive detection of Escherichia coli O157:H7, Langmuir 31 (2015) 5537–5544.

[371] G.B. John, R. Alicia, Aptamer-quantum dot lateral flow test strip development for rapid and sensitive detection of pathogenic Escherichia coli via intimin, O157-specific LPS and shiga toxin 1 aptamers, Curr. Bionanotechnol. (Discontinued) 1 (2015) 80–86.
[372] W. Wu, M. Zhou, H. He, C. Liu, P. Li, M. Wang, Y. Liu, X. Hao, Z. Fang, A sensitive aptasensor for the detection of Vibrio parahaemolyticus, Sensor. Actuator. B Chem. 272 (2018) 550–558.
[373] X. Fu, Z. Cheng, J. Yu, P. Choo, L. Chen, J. Choo, A SERS-based lateral flow assay biosensor for highly sensitive detection of HIV-1 DNA, Biosens. Bioelectron 78 (2016) 530–537.
[374] S. Díaz-Amaya, M. Zhao, L.-K. Lin, C. Ostos, J.P. Allebach, G.T.-C. Chiu, A. J. Deering, L.A. Stanciu, Inkjet printed nanopatterned aptamer-based sensors for improved optical detection of foodborne pathogens, Small 15 (2019) 1805342.